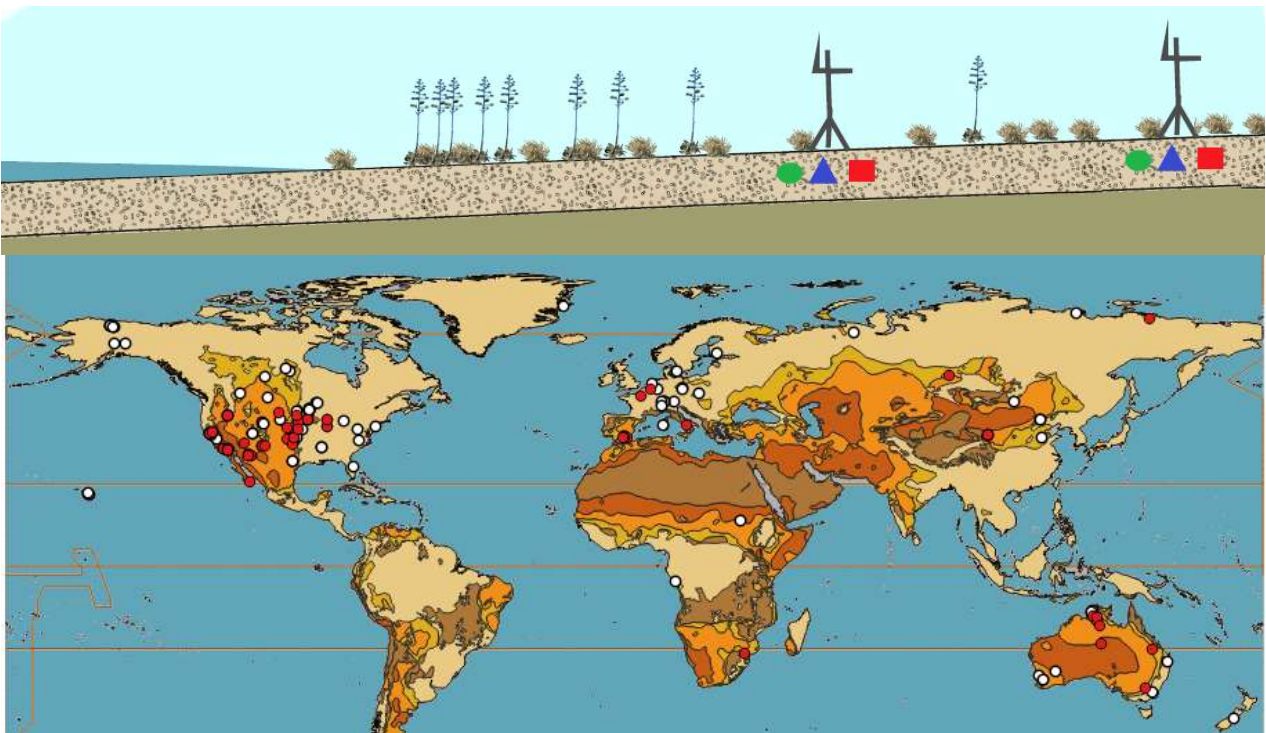*Ph. D. DISSERTATION*/TESIS DOCTORAL

Author: María Rosario Moya Jiménez

CHARACTERIZATION OF SUBSOIL CO₂ DYNAMICS IN TWO SEMIARID ECOSYSTEMS: GLOBAL SCALE IMPLICATIONS

Promoters: Enrique Pérez Sánchez Cañete

Francisco Domingo Poveda

Universidad de Granada

Programa doctorado Ciencias de la Tierra

Diciembre 2020

Ph. D. DISSERTATION/TESIS DOCTORAL

CHARACTERIZATION OF SUBSOIL CO$_2$ DYNAMICS IN TWO SEMIARID ECOSYSTEMS: GLOBAL SCALE IMPLICATIONS

CARACTERIZACIÓN DE LA DINÁMICA DEL CO$_2$ EN EL SUBSUELO DE DOS ECOSISTEMAS SEMIÁRIDOS: IMPLICACIÓN A ESCALA GLOBAL

Memoria presentada por <u>María Rosario Moya Jiménez</u> para optar al grado de Doctor en Ciencias de la Tierra por la Universidad de Granada

AGRADECIMIENTOS

Especialmente, me gustaría expresar mi agradecimiento a los dos grandes pilares que me han acompañado en este proyecto y por los que he conseguido llevar esta tesis a término:

Por un lado a mis directores, Enrique y Paco. Les agradezco enormemente que hayan confiado en mí trabajo a pesar del tiempo que he acabado demandando. He tenido la suerte de tener unos directores a los que buscaba más como amigos, que como supervisores. Porque ellos nunca se han quejado y han aportado su conocimiento, energía y experiencia siempre que han podido.

Por otro lado, agradecer a mi pareja Santiago y a mi familia, quiénes siempre están ahí y lo aguantan todo, por su amor, compañía y apoyo. Por saber que por mucho que me falle el cuerpo, siempre los tendré para lo que necesite.

En lo personal, esta ha sido una época intensa y emocionante. Al contrario que en la carrera o el máster donde me encontraba como pez en el agua, el doctorado ha acabado siendo algo mucho más serio y difícil. He tenido muchas carencias e inseguridades y finalmente a mi propio cuerpo como mi peor enemigo. Sin embargo, y a pesar de todo, sin duda estoy muy contenta con la elección elegida y el desarrollo de esta etapa.

Gracias al doctorado he podido seguir desarrollando la curiosidad que forma parte de mí persona. Durante estos años he trabajado de forma independiente y plena en un proyecto que al principio es guiado, pero que con los años vas moldeando y desarrollando como propio. He podido conocer a muchas personas y trabajar con ellas. He podido dar clase. He podido exponer en inglés en numerosas ocasiones. He podido conocer y formar parte de la comunidad científica. He podido escribir una tesis doctoral. Y he acabado disfrutando de todo ello.

Ahora empieza para mí una nueva etapa. Y la comenzaré con la ilusión y motivación de saber de todo lo que puedo ser capaz.

Rosario

28 de Diciembre de 2020

TABLE OF CONTENTS

ABSTRACT

Understanding the factors that influence patterns of terrestrial CO_2 fluxes across the globe is essential to know and predict the changes in the relation between climate change and land ecosystems. Semi-arid ecosystems occupy approximately 45% of the terrestrial surface and constitute the largest biome on the planet, but they are under-represented in ecological research networks. This is relevant because, due to the reduced biological activity of drylands ecosystems, their carbon dynamics include characteristics that make them unique. Here, the ecosystem carbon balance is strongly associated with variations of abiotic factors.

Pressure pumping, pressure tides and subterranean ventilation are non-diffusive transport processes affected by wind or changes in atmospheric pressure at different temporal scales. These processes can result in more efficient transport compared to molecular diffusion alone and can dominate the ecosystem flux during the dry season. They are especially relevant in well-aerated soils (with a high quantity of pores and fissures) with a CO_2 rich vadose zone (between the water table and the soil surface) and when the soil pores have low water content to allow gas flow. Hence, the vadose zone becomes a key element to be studied. Unluckily most studies in soils, which are key components in the carbon balance in semi-arid ecosystems, have focused on shallow (e.g., <30 cm depth) soil CO_2 dynamics neglecting processes in deeper soil layers where highly CO_2 enriched air can be stored or transported through soil pores and fissures by these processes.

In Chapter I, this thesis tried examines the relationship among variations in subterranean CO_2 molar fraction, volumetric water content, soil temperature and atmospheric pressure during three years (2014-2016)

within soil profiles (0.15, 0.50, and 1.50 m depths) in two semi-arid grasslands located in southeastern Spain. Results using statistical and wavelet analysis shown that CO_2 dynamics were strongly influenced by changes in atmospheric pressure (pressure tides) from semidiurnal, diurnal and synoptic to monthly time scales for all soil depths. In contrast, regarding soil temperature and volumetric water content, only weak daily dependencies were found at the sub-surface level (0.15 m). These results provided clear insights that were visible during the three years of the experiment, into the importance of subterranean storage and non-diffusive gas transport in soils and gave the first insights into the relation between lunar forcing and subterranean CO_2 fluctuation. This chapter resulted in a publication in a Q1 journal.

In Chapter II, this thesis tried to move forward in this direction, including the surface soil horizon (0.05 m) and the study of a new variable, the friction velocity, in the analysis, in order to differentiate the CO_2 dynamic between the surface and deep soil, and the possible presence of pressure pumping and ventilation in subterranean CO_2 dynamics. Through the analysis of the CO_2 molar fraction and main soil and environmental variables related with biotic (soil temperature and soil water content) and abiotic (atmospheric pressure and friction velocity) factors continuously measure during three years, a clear functional decoupling was found between layers. Wavelet analysis revealed that the CO_2 concentration at 0.05 m depth was controlled by soil moisture, soil temperature, pressure pumping and ventilation, with rain-pulse events being the most important factor controlling the carbon dynamics. The concentrations in the deeper soil, on the other hand, were influenced mainly by pressure tides. The subsurface layer acted as an interphase layer and was affected by soil temperature, soil water content, pressure tides, pressure pumping and ventilation. The physical decoupling found between pressure tides, pressure

pumping and ventilation suggests that pressure tides are not directly responsible for CO_2 emissions, and their role in ecosystem carbon dynamics – related to underground, vertical CO_2 transport – merely facilitates CO_2 emission by pressure pumping and ventilation. A manuscript related with this chapter is being prepared for its publication.

Considering that subterranean ventilation would be the most important factor determining the variability in the annual ecosystem carbon balance in our ecosystems under study, the presence of subterranean ventilation at the global scale was studied for first time in chapter III. For this purpose, an algorithm was designed, based on previous scientific evidence, to systematically detect ventilation events in the 145 non-forested open ecosystems selected for this study. The analyzed database was selected from FLUXNET2015, AmeriFlux, OzFlux and AsiaFlux networks. Despite some limitations, it was confirmed that subterranean ventilation CO_2 emissions occur globally. Of the sites analyzed, 34% reported the occurrence of ventilation events. This vented CO_2 was found mainly in arid ecosystems (84%) and sites with hot and dry periods. A manuscript related with this chapter had been submitted for publication.

Unfortunately, the lack of a standardized global database with information on CO_2 dynamics below the soil surface made it impossible to analyze the presence of pressure tides at global scale.

Rates of biological activity per unit of drylands are low compared with many terrestrial ecosystems but the large surface area of drylands gives their carbon dynamics a relevant global significance. In particular, variability in the global CO_2 sinks is dominated by that semi-arid ecosystems, which are the ecosystems most vulnerable to climate change and can be switched to a CO_2 source in response to global warming or changes in precipitation. Under this premise, subterranean ventilation could be the most important factor determining the variability in the annual

ecosystem carbon balance in many ecosystems around the world. Understanding the occurrence of processes, feedbacks and driving factors that modulate the carbon source capacity of natural ecosystems due to ventilation events is needed to advance towards more robust model projections for future climate as well as more adequate design of mitigation policies. Additionally, the improvement of the gradient method, considering the role of abiotic factors in deep soil CO_2 dynamics, will be essential to produce reliable estimations of soil CO_2 efflux in ecosystems affected by non-diffusive gas transport processes.

RESUMEN

Comprender los factores que influyen en la dinámica de CO_2 de los ecosistemas terrestres a lo largo del mundo es esencial para conocer y predecir los cambios que se pueden producir en la relación entre estos y el cambio climático. Los ecosistemas semiáridos ocupan aproximadamente el 45% de la superficie terrestre y constituyen el mayor bioma del planeta. Sin embargo, son ecosistemas poco estudiados en las redes internacionales de investigación ecológica. Este hecho es relevante, ya que debido a la baja producción biológica, la dinámica del carbono de los ecosistemas semiáridos tiene características que los hacen únicos. En ellos, la dinámica del carbono está fuertemente asociada con las variaciones en los factores abióticos.

Las mareas de presión, el bombeo por presión y la ventilación subterránea son procesos de transporte no difusivos afectados por el viento o cambios en la presión atmosférica a diferentes escalas temporales. Estos procesos resultan en una forma de transporte mucho más eficiente que la difusión molecular y pueden llegar a dominar el flujo a escala de ecosistema durante la estación seca. Estos procesos son especialmente relevantes en aquellos suelos bien aireados (con un gran número de poros y fisuras) con una zona vadosa (entre la superficie y el nivel freático) rica en CO_2 y cuando los poros del suelo tengan poco contenido en agua que permita el flujo de aire. Así pues, la zona vadosa, se vuelve un elemento fundamental a ser estudiado. Lamentablemente, la mayoría de estudios en suelos, que son componentes claves en el balance del carbono de los ecosistemas semiáridos, se centran en el perfil más superficial del suelo (unos 30 cm), negando los procesos en profundidad, donde gran parte del aire enriquecido en CO_2 puede ser almacenado y transportado por estos procesos.

En el capítulo I, esta tesis intenta investigar la relación existente entre las variaciones de la fracción molar de CO_2, el contenido del agua en

el suelo, la temperatura del suelo y la presión ambiental a lo largo de tres años (2014-2016) en varios perfiles del suelo (0.15, 0.50 y 1.50 m) en dos pastizales semiáridos localizados en el sureste de España. Los resultados, aplicando el análisis de wavelets, mostraron que la dinámica del CO_2 del suelo estaba fuertemente influenciada por los cambios en la presión atmosférica (mareas de presión) a escala semidiurna, diurna, sinóptica y mensual, para todas las profundidades. Por el contrario, la temperatura y contenido de agua del suelo mostraron débiles dependencias sólo a escala diaria a los 0.15 m de profundidad. Estos resultados mostraron este patrón de forma clara durante los tres años de experimento, demostrando la importancia del almacenamiento subterráneo y el transporte no difusivo del suelo. Este trabajo también aportó las primeras evidencias de la relación existente entre la influencia de la luna y las variaciones de CO_2 subterráneo. El capítulo resultó en una publicación en una revista de alto impacto (Q1).

En el capítulo II, esta tesis intenta avanzar un paso más en esta dirección incluyendo el horizonte superficial del suelo (a 0.05 m) y el estudio de una nueva variable, la velocidad de fricción, para poder estudiar las diferencias en la dinámica del CO_2 entre el suelo superficial y el suelo profundo, así como la posible presencia del bombeo por presión y la ventilación subterránea en estas dinámicas. A través del análisis de la fracción molar del CO_2 y las principales variables ambientales y del suelo relacionadas con factores bióticos (temperatura y contenido en agua del suelo) y abióticos (presión ambiental y velocidad de fricción) medidos de forma continua durante tres años, se encontró un evidente desacoplamiento entre las capas del suelo. El análisis de wavelets reveló que la concentración de CO_2 a 0.05 m estaba controlada por la humedad del suelo, la temperatura del suelo, el bombeo por presión y la ventilación subterránea, siendo los eventos de pulsos de lluvia los principales condicionantes de cambio. La concentración en el perfil profundo, por otro lado, estaba principalmente

condicionada por las mareas de presión. La capa sub-superficial en este caso actuó como una interfase y estuvo afectada por la humedad del suelo, la temperatura del suelo, las mareas de presión, el bombeo por presión y la ventilación subterránea. El desacoplamiento físico existente entre capas con respecto a la presencia de mareas de presión, ventilación o bombeo por presión, sugieren que las mareas de presión podrían no estar relacionadas con las emisiones de CO_2 y que su papel en la dinámica del ecosistema podría ser la de facilitar el transporte del CO_2 a la superficie del suelo para ser ventilado por bombeo de presión o ventilación. Un artículo relacionado con este capítulo está siendo preparado para su publicación.

Considerando que la ventilación subterránea podría ser el factor más importante que determina la variabilidad en el balance anual de carbono de nuestros ecosistemas estudiados, la presencia de ventilación se estudió a escala global por primera vez en el capítulo III. Con este propósito se diseñó un algoritmo, basado en la evidencia científica conocida hasta ahora, capaz de detectar la presencia de eventos de ventilación en los 145 ecosistemas abiertos (zonas no forestales) seleccionados para este estudio. Las bases de datos analizadas son pertenecientes a las redes FLUXNET2015, Ameriflux, OzFlux y AsiaFlux. A pesar de algunas limitaciones encontradas en las bases de datos, se confirmó la presencia de los eventos de ventilación a escala global. El 34% de los sitios analizados reportaron la ocurrencia de este fenómeno. La ocurrencia de ventilación fue principalmente encontrada en ecosistemas áridos (84%) y lugares con períodos cálidos y secos. Un artículo relacionado con este capítulo ha sido enviado para su publicación a una revista de alto impacto.

Lamentablemente, no existe una base de datos estandarizada a nivel global con información de la dinámica del CO_2 en el suelo que permita el análisis de las mareas de presión a escala global.

Las tasas de actividad biológica por unidad de área son bajas en los ecosistemas áridos y semiáridos en comparación con otros ecosistemas terrestres, pero su gran superficie, da a este tipo de ecosistemas una gran relevancia a nivel global. En concreto, la variabilidad global de los ecosistemas a ser sumideros de CO_2 está dominada por los ecosistemas áridos y semiáridos, que son a la vez los ecosistemas más vulnerables al cambio climático y pueden revertir a ser emisores de este gas de efecto invernadero como consecuencia del calentamiento global y los cambios en la precipitación. Bajo esta premisa, la ventilación subterránea puede ser el factor más importante a la hora de determinar la variabilidad en el balance anual del ecosistema en muchos ecosistemas a lo largo del planeta. Comprender la ocurrencia, relevancia y retroalimentaciones de estos procesos que pueden modular la capacidad de un ecosistema de ser fuente o sumidero de carbono debido a procesos de ventilación es necesario para obtener modelos de predicción de cambio climático más robustos y un mejor diseño de políticas de prevención. Por otro lado, la mejora del método de gradiente, considerando los factores abióticos en la dinámica del suelo profundo, será esencial para tener estimaciones fiables de flujos de emisión de CO_2 del suelo en los ecosistemas afectados por los procesos de transporte no difusivos.

INTRODUCTION

1.1 THE ROLE OF TERRESTRIAL ECOSYSTEMS IN THE EARTH SYSTEM. THE EFFECT OF GLOBAL WARMING

Terrestrial ecosystems play a key role in the climate system. Due to their large carbon pools and carbon exchange fluxes with the atmosphere, they interact in complex ways with multiple biophysical and biogeochemical feedbacks across different spatial and temporal scales (Ciais et al., 2013; Le Quere et al., 2015). Globally, terrestrial ecosystems act as a large CO_2 sink (Canadell & Schulze, 2014; Zhu et al., 2016) that has slowed the rise in global land-surface air temperature by 0.09 ± 0.02 °C since 1982 (Zeng et al., 2017).

Earth's climate has changed throughout history. However, the current global warming is of particular relevance because most of it is the result of human activity especially since the mid-20th century (Hegerl et al., 2018; Santer et al., 1996). The mean earth temperature for the period 2006–2015 was 1.53 °C higher than for the period 1850–1900. At this rate of change, terrestrial ecosystems and land processes are exposed to disturbances beyond the range of current natural variability as a result of global warming, with far reaching impacts on ecosystems (IPCC, 2019). In this context, there have been many modelling studies that reported impacts of global warming on ecosystems (e.g. Pielke et al., 2011).

The global warming affects terrestrial ecosystems from different ways. E.g. it is expected to result in desertification, increasing heat waves, wildfires and droughts (Fasullo et al., 2018). Increases in extreme events produced by global warming are generating changes in the structure, composition, and function of ecosystems globally (Holmgren & Hirota,

2013; Seddon et al., 2016; Seidl et al., 2017; Settele et al., 2014). If the ecosystems are going to maintain their carbon sink role or switch to a CO_2 source in response to warming or changes in precipitation (Davies-Barnard et al., 2015; Gonzalez et al., 2010; Wärlind et al., 2014) is one of the largest uncertainties in carbon cycle and climate modelling (Bloom et al., 2016; Ciais et al., 2013; Friend et al., 2014; Le Quere et al., 2018).

In general, the effect of global warming in ecosystems, depends on the degree of exposure and the intrinsic sensitivity (the degree to which a system changes after a disturbance) and resilience (the ability of an ecosystem to return to its original state after a disturbance) of each biome (Pimm, 1984). At global scale, the arid and semi-arid ecosystems are considered the most vulnerable biomes to the effects produced by global warming (Fu & Feng, 2014; Li et al., 2018; Sherwood & Fu, 2014).

1.2 THE IMPORTANCE OF ARID LANDS

The geographic classification of drylands is often based on the aridity index (AI), the ratio of average annual precipitation amount (P) to potential evapotranspiration amount (PET). The United Nations Convention to Combat Desertification (UNCCD 1994) defined drylands as the arid, semi-arid, and dry sub-humid areas resulting from many factors, including climatic variations and human activities. The UNCCD definition excluded the hyper-arid areas, considered in the United Nations Environment Programme (UNEP 1992) definition.

UNCCD and CBD dryland definitions
- arid: P/PET 0.05 - 0.20
- semiarid: P/PET 0.20 - 0.50
- dry subhumid: P/PET 0.50 - 0.65
- additional areas included in CBD definition
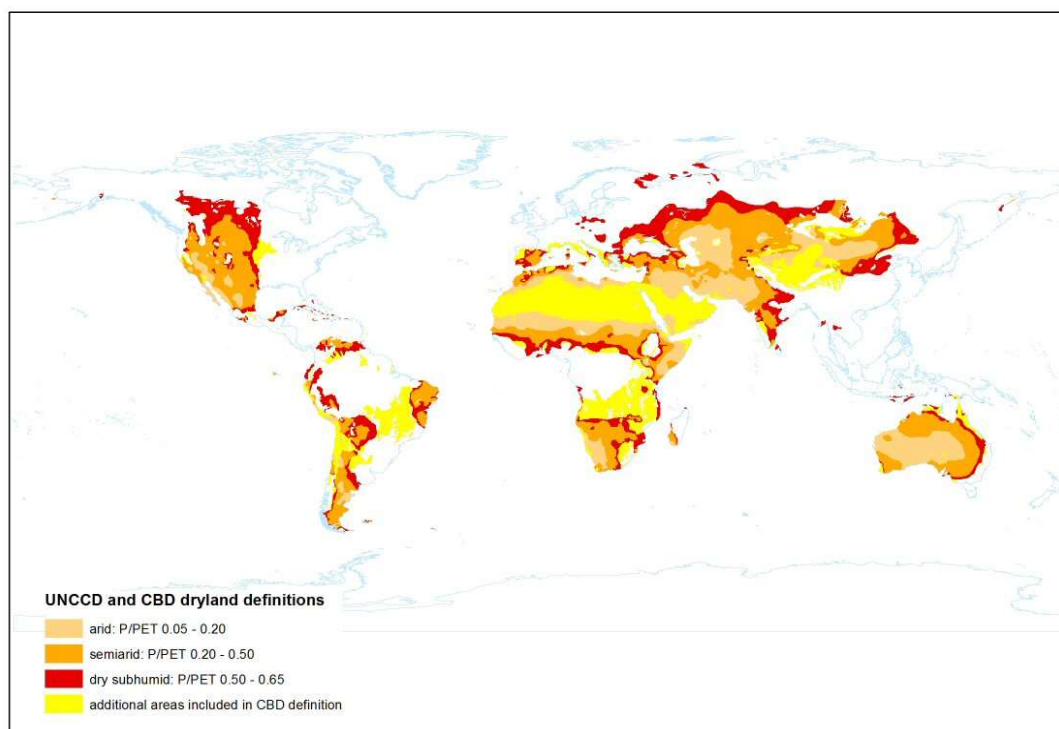
Figure 1. *World dryland distribution according to the UNCCD classification. Source: (UNEP-WCMC; Sorensen, 2007).*

Anothers relevant concepts are aridity and drought. Aridity is a long-term climatic feature characterized by low average precipitation or available water (Gbeckor-Kove, 1989) while drought is defined as a temporary climatic event (Maliva & Missimer, 2012).

Drylands are home to approximately 38.2% (± 0.6%) of the global population (Esch et al., 2017; Koutroulis, 2019), that is about 3 billion people. These regions cover up to about 46% of the total terrestrial surface (about 60 million km², D'Odorico et al., 2013; Maestre et al., 2016; Pravalie, 2016). From them, approximately 70% of dryland areas are located in Africa and Asia and according to the European Environment Agency (European Court of Auditors (ECA), 2018), in the areas of Southern, Central and Eastern European the 8% of the territory show "very high" and "high

sensitivity" to desertification including a large part of the Mediterranean Spain.

1.3 THE EFFECT OF GLOBAL WARMING ON DRYLANDS. THE MEDITERRANEAN REGION

Warming trends over drylands are twice the global average (Lickley & Solomon, 2018). A warming climate will result in regional increases in the spatial extent of drylands and that regions will warm faster than the global average warming rate. As a result of an increased drought frequency and reduced soil moisture availability in the growing season, the range and intensity of desertification have increased over the past several decades (Engelbrecht et al., 2015; Schlaepfer et al., 2017). Arid ecosystems are more sensitive to changes in precipitation and temperature (Li et al., 2018; Seddon et al., 2016; You et al., 2018), increasing vulnerability to desertification. Social drivers, as land use changes or anthropogenic disturbances, can also play an important role with regards to future vulnerability (Emmerich, 2003; Eswaran et al., 2000; Huenneke et al., 2002; Schlesinger, 1990).

Mediterranean climate is also projected to become drier (Alessandri et al., 2014; Polade et al., 2017). Regional trends in frequency and intensity of drought also considerate that Mediterranean areas will be clearly affected by global warming (Kelley et al., 2015; Wilcox et al., 2018). Also, the locally increased incidence of extreme rainfall events over the Mediterranean region has been suggested (Giannakopoulos et al., 2009) join to an expected decrease in annual rainfall (Capolongo et al., 2008). Rodriguez-Caballero et al., (2018) found a possible reduction in the biological soil crust in eastern Spain of $25 - 40\%$ by 2070, and García-Fayos & Bochet, (2009) found a

possible reduction in plant species richness and plant cover in semi-arid Mediterranean shrublands in eastern Spain. For that, is so important to study how loss of biodiversity and modification of the ecosystem functions is inducing changes on the global carbon exchanges in the terrestrial ecosystems.

1.4 THE EDDY COVARIANCE TECHNIQUE. FLUXNET AND REGIONAL NETWORKS

The eddy covariance technique (EC) is the standard method used by biometeorologists to measure the net ecosystem exchange (NEE) fluxes of trace gases between ecosystems and atmosphere. The EC is a powerful tool (Aubinet et al., 2012; Baldocchi, 2014) that helps the scientific community to reach a better understanding of the Earth's climate system in the global change context (Reich, 2010; Solomon & Quin 2007). Key attributes of the eddy covariance method are its ability to measure NEE fluxes directly, *in situ*, without invasive artifacts, at a spatial scale of hundreds of meters, and on time scales spanning from hours to decades (Baldocchi et al., 2001). Despite some limitations inherent to the technique (i.e. its application is generally restricted to periods when atmospheric conditions are turbulent), annual integrations of CO_2 exchange have been demonstrated feasible (Wofsy et al., 1993) and the use of the EC towers has spread around the world with more than eight hundred of towers dedicated to the estimation of annual CO_2 exchange at different ecosystem surfaces.

A set of regional (Aubinet et al., 1999; Isaac et al., 2016; Novick et al., 2018; Reich, 2010; Yu et al., 2006) and global networks (Pastorello et al., 2020) of EC flux measurement stations has been established compiling data for different EC stations. Some regional networks are AmeriFlux in the United States of America, CarboEurope in Europe; AsiaFlux in Asia,

OzFlux in Australia and ChinaFlux in China. FLUXNET is the global network that integrates information of many of the experimental sites included in these regional networks together. They provide an infrastructure for compiling, storing, and distributing open data of carbon, water, energy fluxes and related meteorological conditions to the scientific community. Although the stations are dispersed across most of the world's climate space and representative biomes, the arid and semi-arid environments are largely under-represented in these networks (Bell et al., 2012).

1.5 PROCESSES INVOLVED IN THE TERRESTRIAL CARBON CYCLE

The total amount of carbon incorporated into the ecosystem through photosynthesis is known as gross primary production (GPP), and the global GPP average is estimated about 123 PgC yr^{-1} (Beer et al., 2010). A proportion of the CO_2 captured by ecosystems returns to the atmosphere via ecosystem respiration (R_{eco}; Falge et al., 2002; Valentini et al., 2000). R_{eco} components include the emission of CO_2 from soils (Vargas et al., 2011) known as total soil respiration (RS), and is composed from the production of CO_2 by heterotrophic organisms (i.e., heterotrophic respiration, Rh) and autotrophic respiration (RA, production of CO_2 by plant roots and organisms directly associated with the rhizosphere; Hanson et al., 2000). The balance between CO_2 captured via GPP and loss through R_{eco} is the net ecosystem exchange (NEE), which ultimately determines if the ecosystem acts as a net carbon source or sink.

Some studies have shown a contribution of geochemical processes to the NEE (Emmerich, 2003; Mielnick et al., 2005; Roland et al., 2013). This other process, different from GPP and R_{eco}, is included in the concept of the

Net Ecosystem Carbon Balance (NECB). As defined by Chapin III et al., (2006), NECB is the net rate of organic and inorganic carbon accumulation in an ecosystem, from all sources and sinks, regardless of the temporal and spatial scale at which it is estimated. Some of these processes include photodegradation (Rutledge et al., 2010), geochemical weathering (Hamerlynck et al., 2013), and subterranean ventilation (Kowalski et al., 2008).
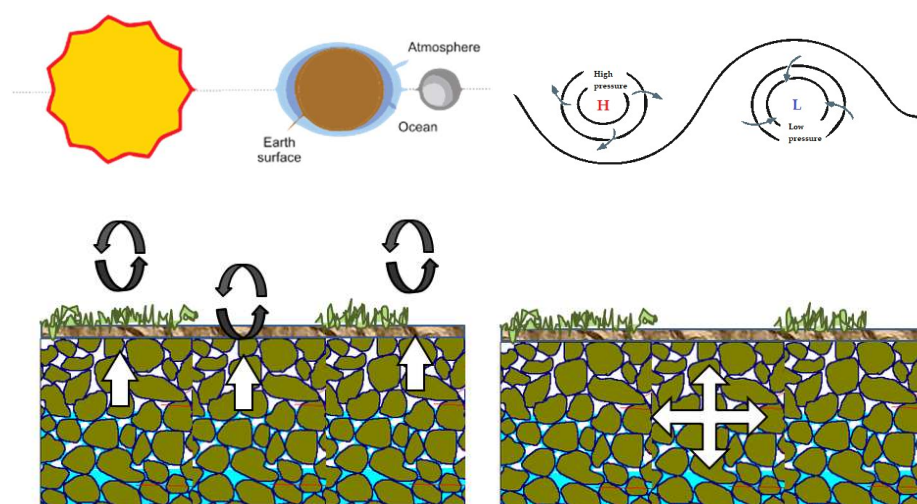
Figure 2. *Diagram of how changes in wind or changes in atmospheric pressure at different temporal scales produces the soil CO_2 transport.*

Pressure pumping (Massman et al., 1997; Mohr, et al., 2016; Roland et al., 2015), pressure tides (Clements & Wilkening, 1974; Kimball & Lemon, 1970; Le Blancq, 2011) and subterranean ventilation (Kowalski et al., 2008; Sánchez-Cañete et al., 2011; Serrano-Ortiz et al., 2010) are non-diffusive transport processes affected by wind or changes in atmospheric pressure at different temporal scales especially relevant in semi-arid and carbonate ecosystems. These processes, results in a more efficient transport mechanism compared to molecular diffusion alone (Bowling & Massman, 2011; Maier et al., 2012; Roland et al., 2015; Takle et al., 2004) and can dominate the NECB in some Mediterranean ecosystems with annual

contributions higher than 50% coming from soil CO_2 reservoirs (Serrano-Ortiz et al., 2014; López-Ballesteros et al., 2017).

1.6 THE SOIL CO2 RESERVOIR IN A GLOBAL CONTEXT

Soils contain about 1500 Gt of organic carbon (Scharlemann et al. 2014), which is about 1.8 times more carbon than in the atmosphere and $2.3 - 3.3$ times more than what is contained in the terrestrial vegetation of the world (Ciais et al. 2013). Soil CO_2 efflux (or soil respiration) constitutes a significant component of CO_2 ecosystem fluxes (Hanson et al., 2000; Raich & Schlesinger, 1992), especially in semiarid and arid ecosystems where most of the carbon resides belowground (Burke et al., 2008; Eswaran et al. 2000). Annually, 119 GtC is estimated to be emitted from the terrestrial ecosystem to the atmosphere, and about 50% is attributed to soil microbial respiration (Auffret et al. 2016; Shao et al. 2013).

Despite its importance, research on the subterranean CO_2 dynamics are focused on surface soils (Davidson et al., 1998; Drewitt et al., 2002; Janssens et al., 2001; Subke et al., 2003), neglecting the deeper layers (Davidson et al., 2006; Hirano et al., 2003; Hirsch et al., 2004; Maier et al., 2010; Risk, 2002; Tang et al., 2003). Currently, the knowledge about the production and transport of CO_2 within the vadose zone (between the water table and the soil surface) remains very vague even though deep soil layers can contain much more carbon than previously assumed (González-Jaramillo et al; 2016).
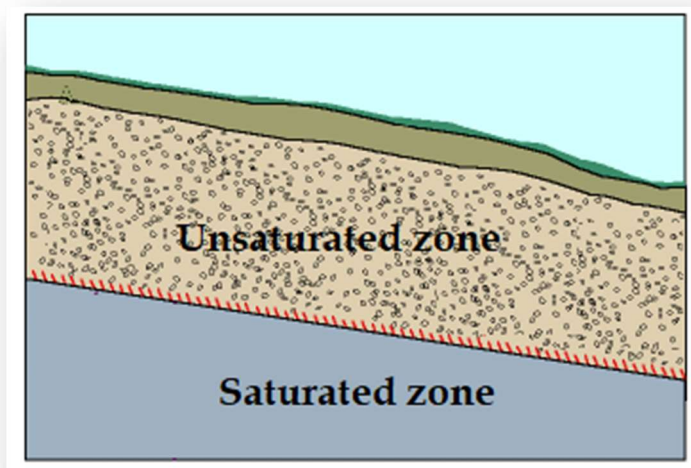
Figure 3. *The CO_2 in soil is storaged and transported mainly in gas form in the vadose zone (unsaturated zone) and dissolve in water in the saturated zone.*

Based on radiocarbon measurements, deep soil organic carbon (SOC) can be very old, with residence times up to several thousand years (Rumpel & Kögel-Knabner 2011) or even several tens of thousands of years (Okuno & Nakamura 2003). Dynamics associated with such deeply buried carbon remain poorly studied, it is widely ignored by the models and is not addressed in most of the ecosystem geochemical studies. Thus, nowadays, the SOC dynamics represents a large source of uncertainties on biogeochemical interactions of soils with atmosphere and climate. One example of this is that the three existing databases (SoilGrids, the Harmonized World Soil Data Base and Northern Circumpolar Soil Database) substantially differ in the estimated size of global SOC stock down to 1 m depth, varying between 2500 Pg to 3400 Pg (Köchy et al. 2015; Tifafi et al. 2018). These values are four to eight times larger than the carbon stock associated with the terrestrial vegetation (Bond-Lamberty et al. 2018).

The deep soil carbon, is assumed to be stable. Unfortunately, recent studies suggest that CO_2 release from deep soils can also be increased by global warming. An increase of 4 °C can increase the annual soil respiration by 34–37% (Hicks Pries et al. 2017). At surface, long-term SOC responses to global warming remain uncertain (Davidson et al. 2006; Dungait et al. 2012; Nishina et al. 2014; Tian et al. 2015).

OBJECTIVES

The main objective of this thesis is to improve the knowledge of subterranean CO_2 dynamics in soil in two semi-arid ecosystems and to study the role of subterranean ventilation at global scale.

In the different chapters, this thesis tries to achieve the main objective by meeting the specific objectives identified for each chapter:

- o To know the role of pressure tides in the CO_2 dynamic in deep soil profiles in two semi-arid ecosystems under study: possible causes, main characteristics and ecosystem functioning (Chapter I).

- o To distinguish which biotic and abiotic processes are the drivers involved in the CO_2 transport and exchange with the atmosphere in shallow and deep profiles in two semi-arid ecosystems (Chapter II).

- o To study the relevance of subterranean ventilation events at global scale (Chapter III).

MATERIAL AND METHODS

2.1 EXPERIMENTAL SITES DESCRIPTION

The study area of this thesis is located in the southeast of Spain, which represents the driest part of Europe. The two experimental sites studied, Balsa Blanca and Amoladeras, are located within the Cabo de Gata-Níjar Natural Park (Almería). The experimental sites are two neighbouring semi-arid grassland sites similar in terms of climate, geology, topography and vegetation: (1) Balsa Blanca (N36º56'26.8" W2º01'58.8″; hereinafter BB), and (2) Amoladeras (N36º50'5" W2º15'1″; hereinafter AM). They are located 23 km apart from each other at an altitude of 65 m (AM) and 208 m (BB) above the sea level. A summary table of this section is available in Chapter I.
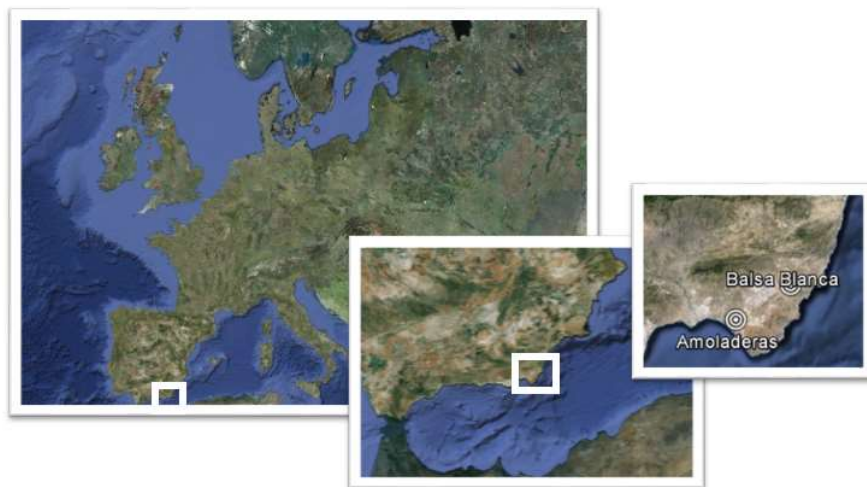
Figure 4. *Location of the study area.*

2.1.1 CLIMATOLOGY AND VEGETATION

The area is classified as a hot arid desert according to Köppen classification (BWh; Rubel & Kottek, 2010). The climate is characterized by

a mean annual precipitation of 220 mm and a mean annual temperature of 18 °C (Figure 1). Climatic conditions are also characterized by a long dry season, which begins in June and ends abruptly in September–October with rain pulse events (López-Ballesteros et al., 2016) when the temperature starts to rise and water resources have not yet become scarce (Serrano-Ortiz et al., 2014).
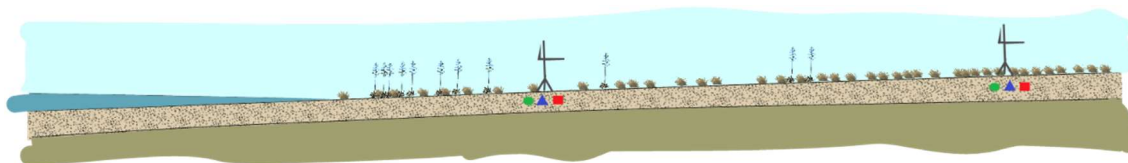
Figure 5. Scheme of Amoladeras (left) and Balsa Blanca (right).

Vegetation is dominated by Machrocloa tenacissima and other drought-tolerant plant species. The rest of vegetation is composed of *Thymus hyemalis* Lange, *Helianthemum almeriense, Sideritis pusilla* (Lange) Pau, *Hammada articulata, Lygeum spartum* L., *Salsola genistoides* Juss. ex Poir., and *Launaea lanifera* Pau in AM and *Chamaerops humilis, Rhamnus lycoides, and Pistacia lentiscus* in BB.

Figure 6. *Amoladeras experimental site during dry season (left) and growing season (right).*

Figure 7. *Balsa Blanca experimental site during dry season (left) and growing season (right).*

2.1.2 GEOLOGY, GEOMORPHOLOGICAL AND SOIL DESCRIPTION

At our experimental sites, geological materials consist of a quaternary conglomerates and Neogene-Quaternary sediments cemented by lime (caliche). The limestone crust is located on a glacis. The glacis in AM has pinkish silts and quartz boulders from the Upper Pleistocene; while in BB it is a calcareous crust "dalle" low detritic from the Lower Pleistocene (MAGNA, 2010). BB is located close to large active tectonic fault system, the Carboneras fault (Reicherter & Reiss, 2001), belonging to the geothermal-volcanic basin of Almería-Níjar (Sanz de Galdeano et al., 1985). The proximity to this experimental site to a fault system has been related to a natural degassing of CO_2 of geological origin in Rey et al., (2012).

Both sites are located geomorphogically on a flat alluvial fan of gentle slopes (2–6%) with petrocalcic horizons (i.e., caliche). Petrocalcic horizons are characterized by bulk densities ranging between 1.6 and 2.3 g cm^{-3} and porosities ranging between 16 and 40% (Duniway et al., 2007; Zamanian et

al., 2016). The characteristics of these materials depend on origin, formation processes and morphology of pedogenic carbonates (Zamanian et al., 2016) producing discontinuities through the vertical layers that are unknown in our experimental sites. The water table is at 50 m depth approximately (Junta de Andalucía, 2013). This fact serves to give an idea about the deep of the vadose zone in the experimental sites.

The dominant soils are classified as Lithic Leptosols (WRB, 2015); they are shallow (10 − 20 cm) and alkaline (pH 8.4 (AM), 7.9 (BB)), with sandy loam texture class and carbonate saturated. In the surface soil horizon, bulk density is lower (1.18 (AM), 1.22 g cm^{-3} (BB)) and porosity is much higher (55.47 (AM), 53.96% (BB)). The soil organic carbon content is 1.24 (AM) and 4.64 kg m^{-2} (BB). The relict degradation level is higher in AM (López-Ballesteros et al., 2018; Rey et al., 2011) due to grazing (Alados et al., 2004).

The vegetation cover varying between 23 (AM) and 63% (BB) of the ground surface. In the soil surface there are patches of bare soil, sections with biological soil crusts, and exposed gravel and rock outcrops.

Figure 8. Aspect of soil texture in Balsa Blanca (left) and caliche horizon in Amoladeras (right).

2.2 APPLIED METODOLOGIES

In this thesis, it is possible to differentiate between the methodologies used to obtain atmospheric data and the methodologies used to obtain data from the vadose zone. For atmospheric data different tasks were performed as data acquisition, instrumentation calibration and preliminary data processing for AM and BB experimental sites. In relation with the vadose zone data, task as data acquisition, instrumentation calibration, data processing, soil CO_2 flux campaigns and gap filling for AM and BB experimental sites were done.

A summary table of the instrumentation used in this thesis is shown in the Table 1.

Table 1. *Sensors and variables used in this thesis in Amoladeras (AM) and Balsa Blanca (BB) experimental sites.*

VARIABLE	SENSOR	SENSOR HEIGHT
Eddy Covariance System (10Hz)		
Wind speed (3-D) and sonic temperature	Three-axis sonic anemometer (CSAT-3, Campbell Scientific, Logan, UT, USA)	3.05 m (AM) 2.90 m (BB)
CO_2 and H_2O vapour densities	Open-path infrared gas analyzer (Li-Cor 7500, Lincoln, NE, USA)	3.05 m (AM) 2.90 m (BB)
Meteorological Measurements (10 Hz)		
Pressure	Open-path infrared gas analyzer (Li-Cor 7500, Lincoln, NE, USA)	3.05 m (AM) 2.90 m (BB)
Photosynthetic Photon Flux Density	PAR sensor (Li-190, Li-Cor, Lincoln, NE, USA)	1.40 m (AM) 1.50 m (BB)
Net Radiation	Net radiometer (NR Lite, Kipp&Zonen, Delft, Netherlands)	1.70 m (AM) 1.50 m (BB)
Air temperature	Thermohygrometer (HMP35-C, Campbell Scientific, Logan, UT, USA)	3.65 m (AM) 1.50 m (BB)
Air humidity	Thermohygrometer (HMP35-C, Campbell Scientific, Logan, UT, USA)	3.65 m (AM) 1.50 m (BB)
Soil heat flux	Heat flux plate (HFP01SC, Hukseflux, Delf, Netherlands)	-0.08 m
Rainfall	A tipping bucket (0.2 mm) rain gauge (785 M, Davis Instruments Corp., Hayward, CA, USA)	1.30 m (AM) 1.40 m (BB)
Subsoil Measurements (30 sec)		
Subsoil CO_2 molar fraction	CO_2 sensor (GMM222, Vaisala, Inc., Finland)	-0.05 m
Subsoil CO_2 molar fraction	CO_2 sensor (GMP-343, Vaisala, Inc., Finland)	-0.15 m, -0.5 m, -1.5 m
Soil temperature	Thermistor (107, Campbell Scientific, Logan, UT, USA)	-0.05 m, -0.15 m, -0.5 m, -1.5 m
Soil water content	Water content reflectometer (CS616, Campbell Scientific, Logan, UT, USA)	-0.05 m, -0.15 m, -0.5 m, -1.5 m
Datalogger system		
EC and meteorological measurements	Datalogger (CR3000 and CR10X, Campbell Scientific, Logan, UT, USA; hereafter, Campbell Scientific, Logan, UT, USA)	Stored as 30 min averages
Subsoil measurents	Datalogger (CR23X, CR1000, CR3000, Campbell Scientific, Logan, UT, USA; hereafter, Campbell Scientific, Logan, UT, USA)	Stored as 30 min averages

2.2.1 THEORY RELATED WITH ATMOSPHERIC DATA ADQUISITION: THE EDDY COVARIANCE TECHNIQUE

The boundary layer is the part of the troposphere that is directly influenced by the presence of the earth's surface, and responds to surface forcing with a timescale of about an hour or less (Stull, 1988). The boundary layer thickness is quite variable in time and space, ranging from hundreds of meters to a few kilometers in a day. Here, turbulent processes are mainly produced by the daily change of temperature in the ground that warms and cools in response to the soil radiation surface. This turbulence produced transport processes of momentum, mass and energy that can be visualized as a set of irregular swirls of motion called eddies (Arya, 1988). Each eddy has 3-D components, including vertical movement of the air. Mathematically such vertical flux can be represented as a covariance between measurements of vertical velocity, the upward and downward movements, and the concentration of the entity of interest. Such measurements require very sophisticated instrumentation.

The eddy covariance (EC) technique is a micrometeorological technique able to measure the covariance of vertical eddies to get wind velocities and scalars such as CO_2, water vapour and temperature (Hutley et al., 2005). Fluxes measured with EC systems are representative of the canopy exchanges in concentration, density or temperature, integrated in the ecosystem (the footprint area ranges from hundreds of hectares to many square kilometers). This technique needs high-resolution temporal sampling (<10 Hz) to capture the turbulent upward and downward movements of eddies produced between the canopy and the lower atmosphere because turbulent fluctuations happen very quickly. Overall, the general physical principle for eddy flux measurement is to measure how

many molecules are moving upward and downward over time, and how fast they travel (Burba, 2013).
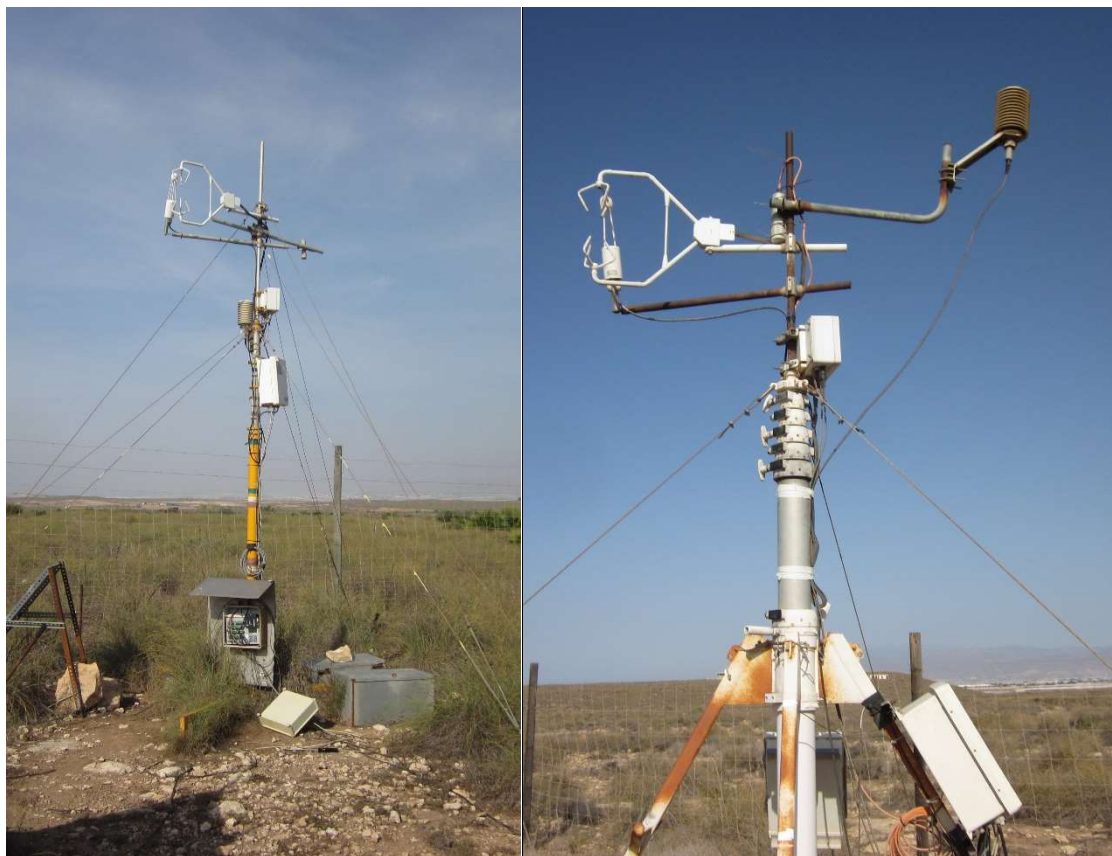
Figure 9. *Eddy covariance stations of Balsa Blanca (right) and Amoladeras (left) experimental sites.*

The EC technique is currently the standard method used in the regional and global networks used in this thesis. The fundamental instrumentation of an EC station is composed by two fast-response sensors that allow the measurement of turbulent fluxes. On one hand, the infrared gas analyzer (IRGA) measures the trace gas (in our case CO_2) and water vapor densities and its functioning is based on Beer-Lambert law. On the other hand, the sonic anemometer measures the 3-D wind speed and the speed of sound, from which sonic temperature is derived. Additionally, other standard meteorological measurements as photosynthetically active

radiation (PAR), net radiation, vapor pressure deficit (VPD), temperature and relative humidity, atmospheric pressure, rainfall, soil heat flux and soil water content were also measured in order to get comprehensive datasets describing biotic fluxes and their abiotic determinants in the ecosystem under study.

2.2.2 ATMOSPHERIC EXPERIMENTAL DESIGN

Two eddy covariance (EC) monitoring stations were installed in AM and BB in July 2007 and June 2006, respectively. The characteristics of both locations are ideal to feasibly use the EC technique, since both areas are quite flat and the surface is very homogeneous. Together with other instrumentation, they were used for meteorological measurements of densities of CO_2 and water vapor as well as atmospheric pressure (IRGA Li-Cor 7500, Lincoln, NE, USA), wind speed and sonic temperature (CSAT-3, Campbell Scientific, Logan, UT, USA), net radiation (NR Lite, Kipp&Zonen, Delft, Netherlands), air temperature and air relative humidity (HMP35-C, Campbell Scientific, Logan, UT, USA) and rainfall (745 M, Davis Instruments Corp., Hayward, CA, USA). The friction velocity (u_*) was determined as the turbulent velocity scale resulting from square root of the (density-normalized) momentum flux magnitude (Stull, 1988).

Data acquire for AM and BB are freely available to the FLUXNET community in http://www.europe-fluxdata.eu/. Sites codes for them in this database are "ES-Amo" and "ES-Agu", for AM and BB respectively.

2.2.3 CALIBRATION AND DATA ADQUISITION IN ATMOSPHERE

Meteorological data were recorded as 30 min averages by data loggers (CR3000 and CR10X, Campbell Scientific, Logan, UT, USA). Power of installation was supply with solar panels (~570 Wp) and batteries (~680 Ah). Missing data for all meteorological variables in both sites corresponded to <10% over the entire period. PC400 or Loggernet are the software used to set up, configure, and retrieve data from EC dataloggers. EddyPro® software (version 5.2.1; LI-COR, Inc. 2014) was used for postprocessing steps.

Figure 10. *Some tasks of atmospheric and soil data maintenance.*

IRGAs were calibrated using a N_2 standard for zero and a standard gas for span (508 μmolCO$_2$ mol^{-1}) gas each six months. Considering the CO_2 deviation (around 5 μmolCO$_2$ mol^{-1}) between calibrations this frequency of

action was suitably for a correct maintenance. The internal chemicals (Ascarite II and magnesium perchlorate) were changed annually as the manual suggest.

2.2.4 THEORY RELATED WITH SUBSOIL DATA ADQUISITION: THE IDEAL GAS LOW AND CO2 MEASUREMENTS

2.2.4.1 HOW CO2 SESONRS WORK

Each gas has an unique infrared (IR) absorption spectrum able to be detectable using IR techniques. In the case of CO_2, there are 3 main bands of IR absorption at wavelengths 2, 2.7, 4.3 and 15 ηm. Both IRGAs and soil CO_2 sensor, used this principle to measure the gas density and transform to volumetric concentration of CO_2 in air. The key components of an IR CO_2 detector are a light source, a measurement chamber, an interference filter (interferometer) and an IR detector. That is how they work: 1) the instrument produces an IR radiation directed from the light source to the measured gas; 2) the filter prevents the wavelets other than the specific gas measured. When the passband of the interferometer coincides with the absorption wavelength of the CO_2 gas; 3) the IR detector sees a decrease in the light transmission. This change in the light intensity detected is converted to a CO_2 density value calculating the ratio between this signal and a reference band (that has no absorption lines). Later, knowing the ambient pressure and temperature can be obtained the CO_2 molar fraction by application of the ideal gas law.

2.2.4.2 THE IDEAL GAS LAW

The ideal gas theory (1) is used to estimate the effect of temperature and pressure changes on CO_2 density (ρ).

$$\rho = \frac{P}{R\,T} \qquad \text{(eq.1)}$$

where (P) is the ambient pressure, (T) is the ambient temperature, and (R) is the universal gas constant (8.3145 J mol^{-1} K^{-1})

If the infrared gas analyzer (IRGA) and soil CO_2 sensor not corrected the CO_2 molar fraction (χ_c) for changes in temperature and pressure, it takes a pressure and temperature constant; so we will have to correct the χ_c by the effect of temperature and pressure changes using this equation:

$$\chi_c = \chi_c{'}\frac{P_{cte}}{P}\frac{T}{T_{cte}} \qquad \text{(eq. 2)}$$

where χ_c is the the CO_2 molar fraction (μmol/mol) corrected by temperature (T, kelvin) and pressure (P, kPa), $\chi_c{'}$ is the CO_2 molar fraction (μmol/mol) measured without correction by T and P. The subscript "cte" is the value of reference used by the IRGA for T (Kelvin) and P (kPa).

2.2.5 SHALLOW SOIL CO2 PROFILE

Shallower sensors were installed at 0.05 m in June 2011 in BB and in June 2012 in AM. The CO_2 sensors were installed vertically with a soil adapter (GMM-222, Vaisala, Inc., Finland) to avoid water entering. Soil moistures were monitored using water content reflectometer (TDR, CS616, Campbell Scientific, Logan, UT, USA). Subsurface temperatures were monitored using thermistors (107, Campbell Scientific, Logan, UT, USA).

Figure 11. *Shallow CO_2 and temperature sensors. Photos from Amoladeras experimental site.*

2.2.6 DEEP SOIL CO2 PROFILE

Vertical profiles were installed in January 2010 in BB and in July 2013 in AM. Boreholes were done with an excavator and the extracted material was used for refilling. A stabilization period of 6 months after the installation of the vertical profile in AM (July 2013) was needed to get reliable data. The stabilization period was selected after comparing CO_2 dynamics in both vertical profiles. Vertical profiles measured soil CO_2 molar fractions (infra-red sensor GMP-343, Vaisala, Inc., Finland), soil temperatures (107 thermistors, Campbell Scientific, Logan, UT, USA) and volumetric soil water content (TDR, CS616, Campbell Scientific, Logan, UT, USA). Sensors were installed horizontally in undisturbed media at three different depths: 0.15 m soil horizons (belonging to edaphic media), and 0.50 m and 1.50 m layers (belonging to underlying media) below the surface. Soil adapters for horizontal positioning made of a PTFE filter were installed with the soil CO_2 sensor (215519, Vaisala, Inc., Finland) for water

protection. During this thesis we have differentiated two levels in the deep soil CO_2 vertical profile: subsurface layer (0.15 m sensors) and deep layer (0.5 m and 1.5 m sensors).

Figure 12. *CO_2, temperature and soil water content sensors at 1.50 m (left) and 0.15 m (right) before refill the boreholes during deep profile installation. Photos from in Balsa Blanca experimental site.*

2.2.7 CALIBRATION AND DATA ADQUISITION IN SOIL

The CO_2 sensors were configured to measure the CO_2 molar fractions at a temperature of 25 °C and 1013 hPa, and during the post-processing they were corrected for variations in temperature and pressure. Data were recorded every 30 s and stored as 30 min averages in a data-logger (CR23X, CR3000 and CR1000, Campbell Scientific, Logan, UT, USA). Power of installation was supply with solar panels (~570 Wp) and batteries (~680 Ah). For the deep profile, missing data vary $3 - 6\%$ over the entire period $(2014 - 2016)$ except in AM for χ_c at 1.50 m (22%), and in BB for soil temperature at 1.50 m (48%) and χ_c at 0.50 m (50%) due to instrument malfunction. Missing data for all shallow variables in both sites corresponded to $<15\%$ in AM and $<20\%$ in BB for the entire period except

in BB for volumetric water content at 0.05 m (46%) due to instrument malfunction during the last months. PC400 was the software used to set up, configure, and retrieve data from soil dataloggers.
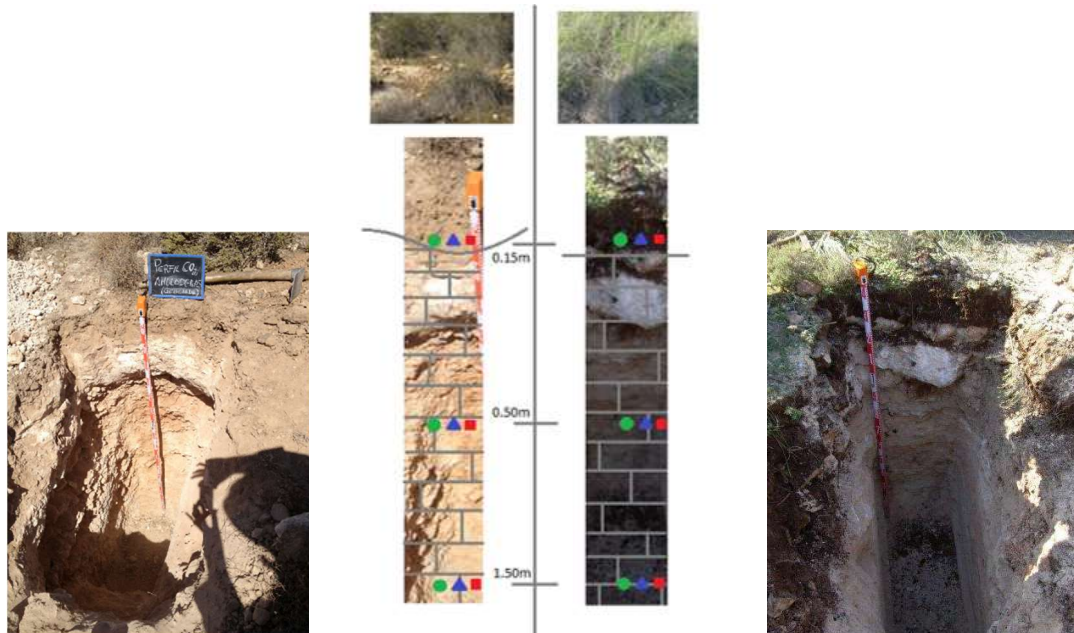
Figure 13. Differences between vertical profiles in Amoladeras (left) and BB (right) experimental sites.

Although soil CO_2 sensors were inherently stable, the superficial sensors were calibrated annually using a CO_2 calibrator (GMK220, Vaisala, Inc., Finland). The to two-point calibration was performed using two reference gases, a low standard gas (508 $\mu molCO_2$ mol^{-1}) and a high standard gas (1989 $\mu molCO_2$ mol^{-1}). The calibrations were performed indicating the air temperature and the air pressure in real time. Unluckily the calibration of the CO_2 sensors situated in the deep profile was impossible without disturb the vertical soil profile.

2.2.8 THE GRADIENT METHOD TO ESTIMATE SOIL CO2 FLUX

Recently, the gradient method has become popular to study the CO_2 transport within the soil and between the soil and the atmosphere (Maier & Schack-Kirchner, 2014; Sanchez-Cañete & Kowalski, 2014). The CO_2 produced in the soil is transported between the soil layers and from the soil to the atmosphere mainly by diffusion. The CO_2 efflux can be determined from concentration gradients in the soil layers and between the soil and the atmosphere. This gradient method is especially suitable for studying the vertical distribution of CO_2 production in the soil and for studying the processes affecting the CO_2 efflux. The diffusivity of CO_2 in the soil depends on total soil porosity, soil tortuosity, soil water content and transport distance. The gradient method was used in our experimental sites to determine the soil CO_2 efflux.

Soil CO_2 efflux for the shallow profile (0.05 m) was calculated assuming that all transport is due to diffusion as:

$$F_s = -k_s \rho_a \frac{d\chi_c}{dz} \qquad \text{(eq. 3)}$$

where F_s is the upward gas flux (µmol CO2 m^{-2} s^{-1}), k_s is the soil CO_2 transfer coefficient (m^2 s^{-1}), ρ_a the mean air molar density (µmol m^{-3}) and $d\chi_c/dz$ is the vertical CO_2 molar fraction gradient (ppm m^{-1}). The CO_2 gradient was calculated using the difference between the mean atmospheric CO_2 molar fraction and the value of the soil CO_2 sensors at 0.05 m depth. The CO_2 molar fraction was corrected for variations in temperature and pressure. The air density (ρ_a) was obtained from the ideal gas law. The empirical k_s is equal to the soil CO_2 diffusion coefficient in absence of production/consumption processes in the monitored layer. It depends not only on diffusion but also can vary with production/consumption processes

in the layer (Sánchez-Cañete et al., 2017), in our case from 0 to 5 cm. The transfer coefficient k_s is obtained from the flux-gradient relationship proposed by Roland et al., (2015):

$$k_s = \frac{F_{chamb}}{\rho_a} \frac{d_z}{d_{\chi c}} \qquad \text{(eq. 4)}$$

where in our study F_{chamb} was measured by a portable soil CO_2 flux chamber (EGM-4; PP-systems, Hitchin, UK) during 14 campaigns in BB and 11 campaigns in AM at differing values of soil water content. These measurements were performed between November 2013 and May 2014 in BB and from April 2016 to October 2016 in AM. F_{chamb} measurements were always performed between 8:00 and 10:00 (solar time) in AM and between 11:00 and 16:00 in BB. For each measurement of soil CO_2 effluxes (F_s), the soil chamber was placed on a PVC collar (5 cm height, 10.5 cm diameter) previously inserted in the soil, leaving $2 - 3$ cm above ground. The chamber system was configured to store temperature, relative humidity, CO_2, and pressure every 3 s during 120 s. The F_s were estimated from the initial slopes of CO_2 molar fractions of the confined air versus time, by using either linear or quadratic regression (Kutzbach et al., 2007; Pérez-Priego et al., 2010; Wagner et al., 1997) for the best regression fit. The raw values of CO_2 molar fraction were previously corrected for dilution (Hubb, 2012) from CO_2 molar fractions referred to wet air. Finally, the flux density was calculated using the ideal gas equation as explained by Pérez-Priego et al. (2015). The chamber fluxes were estimated as:

$$F_{chamb} = \frac{d\chi_c}{d_t} \frac{V}{S} \frac{P_0 (1-w_0)}{R T_0} \qquad \text{(eq. 5)}$$

Figure 14. *Soil CO₂ efflux campaign using a portable chamber in Amoladeras experimental site.*

where F_{chamb} is the soil CO_2 efflux (µmol m^{-2} s^{-1}) derived from the chamber system, $d\chi_c/d_t$ is the initial rate of change in CO_2 molar fraction referenced to dry air (µmol mol^{-1} s^{-1}), V is the total volume (chamber+collar, m³), S is the projected surface area (m²), P_0 is the initial atmospheric pressure (Pa), w_0 is the initial water vapor mole fraction (mol mol^{-1}), R is the universal gas constant (8.314, m³ Pa K^{-1} mol^{-1}), and T_0 is the initial air temperature (K). Therefore, knowing $F_{chamber}$ and applying equation (2), we obtain the soil CO_2 transfer coefficient (k_s). To model k_s, it was fit using a power function against soil tortuosity (ξ):

$$\frac{k_s}{D_a} = a\, \xi^{\, b} \qquad \text{(eq. 6)}$$

where D_a is the diffusion coefficient of the CO_2 in free air, calculated according to Jones (1992), and ξ is obtained as the soil porosity (φ, cm³ cm⁻³) minus the soil water content (θ, cm³ cm⁻³) and the coefficients a and b were obtained by least squares regression. Finally, we used our calculated soil CO_2 transfer coefficient (k_s) to estimate soil CO_2 fluxes during whole the period using the equation (3).

2.2.9 TIME SERIES ANALYSIS: THE ANALYSIS OF TIME SERIES IN THE FREQUENCY DOMAIN

In biogeosciences environmental time series are non-stationary signals that can switch between different patterns by small environmental changes. For this kind of data the wavelet analysis is a powerful tool used for the characterization of time series and the analysis of their possible association with other environmental signals through the decomposition of the signal (Torrence & Campo, 1998). During my research stay in the *University of Delaware*, I could learn the basics of this analysis that are applied in Chapter I and II. In order to approach the reader to a better understanding of the technique, a brief of theory is explained below.

The wavelet analysis let us to examine one time series in the time and frequency domain for visual interpretation or two time series together that may be expected to be linked in some way (Cazelles et al., 2008; Govindan et al., 2005 Grinsted et al., 2004; Torrence & Compo, 1998). The signal (the time series) is decomposed into harmonic components based on Fourier analysis. This can be regarded as a partition of the variance of the series into its different oscillating components with different frequencies (periods). Peaks in the periodogram (an estimate of the spectral density of a signal) or in the spectrum indicate which frequencies are contributing the

most to the variance of the series. In this manner, periodicities, if present, are detected (Chatfield, 1989).

The wavelet transform overcome the limitations of Fourier transform and is used to analize the time series at different frequencies (Daubechies, 1992). It decomposes signals over dilated and translated functions called "mother wavelets" $\phi(t)$ that can be expressed as the function of two parameters, one for the time position (τ), and the other for the scale of the wavelets (α). The wavelet transform can be thought as a cross-correlation of a signal $x(t)$ with a set of wavelets of various "scales" α, at different time positions τ (Cazelles et al., 2006). The mother wavelets, are grouped into different types of wavelet families with different properties. Morlet mother wavelets provide a good balance between time and frequency space and are used to find temporal periodicities (Grinsted et al., 2004) and are used in this thesis.

Using the discrete wavelet transform (DWT, not used in this thesis) or the continuous wavelet transform (CWT, used in Chapter II) we can describe the temporal variability of a signal and track how the different scales related to the periodic components of the signal change over time, i.e. to filter data series in high-frequency events or low-frequency events. By other side, cross wavelet transform (XWT, not used here) and wavelet coherency analysis (WCA, used in Chapter I and II) generalize these methods, allowing the analyses of dependencies between two signals. The XWT reveals areas with high common power while the WCA localized correlation coefficient in time frequency space (Grinsted et al., 2004). Thus, WCA ranges between 0 and 1, where 1 indicates the highest temporal correlation and 0 no correlation between variables. The statistical significance level in the WCA is estimated using Monte Carlo methods with 10.000 iterations. The filtering of any finite-length signal through the wavelet functions produces some edge effects, which reduce the reliability

region of the wavelet results. This area is delimited in the wavelet power spectrum as curved lines in "the cone of influence". In addition, arrows show in the power spectrum or calculated as angles outline the phase-locked angle relationship between both time series (Govindan et al., 2005; Grinsted et al., 2004).

RESULTS

This section is divided in three different chapters estructurated as a scientific journal format. Introduction and Material and Methods of each chapter include the specific information refereed in the "Introduction" and "Material and Methods" sections of this thesis.

CHAPTER 1. CO2 DYNAMICS ARE STRONGLY INFLUENCED BY LOW FREQUENCY ATMOSPHERIC PRESSURE CHANGES IN SEMIARID GRASSLANDS

ABSTRACT

Due to their large carbon storage capacity and ability to exchange subterranean CO_2 with the atmosphere, soils are key components in the carbon balance in semi-arid ecosystems. Most studies have focused on shallow (e.g., <30 cm depth) soil CO_2 dynamics neglecting processes in deeper soil layers where highly CO_2-enriched air can be stored or transported through soil pores and fissures. Here, we examine the relationship among variations in subterranean CO_2 molar fraction, volumetric water content, soil temperature and atmospheric pressure during three years within soil profiles (0.15, 0.50, and 1.50 m depths) in two semi-arid grasslands located in southeastern Spain. We applied a wavelet coherence analysis to study the temporal variability and temporal correlation between the CO_2 molar fraction and its covariates (soil temperature, soil moisture and atmospheric pressure). Our results show that CO_2 dynamics are strongly influenced by changes in atmospheric pressure from semidiurnal, diurnal and synoptic to monthly time-scales for all soil depths. In contrast, only weak daily dependencies were found at the surface level (0.15 m) regarding soil temperature and volumetric water content. Atmospheric pressure changes substantially influence variations in the CO_2 content (with daily fluctuations of up to 2000 ppm) denoting transportation through soil layers. These results provide insights into the importance of subterranean storage and non-diffusive gas transport that could influence soil CO_2 efflux rates, processes that are not considered when applying the flux-gradient approach and, which can be especially important in ecosystems with high air permeability between the unsaturated porous media and the atmosphere.

1. INTRODUCTION

Semi-arid ecosystems occupy approximately ~40% of the terrestrial surface and are home to more than 38% of the total global population (Reynolds et al., 2007), but they are under-represented in ecological research networks (Reichstein et al., 2013; Schimel, 2010; Villarreal et al., 2018). In these ecosystems, soils play a key role in the uptake and emissions of the main greenhouse gases (Ahlström et al., 2015; Poulter et al., 2014). Unfortunately, most studies have focused on shallow soil CO_2 dynamics (<30 cm depth) neglecting what occurs in deeper soil layers. The vadose zone may contain large amounts of CO_2-enriched air in pores, cracks and fissures with concentrations higher than 5% by volume in the first tens of meters (Benavente et al., 2010; Denis et al., 2005). Soil CO_2 content is characterized by a vertical profile of concentration increasing with depth, which is affected by the transport of dissolved atmospheric and soil CO_2 in waters and gravitational percolation (Baldini et al., 2006; Sánchez-Cañete et al., 2013b) where deeper soil layers can reach *c.a.* 100 times more CO_2 content than shallower layers (Buyanovsky & Wagner, 1983). This CO_2-enriched air stored in the soil pores shows clear seasonal and daily patterns of variation driven by a set of biological, physical and chemical processes that are involved in CO_2 production and transport that ultimately influence soil CO_2 efflux rates to the atmosphere.

The diffusion process, driven by a gradient of molar fraction, is considered the main mechanism of gas exchange between the atmosphere and vadose zone (including shallow horizon and deep soil layers; Rolston & Moldrup, 2012). Advective gas transport, driven by bulk flow acting on a concentration gradient, can also strongly affect soil gas migration (Corey et al., 2010; Garcia-Anton et al., 2014). Both transport processes are highly

interconnected. Diffusion is a slow transport process modelled by Fick's first law (only dependent on soil CO_2 production and diffusivity; Maier & Schack-Kirchner, 2014), while bulk flow is typically modelled using Darcy's law (Webb, 2006). Non-diffusive transport processes are usually not considered in the flux model calculations (Maier et al., 2010; Webb & Pruess, 2003). Although its effect is limited in time (Maier et al., 2010), non-diffusive transport can also participate, increasing the gas exchange rates, which results in a more efficient transport mechanism compared to molecular diffusion alone (Bowling & Massman, 2011; Maier et al., 2012; Roland et al., 2015; Takle et al., 2004).

Non-diffusive and diffusive transport processes can be affected by several biotic and abiotic factors, such as volumetric water content (Martinez & Nilson, 1999), soil temperature (Roland et al., 2015), gas content (Elberling et al., 1998), soil texture (Kimball & Lemon, 1971), soil porosity (Nilson et al., 1991; Takle et al., 2004), wind (Bowling & Massman, 2011; Kowalski et al., 2008; Sanchez-Cañete et al., 2011), water table fluctuations (Jiao & Li, 2004; Maier et al., 2010) or atmospheric pressure. The movement of CO_2-enriched air driven by pressure changes is also known as pressure pumping. The potential relevance of non-diffusive transport caused by pressure pumping has been mostly addressed at short time-scales (<1 s; Kimball & Lemon, 1970; Massman et al., 1997; Mohr et al., 2016; Takle et al., 2004), although it also has been studied at half-hourly and longer temporal scales (Bowling & Massman, 2011; Clements & Wilkening, 1974; Elberling et al., 1998; Sánchez-Cañete et al., 2013a). To a lesser extent, pressure oscillations produced at low frequency scales have also been termed as atmospheric or pressure tides (Kuang et al., 2013; Le Blancq, 2011; Lindzen, 1979; Massmann & Farrier, 1992). Through this pressure fluctuation, the direction and magnitude of soil gas efflux can be altered substantially (Bowling & Massman, 2011; Takle et al., 2004). This

phenomenon can be more relevant in carbonated ecosystems, where the presence of fissures and cavities increases the degree of permeability between deeper layers and the soil surface (Cuezva et al., 2011; Serrano-Ortiz et al., 2010), increasing pressure pumping and pressure tides effects.

This chapter focuses on how CO_2 dynamics in the vadose zone is affected by changes in environmental and subterranean conditions by comparing two nearby semi-arid grassland sites. For that, we used a 3-year (2014-2016) record of edaphic (soil profile at 0.15 m, 0.50 m and 1.50 m) and environmental variables. We hypothesize that due to the scarce vegetation and impoverished soils (Lithic Leptosols with thin soil depth and low content in soil organic carbon; WRB, 2015), and the dry conditions of the layers (generally volumetric water content <10%), variations in the vadose zone CO_2 molar fraction will be dominated by abiotic factors. We expect that atmospheric pressure will be the main environmental variable influencing CO_2 dynamics at daily and weekly time-scales because pressure differences in permeable soils could enhances CO_2 transport. A better understanding about the driving factors determining CO_2 dynamics, as well as their temporality, is especially relevant to improve future models related with subterranean CO_2 storage and non-diffusive gas transport in the vadose zone.

2. MATERIAL AND METHODS

2.1 STUDY SITE

The study area is located in Cabo de Gata-Níjar Natural Park, in the province of Almeria in the SE of Spain. We selected two neighbouring semi-arid grassland sites similar in terms of climate, geology, topography and vegetation: (1) Balsa Blanca (N36°56'26.8" W2°01'58.8"; hereinafter BB), and (2) Amoladeras (N36°50'5" W2°15'1"; hereinafter AM). However, the footprint of past degradation, likely due to grazing (Alados et al., 2004), is more evident in Amoladeras (López-Ballesteros et al., 2018; Rey et al., 2011). The area is classified as a hot arid desert according to Köppen classification (BWh; Rubel & Kottek, 2010). The climate is characterized by a mean annual precipitation of 220 mm and a mean annual temperature of 18 °C (Figure 1). Climatic conditions are also characterized by a long dry season, which begins in June and ends abruptly in September-October with rain pulse events (López-Ballesteros et al., 2016). At our experimental sites, geological materials consist of a quaternary conglomerates and Neogene-Quaternary sediments cemented by lime (caliche). The limestone crust is located on a glacis. The glacis in AM has pinkish silts and quartz boulders from the Upper Plesictocene; while in BB it is a calcareous crust "dalle" low detritic from the Lower Pleistocene (MAGNA, 2010). Both sites are located geomorphogically on a flat alluvial fan of gentle slopes (2-6%) with petrocalcic horizons (i.e., caliche). Petrocalcic horizons are characterized by bulk densities ranging between 1.6 and 2.3 g cm⁻³ and porosities ranging between 16 and 40% (Duniway et al., 2007; Zamanian et al., 2016). The characteristics of these materials depend on origin, formation processes and morphology of pedogenic carbonates (Zamanian et al., 2016) producing

discontinuities through the vertical layers that are unknown in our experimental sites. In the surface soil horizon, bulk density is lower (1.18-1.22 g cm^{-3}) and porosity is much higher (55.47-53.96%). The water table is at 50 m depth approximately (Junta de Andalucía, 2013). The dominant soils are classified as Lithic Leptosols (WRB, 2015); they are shallow (10-20 cm) and alkaline (pH 7.9-8.4), with sandy loam texture class and carbonate saturated (Figure 1). Vegetation is dominated by *Machrocloa tenacissima* (previously known as *Stipa tenacissima*) and other drought-tolerant plant species. In the soil surface there are patches of bare soil, sections with biological soil crusts, and exposed gravel and rock outcrops. Absolute pressure in AM (65 m in altitude) is greater than in BB (208 m in altitude) by about 2 kPa (Figure 2). The sites are 23 km apart, and AM is closer to the coast (Figure 1).

2.2 EXPERIMENTAL DESIGN

Vertical profiles were installed in January 2010 in BB and in July 2013 in AM. Boreholes were done with an excavator and the extracted material was used for refilling. The study period covered from January 2014 to December 2016, rejecting a stabilization period of 6 months after the installation of the vertical profile in AM (July 2013). The stabilization period was selected after comparing CO_2 dynamics in both vertical profiles. Vertical profiles measured soil CO_2 molar fractions (χ_c; infra-red sensor GMP-343, Vaisala, Inc., Finland), soil temperatures (T_{soil}; 107 thermistors, Campbell Scientific, Logan, UT, USA) and volumetric soil water content (VWC; TDR, CS616, Campbell Scientific, Logan, UT, USA). Sensors were installed horizontally in undisturbed media at three different depths: 0.15 m soil horizons (belonging to edaphic media), and 0.50 m and 1.50 m layers

(belonging to underlying media) below the surface. Soil adapters for horizontal positioning made of a PTFE filter were installed with the soil CO_2 sensor (215519, Vaisala, Inc., Finland) for water protection. The CO_2 sensors were configured to measure the CO_2 molar fractions at a temperature of 25 °C and 1013 hPa, but during the post-processing measurements were corrected for soil temperature and pressure at the time of measurements. Data were recorded every 30 s and stored as 30 min averages in a datalogger (CR23X and CR1000, Campbell Scientific, Logan, UT, USA; respectively for AM and BB). Missing data vary 3-6% over the entire period (2014-2016) except in AM for χ_c at 1.50 m (22%), and in BB for soil temperature at 1.50 m (48%) and χ_c at 0.50 m (50%) due to instrument malfunction.

At both experimental sites, meteorological measurements of atmospheric pressure (p; open-path infrared gas analyzer Li-Cor 7500, Lincoln, NE, USA), wind speed (CSAT-3, Campbell Scientific, Logan, UT, USA), net radiation (NR Lite, Kipp&Zonen, Delft, Netherlands), air temperature and air relative humidity (HMP35-C, Campbell Scientific, Logan, UT, USA) and rainfall (745M, Davis Instruments Corp., Hayward, CA, USA) were acquired since 2009. Meteorological data were recorded as 30 min averages by a data logger (CR3000, Campbell Scientific, Logan, UT, USA). Missing data for all meteorological variables in both sites corresponded to < 10% over the entire period. For more information about the site and meteorological equipment see López-Ballesteros et al., (2018).

Sea →
Vadose zone →
Saturated zone →
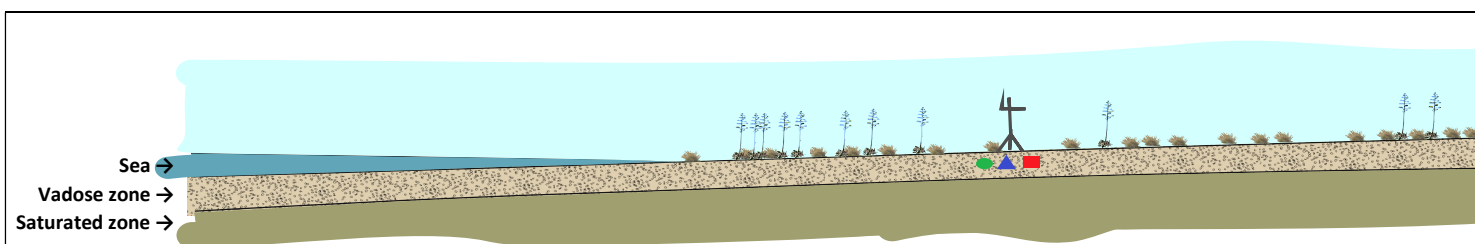
	Amoladeras				
Site characteristics		**Soil depth (m)**	**Morfology of horizons and carbonates content (%)**		
Altitude (m)	65				208
Distance from the sea (m)	3600				6300
Water table depth (m)	50				50
Slope (%)	2-6				2-6
Climate	Cold arid steppe, dry, semi-arid		Ah (11.3)		Cold arid steppe, dry, semi-arid
Mean annual T^re (ºC)	18				18
Annual precipit. (mm)	220	0.15	Petroc. horizon		220
Predominant Sp.	*Machrocloa tenacissima*				*Machrocloa tenacissima*
Relict degradation level	*High*				*Low*
Soil properties			Cmk1 (79.6)		
Vegetation cover (%)	23				63
Biological crust and litter cover (%)	34				26
Bare soil cover (%)	8				1
Gravel and rock cover (%)	35				10
Soil type	Lithic Leptosol (Calcaric)				Mollic Lithic Leptosol (Calcaric)
Maximum soil depth (cm)	15	0.50			20
Soil texture class (%)			2Cmk2 (65)		
Clay	15				16
Silt	27				23
Sand	58				61
Bulk density (g cm^-3)	1.18		3Cmk3 (89.5)		1.22
Porosity (%)	55.47				53.96
pH	8.4				7.9
Soil organic C (kg m^-2)	1.24	1.50			4.64
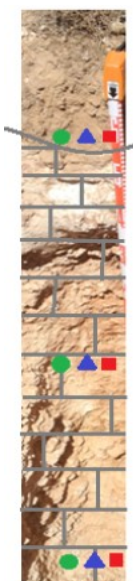
Figure 1. *Description of site and soils characteristics in Amoladeras and Balsa Blanca. The information is coupled with a schematic illustration of our experimental design. Soil molar fraction sensors, soil thermistors and volumetric water content reflectometers are represented as geometric figures. Pedological characteristics (pedogenic maximum depth and petrocalcic horizon) are represented with drawn lines. Morphological horizons are described according to (FAO, 2009). Water table depth is determined from (Junta de Andalucía, 2013).*

2.3 DATA ANALYSIS

Outliers were detected with a 2.5-hour sliding standard deviation window across neighbouring values. Small gaps (less than a week) were filled by estimating extrapolated values from forward and reverse auto-regressive fits of the remaining samples. Gaps of more than a week were filled with a simple regression fit with the same soil depth profile from the other experimental site, (except for CO_2 at 0.50 m in BB where correlation was higher with CO_2 at 1.50 m in AMO, $R^2 > 0.5$). Atmospheric pressure gaps where filled using a simple regression with measurements from the other experimental site ($R^2 > 0.96$). In order to analyse the relationship between differences at 30 min averages in T_{soil} and subsoil χ_c variations, both simple regression and Spearman partial correlation analyses were performed considering the effect of T_{soil} or VWC. In order to study the time series at the seasonal scale, we distinguish in the database between growing or wet (March-April) and dry (July-August) season. The periods selected are periods in which is that "dry" and "wet" conditions occurs in each year analysed.

We used the continuous wavelet transform to describe the temporal variability, explore the spectral properties and investigate the temporal

correlations (Cazelles et al., 2008; Govindan et al., 2005; Grinsted et al., 2004; Torrence & Compo, 1998) between χ_c and p, T_{soil} and VWC during three years. Wavelet coherence analysis (WCA) is useful to identify significant temporal correlations between two time series (Grinsted et al., 2004). We calculated the WCA between χ_c and p and the soil variables (T_{soil} and VWC) with statistical significance ($p < 0.05$) using 1000 Monte Carlo simulations. As a mother function, we used the Morlet wavelet, which is a widely used non-orthogonal wavelet for time and scale resolution (Torrence & Compo, 1998). All time series were analysed using a 1-hour time step. WCA ranges between 0 and 1, where 1 indicates the highest temporal correlation (and 0 for no correlation) between variables. Yellow areas with black contour lines represent a high significant temporal correlation with 5% significance level. In addition, arrows show the phase-locked angle relationship between both time series (Govindan et al., 2005; Grinsted et al., 2004; Xu et al., 2014). The WCA has been previously used for continuous measurements of soil carbon dynamics (Vargas et al., 2012; Vargas et al., 2018; Xu et al., 2014). All data analyses were performed using MATLAB R2017a (MathWorks, Natick, Massachusetts, USA).

3. RESULTS

3.1. ENVIRONMENTAL CONDITIONS

The annual mean air temperature during the study period was 18.5 ± 5.9 °C in AM and 17.7 ± 6.4 °C in BB. The warmest summer and winter were in 2015 and 2016, respectively. Both ecosystems show the same rainfall pattern although BB always had a slightly higher precipitation regime (15%). The driest year was 2014 with 134 mm in AM and 166 mm in BB, with lower precipitation than the typical precipitation regime established in the area (220 mm). In contrast, 2015 and 2016 were rainy years with 201 mm and 264 mm respectively in AM and 237 mm and 284 mm in BB.

Seasonal and annual patterns of atmospheric pressure (*p*), volumetric water content (VWC), soil temperature (T_{soil}) and precipitation are shown for both experimental sites in Figure 2. Fluctuations in *p* were similar in BB and AM. There was a seasonal pattern in the range of variation, with winter months having the highest maximum and minimum values. Regarding T_{soil}, both ecosystems showed similar values. Maxima and minima were reached in the shallower layer (0.15 m) with values ranging between 9 °C and 34 °C in AM, versus 5 °C and 35 °C in BB. With a slight decrease in the amplitude of daily fluctuations in comparison with the shallower layer, T_{soil} was very similar at 0.50 m in both ecosystems. At 1.50 m the lowest range of variation was observed and the maximum and minimum values were reached with a ~20 days delay in relation with the shallowest layer. At this depth maximum T_{soil} was reached in August (~27 °C) while minimum was reached in February (~18 °C). Finally, the annual mean VWC was 7.5 ± 2.6% in AM and 8.7 ± 2.9% in BB with minima around 5-6% in AM and 3-

4% in BB and maxima of 42% in AM and 50% in BB coinciding with local storms. After these storms, the VWC in AM returned rapidly to its base level in comparison with a longer recovery in VWC for BB.
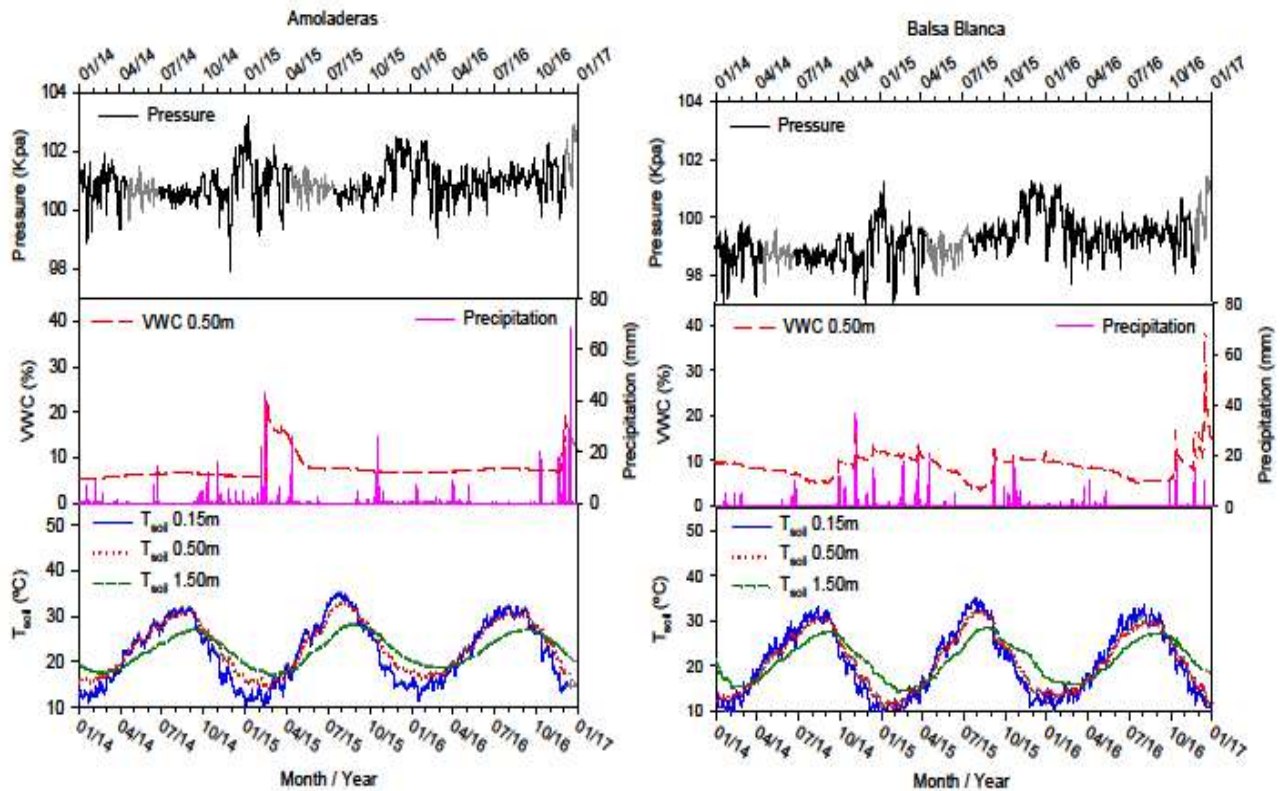
Figure 2. *Daily-averaged values of atmospheric pressure, volumetric water content (VWC) at 0.50 m, soil temperature (T_{soil}) at soil depths of 0.15 m (solid lines), 0.50 m (dotted lines) and 1.50 m (dashed lines); and daily precipitation during the study period (January 2014-December 2016). Shaded lines represent gaps in the time series.*

3.2. DYNAMICS OF SOIL CO2 MOLAR FRACTIONS AT DIFFERENT TEMPORAL SCALES

Soil CO_2 showed a clear vertical profile with higher concentration at depth, and similar means over the three years (Figure 3). The year with the highest χ_c was 2015 (with an annual average across the multiple soil depths of 1558 ± 429 ppm in AM and 1161 ± 329 ppm in BB). The χ_c showed clear annual patterns with maxima in summer and minima in winter. Generally, AM had higher CO_2 concentrations across the multiple soil depths. For example, χ_c at 1.50 m had an annual average of 2029 ± 113 ppm in AM and 1268 ± 154 ppm in BB. AM also showed higher variability, particularly at 0.15 m (Figure 3).

During the whole study period, we detected sub-daily and synoptic patterns in p and χ_c, even during the first precipitation events at the end of the dry season, with inverse correlation between both variables (Table 1; Figure 4). At the synoptic scale (oscillation in p induced by the passage of high and low pressure systems and fronts), p changes lasted from 3 to 8 days approximately. However, at daily scale there were two cycles per day, and the first generally had a lower amplitude than the second. Regarding χ_c, daily fluctuations up to 2000 ppm CO_2 occurred during periods of less than 6 hours (*c.a.* 19 September 2014; Figure 4). At all depths, χ_c was generally higher in AM (Figures 3 and 4). On the other hand, χ_c showed similar values at 0.50 m and 1.50 m in BB (Figure 4), while in AM an increment in χ_c with depth was more evident.
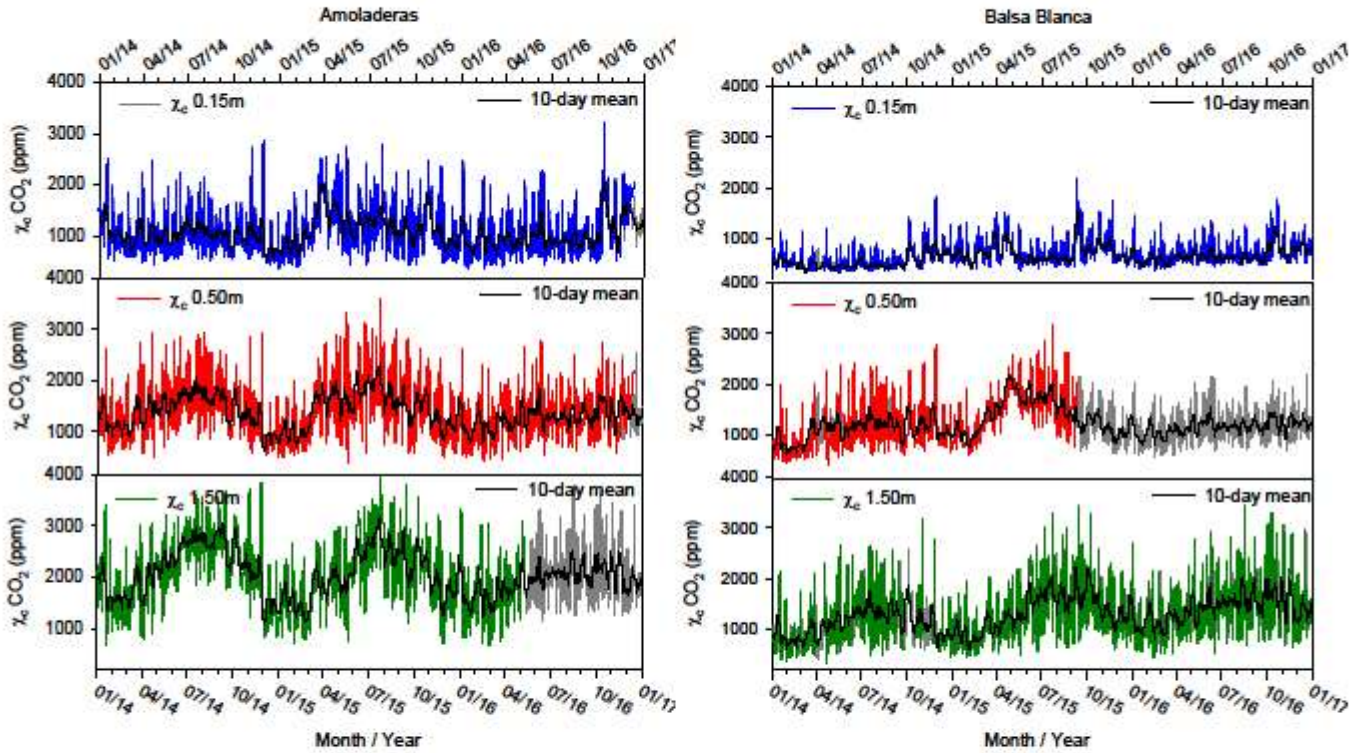
Figure 3. *Daily-averaged (solid lines) and 10-day mean (dotted lines) values of soil CO_2 molar fraction (χ_c) at 0.15 m, 0.50 m and 1.50 m depth during the study period (January 2014-December 2016). Shaded lines represent gaps in the time series.*

3.3. THE EFFECT OF ATMOSPHERIC PRESSURE ON CO2 MOLAR FRACTION FLUCTUATIONS

We found strong significant partial correlations between variations in atmospheric p and variations in χ_c (p<0.01; Table 1). This correlation was not influenced by the indirect effect of T_{soil} or VWC, and was always higher at AM. In general, the degree of correlation increased with depth reaching correlation coefficients of -0.79 in AM for wet season and -0.70 in BB at 1.50 m for dry season. We also found seasonal differences, with more

correlation in the shallower layer (0.15 m) during the dry season in both sites, whereas the growing season presented the highest partial correlation at 1.50 m and 0.50 m in AM. The weakest correlation was found at 0.50 m in BB (-0.28 during the wet season; $p < 0.01$; Table 1).
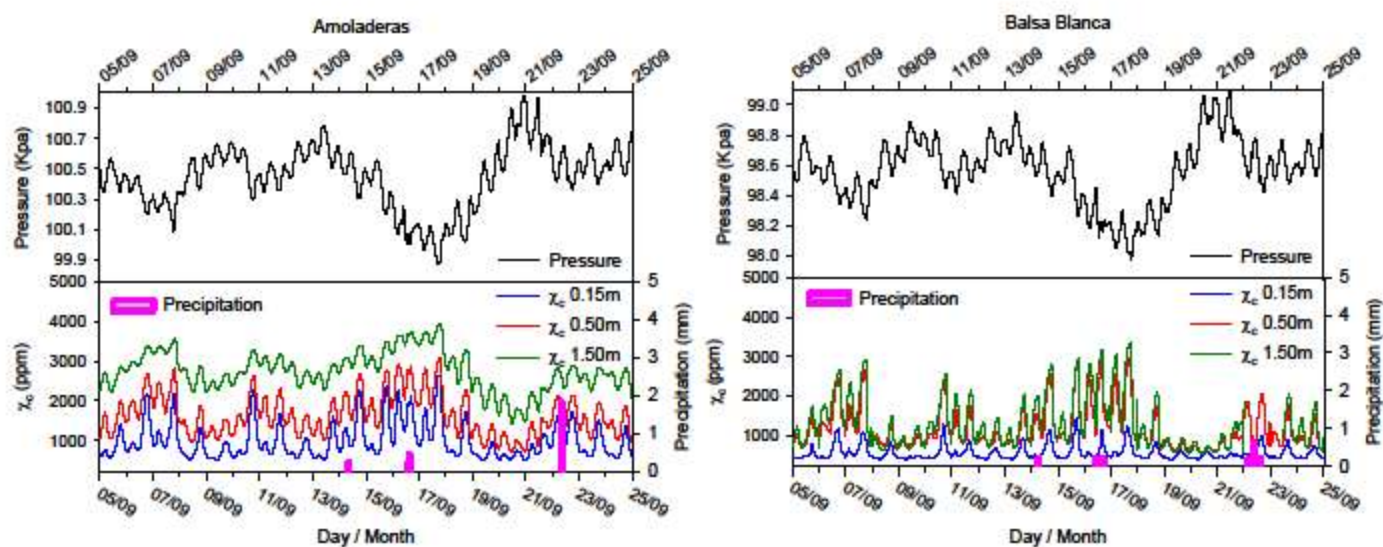
Figure 4. *Average half-hour values of atmospheric pressure and soil CO_2 molar fraction (χ_c) at 0.15 m, 0.50 m and 1.50 m depth during the period 05 -25 September of 2014.*

Amoladeras		Δp	$\Delta p(\Delta T_{soil})$	$\Delta p(\Delta VWC)$	$\Delta p(\Delta T_{soil}, \Delta VWC)$	Balsa Blanca		Δp	
$\Delta \chi_c$ 0.15m	year	-0.59	-0.55	-0.54	-0.54	$\Delta \chi_c$ 0.15m	year	-0.41	
	dry	-0.67	-0.62	-0.66	-0.62		dry	-0.45	
	wet	-0.58	-0.54	-0.58	-0.53		wet	-0.40	
$\Delta \chi_c$ 0.50m	year	-0.75	-0.75	-0.75	-0.75	$\Delta \chi_c$ 0.50m	year	-0.43	
	dry	-0.76	-0.76	-0.76	-0.76		dry	-0.66	
	wet	-0.78	-0.78	-0.78	-0.78		wet	-0.28	
$\Delta \chi_c$ 1.50m	year	-0.75	-0.75	-0.74	-0.74	$\Delta \chi_c$ 1.50m	year	-0.62	
	dry	-0.71	-0.71	-0.70	-0.70		dry	-0.70	
	wet	-0.79	-0.79	-0.79	-0.79		wet	-0.62	

Table 1. *Correlation coefficients (r) of Spearman partial correlation between variations in atmospheric* *soil CO_2 molar fraction ($\Delta \chi_c$) at three depths (0.15 m, 0.50 m and 1.50 m) in half-hour values during* *2014- December 2016), considering growing wet (wet; March-April) and dry season (dry; July-August* *soil temperature (ΔT_{soil}) at three depths (0.15 m, 0.50 m and 1.50 m), variations in volumetric water* *the combined effect of soil temperature and volumetric water content ($\Delta T soil$, ΔVWC) are controlled* *data are not considered for this analysis (sample size, n≥8784; all the coefficients had p-value<0.01).*

3.4. WAVELET COHERENCE ANALYSIS

We used wavelet coherence analysis (WCA) to test the temporal correlation between χ_c and ancillary variables. The yellow areas inside the contour lines represent high local temporal correlation between both series (Figures 5, 6 and 7). This analysis showed that p had a strong temporal correlation with χ_c in the deep soil (Figure 5), much higher than T_{soil} (Figure 6) or VWC (Figure 7). The WCA also indicated the main periodic components in the frequency domain between time series, showing a strong spectral coherence between variations of p and changes in χ_c (Figure 5), at periodicities ranging from 0.5 day to ~30 days (shown as yellow areas with black contour lines during this period) throughout the study period. Finally, the almost horizontal arrows pointing left indicated that oscillations were out of phase (Figure 5). This means that increments in χ_c corresponded to decreases in p and *viceversa*, at these temporal scales. This interpretation was consistent with the temporal pattern visible in Figure 4 and Table 1, which showed semidaily, daily and a synoptic patterns of variation, while the quasi-monthly pressure-CO_2 fluctuation was not evident from the wavelet coherence analysis.

The WCA showed strong spectral coherence between variations of T_{soil} or VWC and changes in χ_c (Figures 6 and 7) at daily and annual scale (shown as yellow areas with black contour lines at 1 day and 256 days) at 0.15 m. Contrary to the p-χ_c relationship, there was a high seasonality in this correlation in the case of T_{soil} in BB and in both ecosystems with VWC, with both variables particularly correlated during dry season. The causality relation − with T_{soil} or VWC forcing variations in χ_c − diminished with depth.
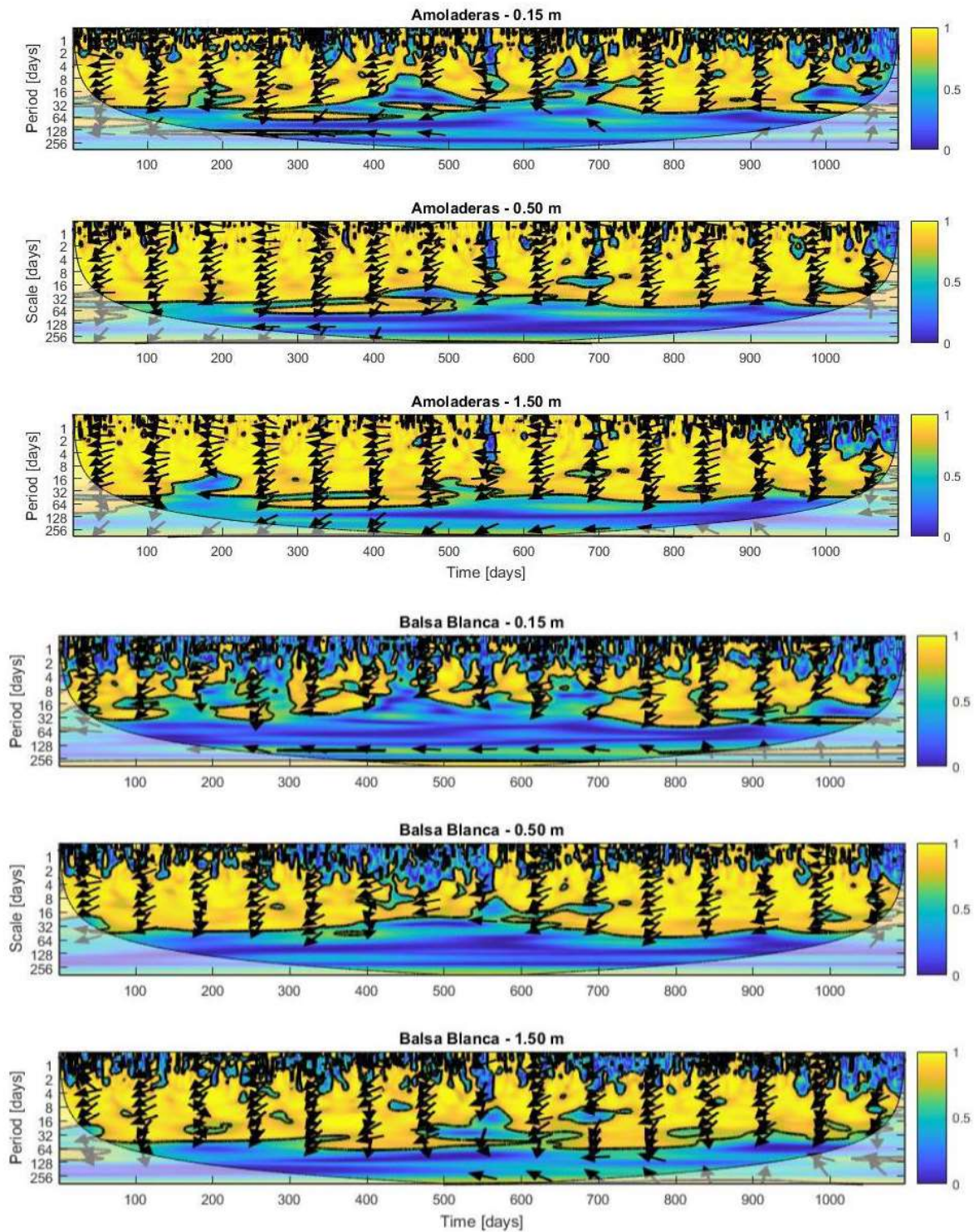
Figure 5. *Average 1-hour wavelet coherence analysis (WCA) to test the influence of atmospheric pressure on soil CO₂ molar fraction at three depths (0.15 m, 0.50 m and 1.50 m) in Amoladeras (AM) and Balsa Blanca (BB) experimental sites. Yellow areas with black contour lines represent a high significant temporal*

correlation with 5% significance level. Shaded area represents the cone of influence, where correlation is not influenced by edge effects. Arrows show the phase-locked angle relationship between the two time series. Horizontal arrows pointing right (phase angle of 0^0) indicate that the two time series are in phase, and horizontal arrows pointing left (phase angle of 180^0) represent when the two time series are out of phase.
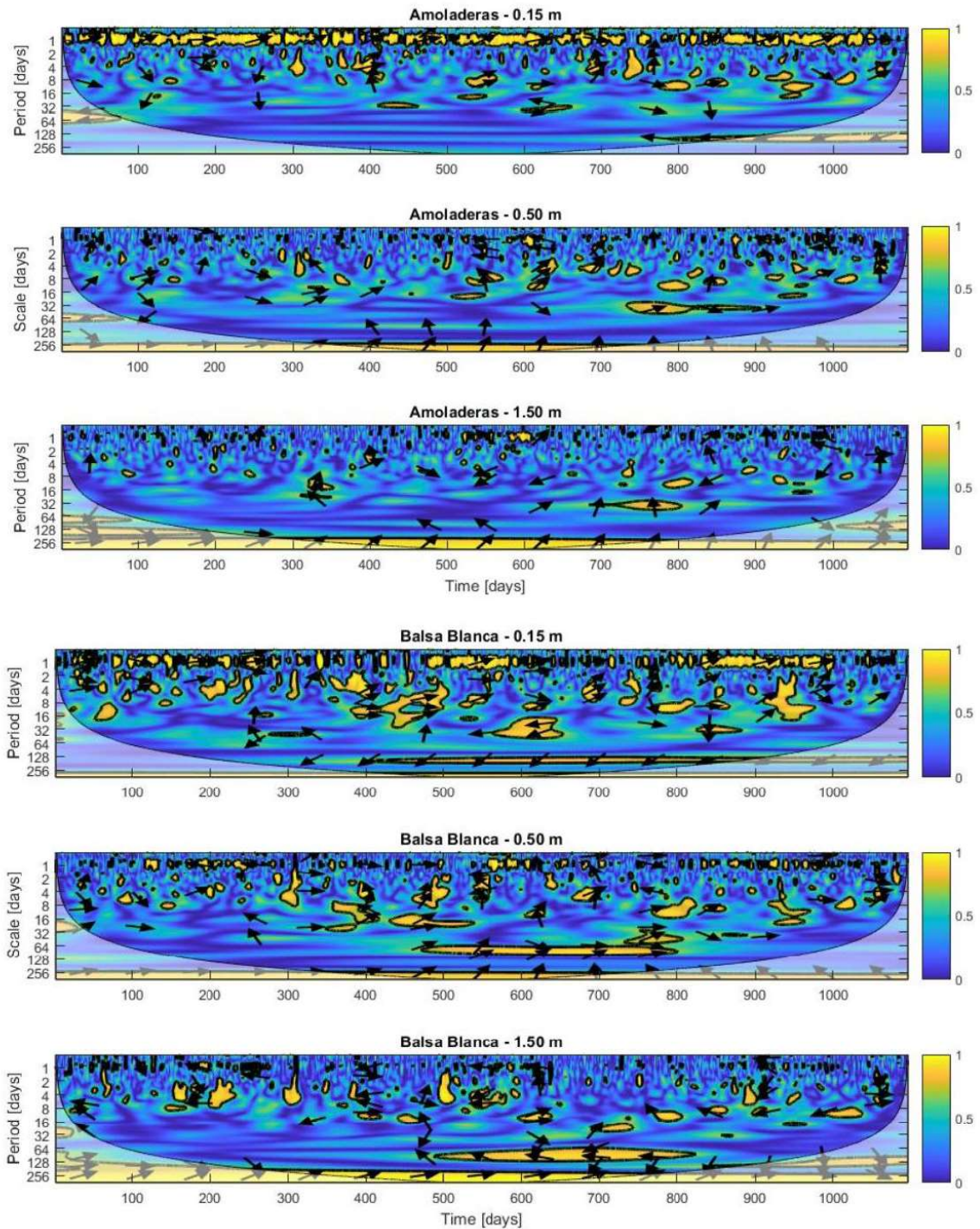
Figure 6. *Average 1–hour wavelet coherence analysis (WCA) to test the influence of soil temperature on soil CO_2 molar fraction at three depths (0.15 m, 0.50 m and 1.50 m) in Amoladeras (AM) and Balsa Blanca (BB) experimental sites. Information about the interpretation of this figure can be found in the caption for Figure 5.*
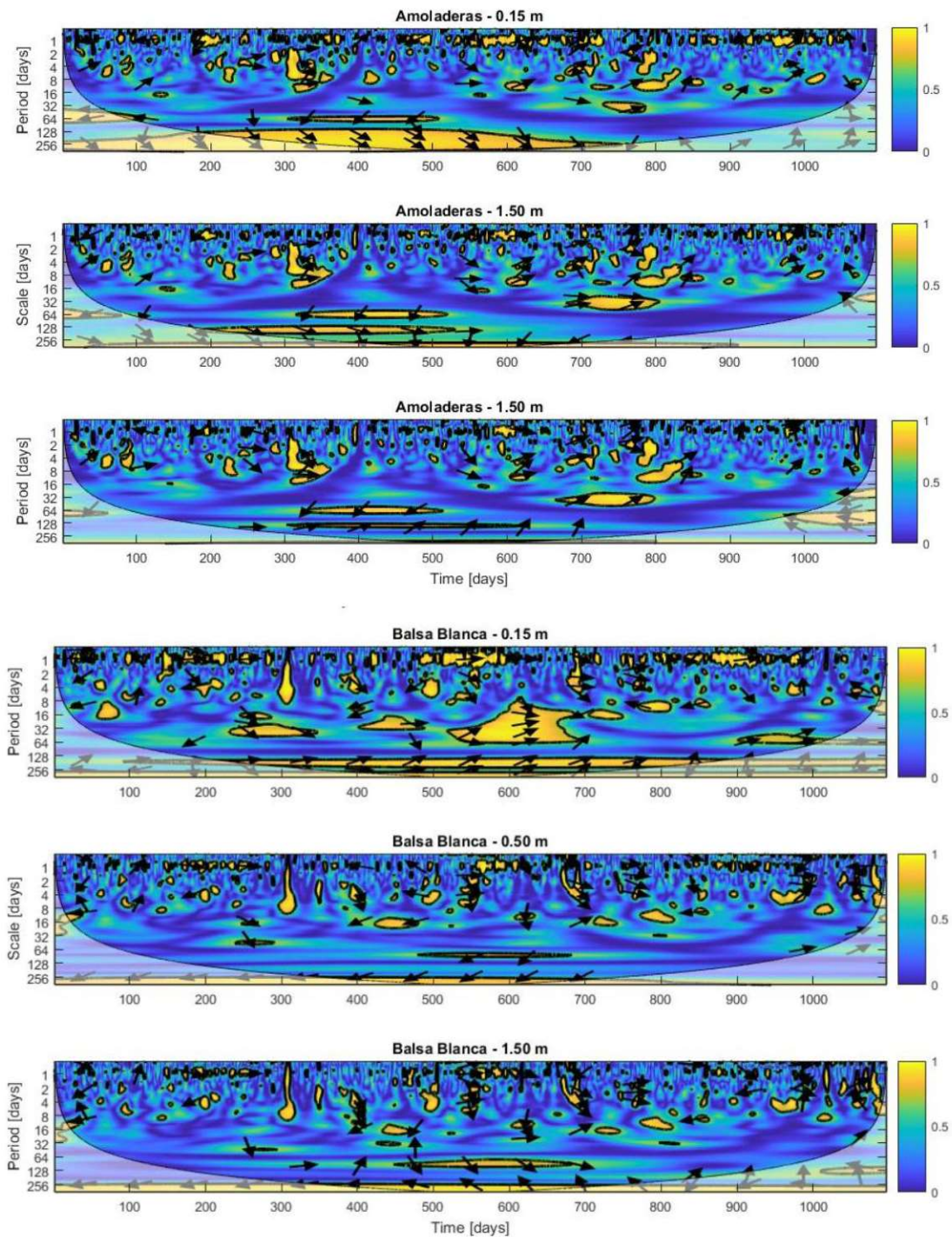
Figure 7. *Average 1-hour wavelet coherence analysis (WCA) to test the influence of volumetric water content at 0.50 m on soil CO_2 molar fraction at three depths (0.15 m, 0.50 m and 1.50 m) in Amoladeras (AM) and Balsa Blanca (BB) experimental sites. Information about the interpretation of this figure can be found in the caption of Figure 5.*

4. DISCUSSION

Changes in atmospheric pressure (p) conditions induce the expansion or contraction of the air stored in soil pores within the vadose zone, which plays a dominant role in regulating CO_2 storage and vertical transport. Simple regressions, Spearman partial correlations and spectral analysis consistently showed that CO_2 dynamics strongly depend on changes in atmospheric pressure (Figures 4, 5 and Table 1). We propose that the underlying physical mechanism is related to pressure tides (Kuang et al., 2013; Le Blancq, 2011; Lindzen, 1979; Massmann & Farrier, 1992). Pressure fluctuations penetrate deep into the soil vertical profile with very little attenuation (Maier et al., 2010; Massmann & Farrier, 1992; Takle et al., 2004), and the soil air expands upward in conditions of falling p or is compressed downward under rising p (Redeker et al., 2015; Sánchez-Cañete et al., 2013a), which may induce a natural "soil breathing phenomenon". The p influence was stronger in the deepest layer (Table 1 and Figure 5), where χ_c was higher and there was a lower influence of soil temperature (T_{soil}) and volumetric water content (VWC). Petrophysical properties of soil medium, such as permeability and connectivity, are pivotal factors in the p influence. These factors differs between layers producing discontinuities (Zamanian et al., 2016) that can slow down or facilitate the circulation of soil gases.

According to wavelet coherence analysis (WCA), the temporal correlation between p and χ_c (Figure 5) presented strong variations at different time scales. The dominant periods range from 0.5 day to ~30 days, implicating clear semidiurnal, diurnal, synoptic (Figure 4) and monthly temporal coherence (Figure 5). At semi-daily and daily scale in our experimental sites, the pressure tides showed two peaks per day, and generally, the first peak was smaller than the second (Figure 4). This

bimodal pattern was produced in the opposite way in the χ_c, with daily fluctuations up to 2000 ppm during intervals of less than 6 hours (Figure 4). Semi-daily and daily fluctuations in CO_2 dynamics have been related with gravitational forcing produced by sun and the moon (Lindzen, 1979; Sánchez-Cañete et al., 2013a), and are mainly forced by daily variations in insolation due to diurnal heating of Earth's surface (Kimball & Lemon, 1970; Le Blancq, 2011). At the synoptic scale, the pressure tide effect was also detected. This pattern of variation ranged between 3 and 8 days (Figure 4) induced by synoptic weather changes (the passage of high and low pressure systems and fronts; Clements & Wilkening, 1974; Elberling et al., 1998; Sánchez-Cañete et al., 2013a). With respect to the monthly scale, we are not aware of any other studies relating CO_2 dynamics to pressure tides. However, the wavelet coherence analysis showed a clear quasi-monthly pressure-CO_2 fluctuation that was visible during the three years of the experiment at both experimental sites (Figure 5). At this temporal scale, lunar forcing is the predominant factor affecting atmospheric tides with a 27.3-day and 13.6-day atmospheric oscillation affected by the lunar declination and the lunar revolution around the Earth (Guoqing, 2005).

At high-frequencies (< 1 Hz; Massman et al., 1997; Mohr et al., 2016; Roland et al., 2015), the friction velocity (indicator of turbulence) drives p fluctuations (Maier et al., 2010; Redeker et al., 2015). There is no clear distinction between pressure pumping and ventilation, a physical phenomena produced by turbulence that is associated with abrupt emissions of CO_2 to the atmosphere via non diffusive transport presented in well-aerated soils (Maier et al., 2010; Redeker et al., 2015). Some authors have stated a positive relationship between both processes (Mohr et al., 2016; Nachshon et al., 2012; Redeker et al., 2015), considering a correlation between p changes and wind perturbations. A low correlation between

pressure tides and wind velocity was detected in BB only at 0.15 m (similar to results obtained by Sánchez-Cañete et al., 2013a) and no correlation was detected in the deep profile in AM (data not shown). Although the high-frequency pressure oscillation and wind turbulence are not measured in this study, ventilation events had been detected in the past in the experimental sites of Balsa Blanca (BB; Rey et al., 2012) and Amoladeras (AM; López-Ballesteros et al., 2017), with AM having the higher ventilation potential (López-Ballesteros et al., 2018). Unlike pressure tides, high-frequency pressure fluctuations caused by winds are known to undergo strong attenuation with soil depth (Redeker et al., 2015; Takle et al., 2004). This different capacity of permeability could create a possible decoupling between the shallower horizons, affected by ventilation, pressure pumping and pressure tides; and deeper layers, that would be affected only by pressure tides. This assumption could explain the lack of relationship found between wind turbulence and p changes in BB and AM in the vertical profile, even though ventilation events have been detected at the ecosystem scale (López-Ballesteros et al., 2017; Rey et al., 2012).

Proximity to the coast (3.6 Km in AM and 6.3 Km in BB), could influence the atmospheric pressure tide effect on soil χ_c and explain the higher range of variation in the χ_c in AM, as well as the higher pressure tidal effect in comparison with BB (Figures 3 and 4). The water table provides a low-permeable boundary between the vadose zone and the soil surface that in coastal areas fluctuates frequently in response to sea tidal variations (Jiao & Tang, 1999; Li & Barry, 2000). At our experimental sites the water table is at 50 m depth approximately (Junta de Andalucía, 2013). Fluctuations in the water table changes the volume of the vadose zone; changing the depth of air penetration (Jiao & Li, 2004; Maier et al., 2010). When the water table rises, air is forced to be compressed in the vadose zone generating positive pressures and therefore, the air stored in the pores

and fissures could be pushed up to shallower layers. On the contrary, when the water table falls, extra pore space and negative pressures are generated (Jiao & Li, 2004). Dong et al., (2014) studied a coastal aquifer near the Ariake Sea, where the groundwater level of the coastal aquifer fluctuated with tidal and barometric variations. Here, spectral analyses also revealed that the sea-tidal effects could influence the semi-monthly, diurnal, and semidiurnal periodicities, associated with the astronomical tidal variations.

Other differences between study sites may be relevant. Firstly, due to its geographical position in the subterranean aquifer system (Junta de Andalucía, 2013), AM would have a higher allochthonous CO_2 recharge than BB explaining its higher χ_c concentration (Figures 3 and 4; López-Ballesteros et al., 2017). Secondly, the higher fraction of bare soil and rocks, the differing content in SOC, lower microbial activity or thinner soil depth are "degradation indicators" exhibited by AM (López-Ballesteros et al., 2018; Rey et al., 2011). These indicators suggest an increase in the interconnectivity between the soil medium and the atmosphere, and could enhance the gas transport and storage capacity of the medium, producing changes at the surface (López-Ballesteros et al., 2018). This would explain why in AM χ_c is more influenced by p changes (driver of physical transport processes in the χ_c dynamics) than in BB (Figure 5), while the influence of VWC and T_{soil} (drivers of biological processes in the χ_c dynamics) is higher in BB and only relevant at 0.15 m depth (Figures 6, 7). Thirdly, in AM the VWC at 0.50 m returns to its base level rapidly after a local storm, while in BB takes longer for VWC to returns to its pre-storm levels (Figure 2). This suggests that the soil in AM favours drainage and is more porous than in BB, enhancing CO_2 storage and vertical transport.

Seasonal differences were also found in both ecosystems. During the dry season, coinciding with the maximum water-free pore space, when the

aeration between soil and atmosphere is higher (Cuezva et al., 2011; Loisy et al., 2013), a higher correlation between χ_c and p was found in the shallower layer (Table 1). Spectral analysis also showed a marked seasonal pattern in the temporal correlations between variations of χ_c and changes in VWC (in BB and AM; Figure 7) and T_{soil} (in BB; Figure 6) in the shallowest layer (0.15 m), which are higher during dry season.

Most studies interpret the soil CO_2 efflux as instantaneous soil respiration and the more basic models are built by using soil temperature and soil water content relationships (Almagro et al., 2009; Davidson et al., 1998). However, at our experimental sites, T_{soil} and VWC are only relevant at 0.15 m for soil χ_c dynamics. Instead, changes in atmospheric pressure is the main driver in the deep soil profile (Figures 5, 6 and 7). Similar effects were detected in different ecosystems by some studies that estimated a temporary transport enhancement by pressure pumping (Bowling & Massman, 2011; Maier et al., 2012; Takle et al., 2004). However, there are no similar studies analysing pressure tides and their relation with CO_2 fluxes at low frequencies (> 1 Hz). Although the air flux induced by pressure fluctuation is only effective for a limited period (Maier et al., 2010), the omission of non-diffusive processes in the flux-gradient approach (Fick's law), generates an underestimation of the real CO_2 efflux rates and its transport in soil that cast doubt on its assumptions. Therefore, we propose that it is important to consider this effect when the soil gas flux is determined using the gradient method, at least, in ecosystems with high interconnectivity between the unsaturated porous media and the atmosphere (Fang & Moncrieff, 1999; Redeker et al., 2015; Vargas et al., 2010). There have been several attempts to incorporate this physical phenomenon. Based on empirical modelling, Mohr et al., (2016) defined a pressure pumping coefficient that would be able to describe the strength of the pressure-pumping effect on injected helium. Goffin et al., (2015) created

an alternative model considering air pressure fluctuations at the soil surface with the air permeability to calculate the soil CO_2 efflux. They concluded that the influence of pressure fluctuations creates a higher instantaneous flux compared to the diffusive flux only observable on very short timescales. Finally, Xu et al., (2014) created a model where the volume of CH_4 transported though porous media was correlated with a pressure change rate. These approaches could serve as bases to improve the gradient method in ecosystems affected by non-diffusive gas transport processes (Maier et al., 2012; Webb & Pruess, 2003).

CONCLUSIONS

This study assessed the main factors controlling soil CO_2 dynamics in the vadose zone of two semi-arid grasslands at different soil depths and time-scales. Our results showed that CO_2 dynamics at two semi-arid grasslands strongly depend on changes in atmospheric pressure. This dependency was consistent across soil depths, time-scales and study periods. We found strong evidence of non-diffusive CO_2 transport at our sites, with fluctuations of up to 2000 ppm CO_2 in less than 6 hours driven by pressure tides at scales ranging from 0.5 to ~30 days, showing semidiurnal, diurnal, synoptic and monthly patterns of oscillation. The atmospheric pressure effect on the soil CO_2 concentration was more evident in deeper layers, during the dry season and in the more degraded ecosystem. Pressure fluctuations penetrated deep into the soil vertical profile with very little attenuation, suggesting a bulk transport mechanism of trace gases throughout the porous medium that is much more effective than diffusion. This approach showed the importance of subterranean storage and non-diffusive gas transport and suggested the need to consider non-diffusive gas transport processes in models. The improvement of the gradient method (beyond Fick's law) will be essential for reliable estimations of the soil CO_2 efflux in ecosystems affected by non-diffusive gas transport processes.

All data used in this study are freely available at https://doi.org/10.6084/m9.fig- share.7381580.v2.

CHAPTER 2. DECOUPLING BETWEEN SHALLOW AND DEEP LAYERS IN SOIL CO2 DYNAMICS IN TWO SEMIARID ECOSYSTEMS
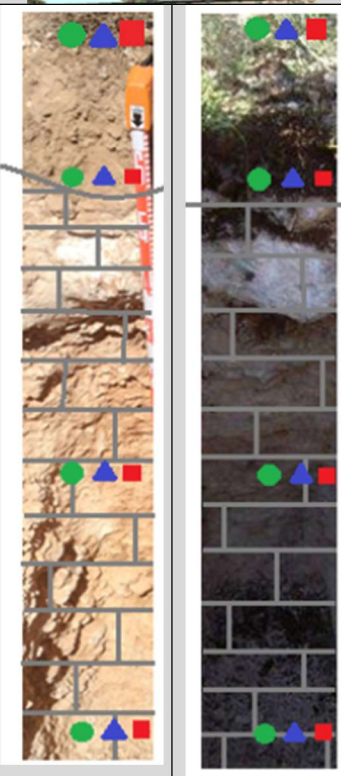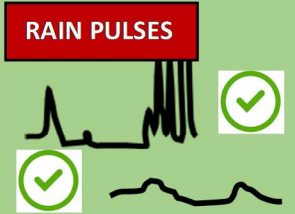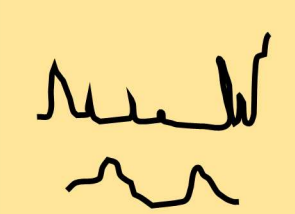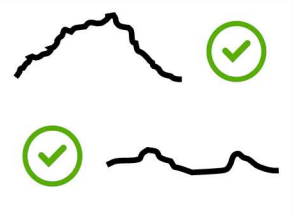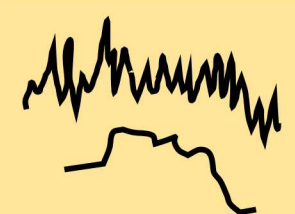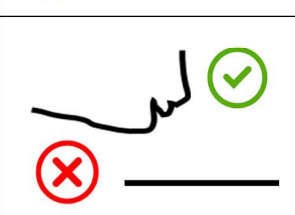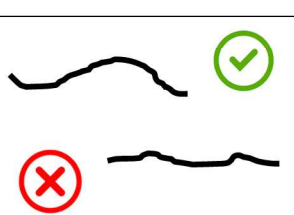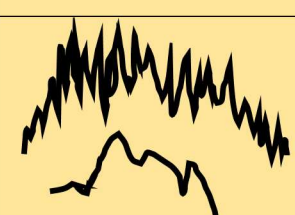
In preparation for publication.

ABSTRACT AND GRAPHICAL ABSTRACT

The carbon dynamic in drylands ecosystems has characteristics that make them unique. The spatial and temporal fluctuations of water availability are, in general, the fundamental drivers of biological processes because water availability is the most important environmental constraint. But also, due to the reduced biological activity of drylands ecosystems, the ecosystem carbon balance is also strongly associated with variations of abiotic factors. Pressure pumping, pressure tides and subterranean ventilation are non-diffusive transport processes affected by wind or changes in atmospheric pressure at different temporal scales. These processes, could results in a more efficient transport mechanism compared to molecular diffusion alone and can dominate the ecosystem flux during the dry season at ecosystem scale. They are especially relevant in well-aerated soils with a CO_2 rich vadose zone. Unluckily most studies in soils, which are key components in the carbon balance in semi-arid ecosystems, have focused on shallow soil CO_2 dynamics neglecting processes in deeper soil layers where highly CO_2-enriched air can be stored or transported through soil pores and fissures by this mechanism.

This study tries to understand either surface and subsurface soil CO_2 dynamics in two semi-arid ecosystems through the analysis of the CO_2 molar fraction and main soil and environmental variables related with biotic (soil temperature and soil water content) and abiotic (atmospheric pressure and friction velocity) factors continuously measure during three years (2014-2016). Different layers in the vadose zone were considered with sensors at 0.05 m (surface layer), 0.15 m (subsurface layer), 0.50 m and 1.50 m (deep layer). Wavelet analysis revealed that CO_2 concentration at 0.05 m depth was controlled by soil moisture, soil temperature, pressure pumping and ventilation, being rain pulses events the most important factor

controlling the carbon dynamic. The concentrations in the deeper soil, however, were influenced mainly by pressure tides. While, the subsurface layer acted as an interphase layer and was relevant affected by soil temperature, soil water content, pressure tides, pressure pumping and ventilation. Futhermore, the long-term soil CO_2 efflux based on the gradient method was estimated in-situ for the experimental sites of this study. The results achieved, especially the physical decoupling found between soil layers, could help us to better understand the different processes behind non-diffusive transport processes in semi-arid ecosystems.

		SOIL WATER CONTENT	SOIL TEMPERATURE	CO₂ MOLAR FRACTION (X$_c$)

ATMOSPHERE

ANNUAL INFLUENCE ON X$_c$ ✓ ✗

✓ ✗ **DAILY AND/OR SYNOPTIC INFLUENCE ON X$_c$**

0.05 m SURFACE — RAIN PULSES ✓ ✓ / ✓ ✓ /
0.15 m SUB-SURFACE — RAIN P. >15MM ✓ ✓ / ✓ ✓ /
0.50 -1.50 m DEEP LAYER — ✓ ✗ / ✓ ✗ /

RELEVANT PROCESS

Ⱳ **ANNUAL PATTERN**

DAILY PATTERN (2d) Ⱳ

(green box) D

1. INTRODUCTION

Understanding the components that influence patterns of terrestrial CO_2 fluxes around the world is essential to predict and manage the effect of the human carbon footprint (Magnani et al., 2007). Semi-arid ecosystems occupy approximately 45% of the terrestrial surface and constitute the largest biome on the planet (Reynolds et al., 2007; Schimel, 2010), but they are under-represented in ecological research networks (Schimel et al., 2015; Villarreal et al., 2018). Rates of biological activity per unit of drylands is low compared with many terrestrial ecosystems (Sitch et al., 2003) but the large surface area of drylands gives drylands carbon dynamic a relevant global significance. In particular, total dryland soil organic carbon reserves contain 27% of the global soil organic carbon reserves (Lal et al., 2004; MA 2005; Schimel, 1995) and the positive global CO_2 sink trend is dominated by semi-arid ecosystems (Ahlström et al., 2015).

Soil temperature and soil moisture are commonly the major abiotic factors controlling soil respiration (Smith et al., 2018; Albertsen, 1979; Davidson et al., 2006). However, in arid and semi-arid ecosystems, subjected to prolonged summer droughts, soil CO_2 efflux (F_s) respond to the most limiting factor (Ma et al., 2007; Rambal et al., 2003; Reinchestein et al., 2007; Saleska et al., 2003). Thus, water availability is the main controlling factor and the temperature dependence of F_s is only relevant during growing season, when water is not a limiting factor (Specht & Moll, 1983; Larcher, 2000). The spatial and temporal fluctuations of water availability are, in general, the fundamental drivers of biological processes (Noy-Meier; 1973). Consequently, the most used F_s models are being proved ineffective in drought-prone regions or modelling the F_s emissions

during rain pulses (Almagro et al., 2009; Migliavacca et al., 2011; Xu & Baldocchi, 2004).

Rain pulses are occasional rain events that cause the sudden activation of the biological activity, which large increases in the CO_2 release, that gradually decrease over some subsequent days following the rain event. The F_s is produced by the enhancing of the soil respiration processes (Birch., 1958; Curiel Yuste et al., 2003; Jarvis et al., 2007) and the displacement of CO_2-rich soil air by water (Liu et al., 2002, Marañon-Jimenez et al., 2011). Rain pulses are common in water-limited systems (Jenerette et al., 2008). These types of events only occur during periods of marked absence of water, so they usually occur during dry season (Ivans et al. 2006; Xu & Baldocchi, 2004) and mark the transition phase between dry and growing season (Cleverly et al., 2013; Lázaro et al., 2001). Multiple studies have highlighted the importance of rain pulses in the ecosystem carbon exchange resulting in dramatic variation in fluxes between seasons and years (Hastings et al., 2005; Huxman, 2004; Reynolds, 2004; Vargas et al., 2012).

Due to the reduced biological activity of drylands ecosystems, the ecosystem carbon balance is also strongly associated with variations of abiotic factors, at least on short time scales (Emmerich, 2003; Mielnick et al., 2005; Roland et al., 2013; Were et al., 2010). Pressure pumping (Massman et al., 1997; Mohr, et al., 2016; Roland et al., 2015), pressure tides (Clements & Wilkening, 1974; Le Blancq, 2011, Sánchez-Cañete et al., 2013a) and subterranean ventilation (Kowalski et al., 2008; Serrano-Ortiz et al., 2010; Sánchez-Cañete et al. 2011) are non-diffusive transport processes affected by wind or changes in atmospheric pressure at different temporal scales. These processes, results in a more efficient transport mechanism compared to molecular diffusion alone (Bowling & Massman, 2011; Maier et al., 2012; Takle et al., 2004), and can dominate the flux

during the dry season at ecosystem scale (Kowalski et al., 2008) with annual contributions >50% (Serrano-Ortiz et al., 2014).

In semiarid and arid ecosystems where most of the carbon resides belowground (Burke et al., 2008; Eswaran et al., 2000), F_s constitutes a significant component of CO_2 ecosystem fluxes (Hanson et al., 2000; Raich & Schlesinger, 1992). Despite its importance, research on the subterranean CO_2 dynamics are focused on surface soils (Davidson et al., 1998; Drewitt et al., 2002; Janssens et al., 2001; Longdoz et al., 2008; Subke et al., 2003), neglecting the deeper layers (Davidson et al., 2006; Hirano et al., 2003; Hirsch et al., 2004; Maier et al., 2010; Risk et al., 2002; Tang et al., 2003). Currently, the knowledge about the production and transport of CO_2 within the vadose zone (between the water table and the soil surface) remains very vague. However, the vadose zone contains large CO_2-enriched air (ca. 5% by volume) in the first meters (Benavente et al., 2010; Denis et al., 2005) and its exchange with the atmosphere can represent from 10 to 90% of total ecosystem CO_2 emissions (Hanson et al., 2000; Sánchez-Cañete et al., 2016).

All of these factors involving non-diffusive processes, along with the fact that studies generally use only the uppermost soil layer neglecting the subsurface, highlight the need to know the potential interaction between different soil layers and the atmosphere and the need to examine in a systemic and integrative way the CO_2 dynamics of the different layers within the vadose zone.

This study tries to understand the differences and similarities between surface and subsurface soil CO_2 dynamics in two semi-arid ecosystems through the analysis of the CO_2 molar fraction and main soil and environmental variables continuously measured at different soil depths (0.05, 0.15, 0.50 and 1.50 m) during three years (2014-2016). We attemp to find the differences in the CO_2 sources and transport processes along the different layers in the vadose zone (surface soil, subsurface soil, and deep

soil) and how they contribute to the annual carbon dynamics. Specifically, we address the following questions: Do all the different layers of the vadose zone have the same behaviour? Is there a decoupling in the soil processes between layers? On the other hand, the secondary objective is to obtain accurate estimates of long-term soil CO_2 efflux based on the gradient method. For that, we determined the in-situ gas transfer coefficient (k_s), measuring the mole fraction of CO_2 at two depths and the CO_2 output from the soil using a portable camera. Finally, a k_s model was obtained for each experimental site based on the porosity and water content of the soil, which is critical to correctly model the CO_2 fluxes based on continuous measurements of soil CO_2 concentration.

2. MATERIAL AND METHODS

2.1 STUDY SITE

The study area is located in Cabo de Gata-Níjar Natural Park, in the province of Almeria in the SE of Spain. We selected two neighboring semi-arid grassland sites similar in terms of climate, geology, topography and vegetation: (1) Balsa Blanca (N36º56'26.8" W2º01'58.8″; hereinafter BB), and (2) Amoladeras (N36º50'5" W2º15'1″; hereinafter AM). The sites are located 23 km apart from each other and at 65 m (AM) and 208 m (BB) of altitude. The area is classified as a hot arid desert according to Köppen classification (BWh; Rubel & Kottek, 2010). The climate is characterized by a mean annual precipitation of 220 mm and a mean annual temperature of 18 °C (Figure 1). Climatic conditions are also characterized by a long dry season, which begins in June and ends abruptly in September–October with rain pulse events (López-Ballesteros et al., 2016) when the temperature starts to rise and water resources have not yet become scarce (Serrano-Ortiz et al., 2014). At our experimental sites, geological materials consist of a quaternary conglomerates and Neogene-Quaternary sediments cemented by lime (caliche). The limestone crust is located on a glacis. The glacis in AM has pinkish silts and quartz boulders from the Upper Pleistocene; while in BB it is a calcareous crust "dalle" low detritic from the Lower Pleistocene (MAGNA, 2010). Both sites are located geomorphogically on a flat alluvial fan of gentle slopes (2–6%) with petrocalcic horizons (i.e., caliche). Petrocalcic horizons are characterized by bulk densities ranging between 1.6 and 2.3 g cm^{-3} and porosities ranging between 16 and 40% (Duniway et al., 2007; Zamanian et al., 2016). The characteristics of these materials depend on origin, formation processes and morphology of pedogenic

carbonates (Zamanian et al., 2016) producing discontinuities through the vertical layers that are unknown in our experimental sites. In the surface soil horizon, bulk density is lower (1.18 (AM) - 1.22 g cm^{-3} (BB)) and porosity is much higher (55.47 (AM) − 53.96% (BB)). The soil organic carbon content is 1.24 (AM) and 4.64 kg m^{-2} (BB). The relict degradation level is higher in AM (López-Ballesteros et al., 2018; Rey et al., 2011) due to grazing (Alados et al., 2004). The water table is at 50 m depth approximately (Junta de Andalucía, 2013). The dominant soils are classified as Lithic Leptosols (WRB, 2015); they are shallow (10–20 cm) and alkaline (pH 8.4 (AM) − 7.9 (BB)), with sandy loam texture class and carbonate saturated. Vegetation is dominated by Machrocloa tenacissima and other drought-tolerant plant species. The rest of vegetation is composed of *Thymus hyemalis* Lange, *Helianthemum almeriense, Sideritis pusilla* (Lange) Pau, *Hammada articulata, Lygeum spartum* L., *Salsola genistoides* Juss. ex Poir., and *Launaea lanifera* Pau in AM and *Chamaerops humilis, Rhamnus lycoides, and Pistacia lentiscus* in BB. The vegetation cover varying between 23 (AM) and 63% (BB) of the ground surface. In the soil surface there are patches of bare soil, sections with biological soil crusts, and exposed gravel and rock outcrops.

2.2. EXPERIMENTAL DESIGN

Vertical profiles were installed in January 2010 in BB and in July 2013 in AM. Boreholes were done with a backhoe and the extracted material was used for refilling. The study period covered from January 2014 to December 2016, rejecting a stabilization period of 6 months after the installation of the vertical profile in AM. The stabilization period was selected after comparing CO_2 dynamics in both vertical profiles. Vertical

profiles measured soil CO_2 molar fraction (χ_c; infra-red sensor GMP-343, Vaisala, Inc., Finland), soil temperature (T_{soil}; 107 thermistors, Campbell Scientific, Logan, UT, USA) and volumetric soil water content (VWC; TDR, CS616, Campbell Scientific, Logan, UT, USA). Sensors were installed horizontally in undisturbed media at three different depths: 0.15 m soil horizons (belonging to edaphic media; heirenafter subsurface layer), and 0.50 m and 1.50 m layers (belonging to underlying media; heirenafter deep layers) below the surface. Soil adapters for horizontal positioning made of a PTFE filter were installed with the soil CO_2 sensor (215519, Vaisala, Inc., Finland) for water protection. The CO_2 sensors were configured to measure the CO_2 molar fractions at a temperature of 25 °C and 1013 hPa, but during the post-processing measurements were corrected for soil temperature and pressure at the time of measurements. Data were recorded every 30 s and stored as 30 min averages in a data-logger (CR23X and CR1000, Campbell Scientific, Logan, UT, USA; respectively for AM and BB). Missing data vary 3–6% over the entire period (2014–2016) except in AM for χ_c at 1.50 m (22%), and in BB for soil temperature at 1.50 m (48%) and χc at 0.50 m (50%) due to instrument malfunction.

Shallower CO_2 sensors were installed at the 0.05 m horizon (heirenafter surface layer), in June 2011 in BB and in June 2012 in AM. The sensors were installed vertically with an in-soil adapter (GMM-222, Vaisala, Inc., Finland) to avoid water entering. Vaisala sensors were configured to obtain the CO_2 molar fraction at 25 °C and 101.3 kPa and later corrected for variations in temperature and pressure. Soil moistures were monitored using water content reflectometer (TDR, CS616, Campbell Scientific, Logan, UT, USA). Subsurface temperatures were monitored using thermistors (107, Campbell Scientific, Logan, UT, USA). All measurements were made every 30 s and stored as 30 min averages in a data- logger (CR3000 and CR1000, Campbell Scientific, Logan, UT, USA;

respectively for AM and BB). Missing data for all meteorological variables in both sites corresponded to <15% in AM and <20% in BB per the entire period except in BB for VWC (46%) due to instrument malfunction during the last months.

At both experimental sites, an eddy covariance tower were installed to measure densities of CO_2 as well as barometric pressure (p; open-path infrared gas analyzer Li-Cor 7500, Lincoln, NE, USA). The net ecosystem carbon balances (NEE) were estimated by integrating the half-hourly CO_2 fluxes calculated and processed with EddyPro 5.1.1 software (Li-Cor, Inc., USA). Wind speed and sonic temperature were measured by a three-axis sonic anemometer (CSAT-3; Campbell Scientific, Logan, UT, USA; hereafter CSI). The friction velocity (u_*) was determined as the turbulent velocity scale resulting from square root of the (density-normalized) momentum flux magnitude (Stull, 1988). Furthermore, meteorological measurements of net radiation (NR Lite, Kipp&Zonen, Delft, Netherlands), air temperature and air relative humidity (HMP35-C, Campbell Scientific, Logan, UT, USA) and rainfall (745 M, Davis Instruments Corp., Hayward, CA, USA) were acquired since 2009. Meteorological data were recorded as 30 min averages by a data logger (CR3000 and CR10X, Campbell Scientific, Logan, UT, USA). Missing data for all meteorological variables in both sites corresponded to <10% over the entire period. For more information about the sites and meteorological equipment see López-Ballesteros et al. (2018).

2.3. DATA ANALYSIS

Outliers were detected with a 2.5-hour sliding standard deviation window across neighboring values. Small gaps (less than a week) were filled

by estimating extrapolated values from forward and reverse auto-regressive fits of the remaining samples. Gaps of more than a week were filled with a simple regression fit with the same soil depth profile from the other experimental site, (except for CO_2 at 0.50 m in BB where correlation was higher with CO_2 at 1.50 m in AM, $R^2 > 0.5$). Atmospheric pressure gaps where filled using a simple regression with measurements from the other experimental site ($R^2 > 0.96$). The rain pulse events non-detected due to instrument malfunction where filled using data the meteorological station from the Almeria airport (15 km from AM and 40 km from BB).

We used wavelet analysis to explore the spectral properties of the times series χ_c, p, u_*, T_{soil} and VWC during three years. The wavelet analysis is a powerful tool to examinate one time series in the time and frequency domain for visual interpretation or two time series together that may be expected to be linked in some way (Cazelles et al., 2008; Govindan et al., 2005 Grinsted et al., 2004; Torrence & Compo, 1998). Specifically, we used the continuous wavelet transform (CWT) to describe the temporal variability of χ_c and the presence of rain pulses and the partial wavelet coherence analysis (WCA) to describe the temporal variability, explore the spectral properties and investigate the temporal correlations between χ_c, p, u_*, T_{soil} and VWC. We calculated the CWT and WCA with statistical significance ($p < 0.05$) and using the Morlet wavelet as a mother function (Torrence & Compo, 1998). The WCA between χ_c and p, u_*, T_{soil} and VWC was computed using 1000 Monte Carlo simulations. All-time series were analyzed using a 1-hour time step. Areas with black contour lines represent a high significant temporal correlation with 5% significance level. WCA ranges between 0 and 1, where 1 indicates the highest temporal correlation (and 0 for no correlation) between variables (Vargas et al., 2012, 2018; Xu et al., 2014). In addition, arrows show the phase-locked angle relationship between both time series (Govindan et al., 2005; Grinsted et al., 2004; Xu

et al., 2014). All data analyses were performed using MATLAB R2017a (MathWorks, Natick, Massachusetts, USA).

2.4 FLUX CALCULATION

The soil CO_2 efflux (F_s) was determined using the gradient method (Maier & Schack-Kirchner, 2014; Sanchez-Cañete & Kowalski, 2014). Soil CO_2 efflux (F_s) was calculated assuming that all transport is due to diffusion as:

$$F_s = -k_s \rho_a \frac{d\chi_c}{dz} \quad \text{(eq. 1)}$$

where F_s is the upward gas flux (µmol CO2 m^{-2} s^{-1}), k_s is the soil CO_2 transfer coefficient (m^2 s^{-1}), ρ_a the mean air molar density (µmol m^{-3}) and $d\chi_c/dz$ is the vertical CO_2 molar fraction gradient (ppm m^{-1}). The CO_2 gradient was calculated using the difference between the mean atmospheric CO_2 molar fraction and the value of the soil CO_2 sensors at 5 cm depth. The CO_2 molar fraction was corrected for variations in temperature and pressure. The air density (ρ_a) was obtained from the ideal gas law. The empirical k_s is equal to the soil CO_2 diffusion coefficient in absence of production/consumption processes in the monitored layer. It depends not only on diffusion but also can vary with production/consumption processes in the layer (Sánchez-Cañete et al.; 2017), in our case from 0 to 5 cm. The transfer coefficient k_s is obtained from the flux-gradient relationship proposed by Roland et al., (2015):

$$k_s = \frac{F_{chamb}}{\rho_a} \frac{d_z}{d_{\chi c}} \qquad \text{(eq. 2)}$$

where in our study F_{chamb} was measured by a portable soil CO_2 flux chamber (EGM-4; PP-systems, Hitchin, UK) during 14 campaigns in BB and 11 campaigns in AM at differing values of soil water content. These measurements were performed between November 2013 and May 2014 in BB and from April 2016 to October 2016 in AM. $F_{chamber}$ measurements were always performed between 8:00 and 10:00 (solar time) in AM and between 11:00 and 16:00 in BB. For each measurement of soil CO_2 effluxes (F_s), the soil chamber was placed on a PVC collar (5 cm height, 10.5 cm diameter) previously inserted in the soil, leaving 2–3 cm above ground. The chamber system was configured to store temperature, relative humidity, CO_2, and pressure every 3 s during 120 s. The F_s were estimated from the initial slopes of CO_2 molar fractions of the confined air versus time, by using either linear or quadratic regression (Kutzbach et al., 2007; Pérez-Priego et al., 2010; Wagner et al., 1997) for the best regression fit. The raw values of CO_2 molar fraction were previously corrected for dilution (Hubb, 2012) from CO_2 molar fractions referred to wet air. Finally, the flux density was calculated using the ideal gas equation as explained by Pérez-Priego et al., (2015). The chamber fluxes were estimated as:

$$F_{chamb} = \frac{d\chi_c}{d_t} \frac{V}{S} \frac{P_0 (1-w_0)}{R \, T_0} \qquad \text{(eq. 3)}$$

where $F_{chamber}$ is the soil CO_2 efflux ($\mu mol \ m^{-2} \ s^{-1}$) derived from the chamber system, $d\chi_c/d_t$ is the initial rate of change in CO_2 molar fraction referenced to dry air ($\mu mol \ mol^{-1} \ s^{-1}$), V is the total volume (chamber+ collar, m^3), S is the projected surface area (m^2), P_0 is the initial atmospheric pressure (Pa), w_0 is the initial water vapor mole fraction ($mol \ mol^{-1}$), R is the universal gas constant (8.314, $m^3 \, Pa \ K^{-1} \ mol^{-1}$), and T_0 is the initial air temperature (K). Therefore, knowing $F_{chamber}$ and applying equation (2),

we obtain the soil CO_2 transfer coefficient (k_s). To model k_s , it was fit using a power function against soil tortuosity (ξ):

$$\frac{k_s}{D_a} = a\,\xi^{\,b} \qquad \text{(eq. 4)}$$

where D_a is the diffusion coefficient of the CO_2 in free air, calculated according to Jones (1992), and ξ is obtained as the soil porosity (φ ,cm³ cm⁻³) minus the soil water content (θ, cm³ cm⁻³) and the coefficients a and b were obtained by least squares regression. Finally, we used our calculated soil CO_2 transfer coefficient (k_s) to estimate soil CO_2 fluxes during whole the period using the equation (1).

In this chapter positive values of F_s denote a CO_2 release to the atmosphere in consistency with NEE measurements.

3. **RESULTS**

3.1 **ENVIRONMENTAL DESCRIPTION**

The annual mean air temperature during the study period was 18.5 ± 5.9 °C in AM and 17.7 ± 6.4 °C in BB (Figure 1). The warmest summer and winter were in 2015 and 2016, respectively. Both ecosystems show the same rainfall pattern although BB always had a slightly higher precipitation regime (15%). The driest year was 2014 with 134 mm in AM and 166 mm in BB, with lower precipitation than the typical precipitation regime established in the area (220 mm). In contrast, 2015 and 2016 were rainy years with 201 mm and 264 mm respectively in AM and 237 mm and 284 mm in BB (Figure 5). Total amount of rainfall corresponding to rain pulses is highly variable. Although the more common are the low-magnitude rain pulses (i.e., <10 mm), several high magnitude rain pulses could fall yearly. It's remarkable the rain pulse event occurred on December in 2016, when the typical total amount of rainfall fallen corresponded to a typical annual value.

Seasonal and annual patterns of atmospheric pressure (p), volumetric water content (VWC), soil temperature (T_{soil}) and precipitation are shown for both experimental sites in Figure 1. Absolute p in AM (65 m in altitude) is greater than in BB (208 m in altitude) by about 2 kPa. Fluctuations in p were similar in BB and AM. There was a seasonal pattern in the range of variation, with winter months having the highest maximum and minimum values. Regarding T_{soil}, both ecosystems showed similar values. Maxima and minima were reached in the shallower layer (0.05 m) with values ranging between 9 °C and 38 °C in AM, versus 6 °C and 40 °C in BB. With a slight decrease in the amplitude of daily fluctuations in comparison with

the shallower layer, T_{soil} was very similar at 0.15 m and 0.50 m in both ecosystems. At 1.50 m the lowest range of variation was observed and the maximum and minimum values were reached with a ~20 days delay in relation with the shallowest layer. At this depth maximum T_{soil} was reached in August (~27 °C) while minimum was reached in February (~18 °C).
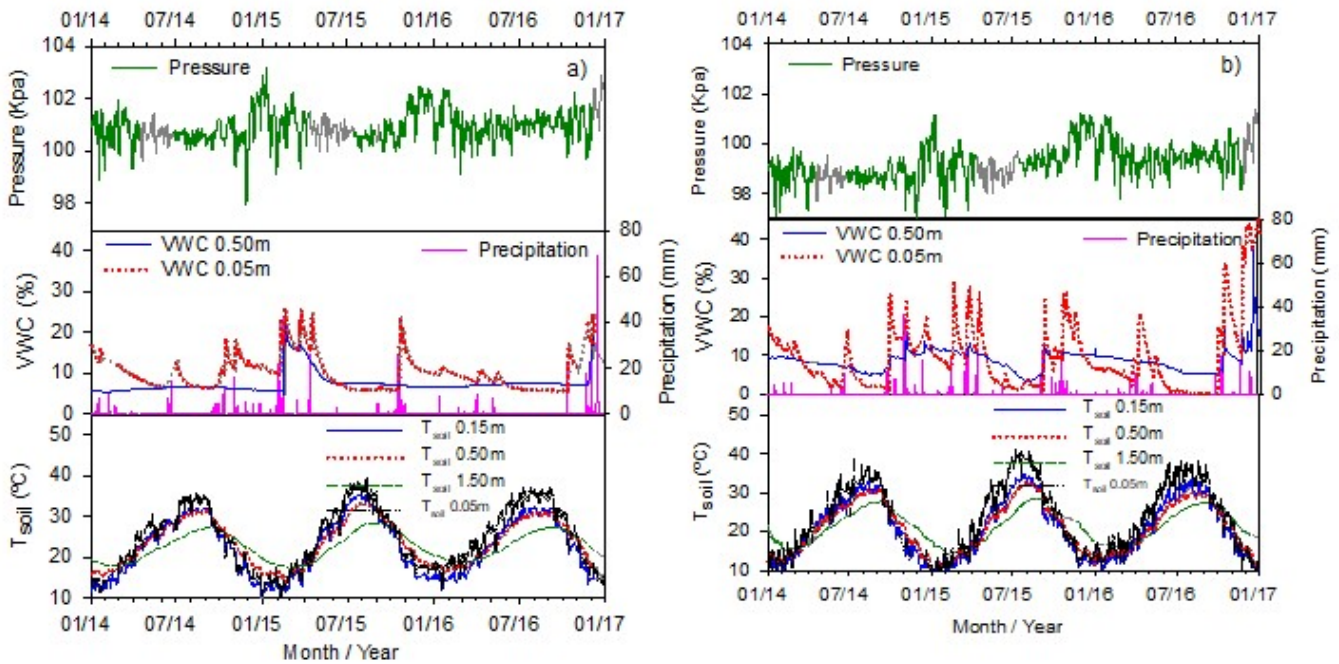
Figure 1. *Daily-averaged values of atmospheric pressure, daily precipitation, volumetric water content (VWC) at 0.05 m (dotted lines) and 0.50 m (solid lines) and soil temperature (T_{soil}) at soil depths of 0.05m (dashed and doted lines), 0.15 m (solid lines), 0.50 m (dotted lines) and 1.50 m (dashed lines) during the study period (January 2014–December 2016) in Amoladeras (a) and Balsa Blanca (b) experimental sites. Gray lines represent gaps in the time series.*
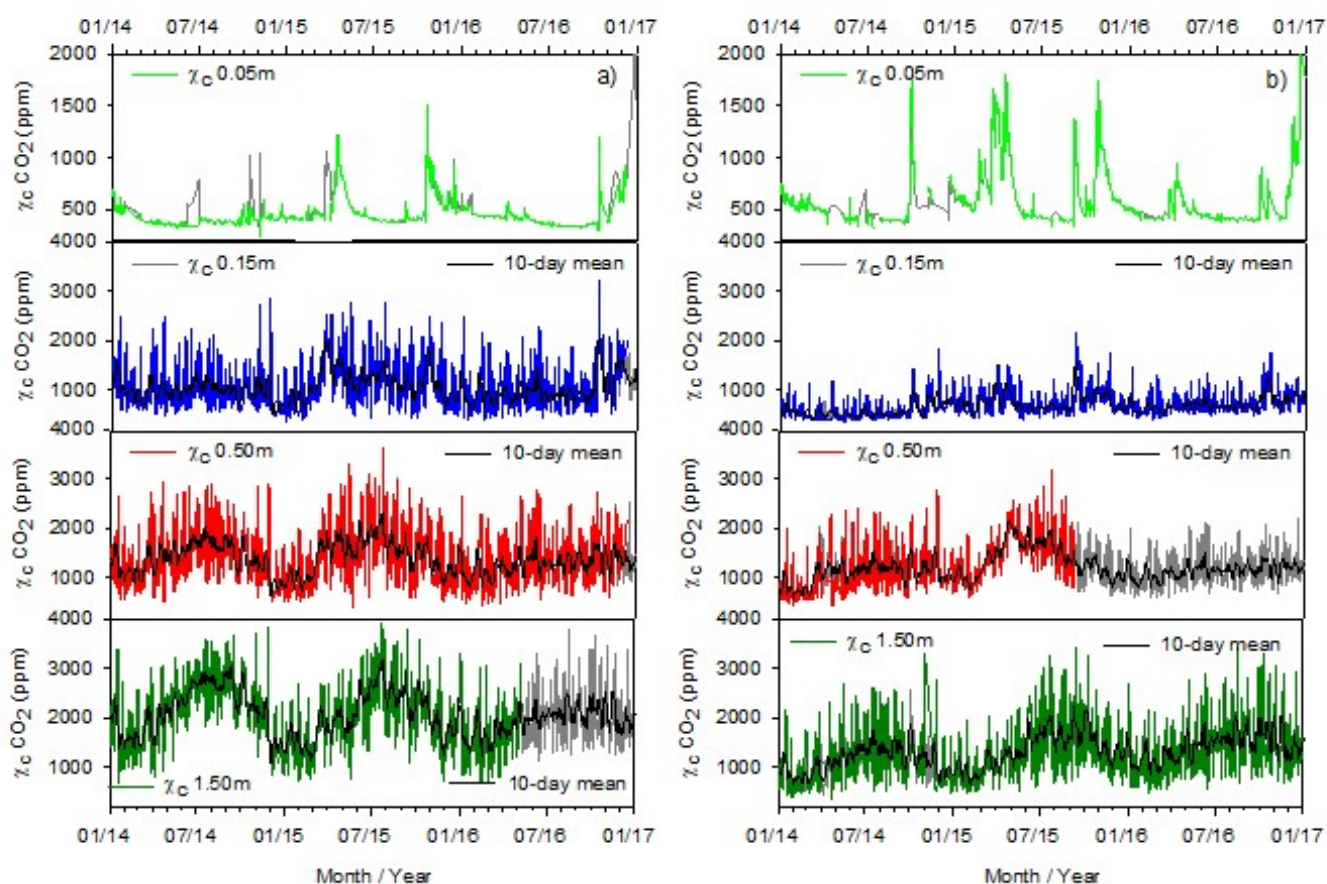
Figure 2. *Daily-averaged and 10-day mean values of soil CO₂ molar fraction (χc) at 0.05m, 0.15 m, 0.50 m and 1.50 m depth during the study period (January 2014–December 2016) in Amoladeras (a) and Balsa Blanca (b) experimental sites. Gray lines represent gaps in the time series.*

Finally, precipitation events conditioned the VWC dynamic at annual and seasonal scale. The annual mean VWC at 0.50 m was 7.5 ± 2.6% in AM and 8.7 ± 2.9% in BB with minima around 5–6% in AM and 3–4% in BB and maxima of 42% in AM and 50% in BB coinciding with local storms. With small precipitation events, the slow water infiltration only permeates into soil surface (0.05 m) and the soil subsurface (0.15 m) layers. During a large precipitation event or events of intense rain (>15 mm) water could

descend up to 1.5 m in the same day (data not shown). Depending if the rainfall is produced during growing or dry season, differences in the increment rate of the volumetric water content were found in BB at 0.50 m. During dry season, less water could permeate at 0.50 m and it required a longer time to recovery the VWC pre-rainfall levels. However, during growing season the infiltration depth was higher and a homogeneous distribution of VWC across the soil profile was produced.

3.2 DYNAMICS OF SOIL CO_2 MOLAR FRACTION AT ANNUAL AND SEASONAL SCALE

Soil CO_2 showed a clear vertical profile with higher concentration at depth, and similar means over the three years (Figure 2). The year with the highest χ_c was 2015 with an annual average across the subsurface (0.15 m) and deep (0.5 m and 1.5 m) soil depths of 1558 ± 429 ppm in AM and 1161 ± 329 ppm in BB. At surface (0.05 m), the year with the highest χ_c was 2016 in AM with an annual average of 515 ± 303 ppm, and 2015 in BB with an annual average of 671 ± 334 ppm.

The χ_c at surface soil showed a clear irregular pattern influenced by rain pulses. At deep soil, the χ_c showed clear annual patterns with maxima in summer and minima in winter. At subsurface soil (0.15 m), the χ_c patterns were more regular throughout the year. The χ_c showed annual patterns with maxima in summer and minima in winter but also with peaks related with days with high precipitation events. Generally, BB had higher CO_2 concentrations in the surface soil and AM in the subsurface soil and deep soil. For example, χ_c at 1.50 m had an annual average of 2029 ± 113 ppm in

AM and 1268 ± 154 ppm in BB. AM also showed higher variability in the subsurface and deep soil, particularly at 0.15 m (Figure 2).
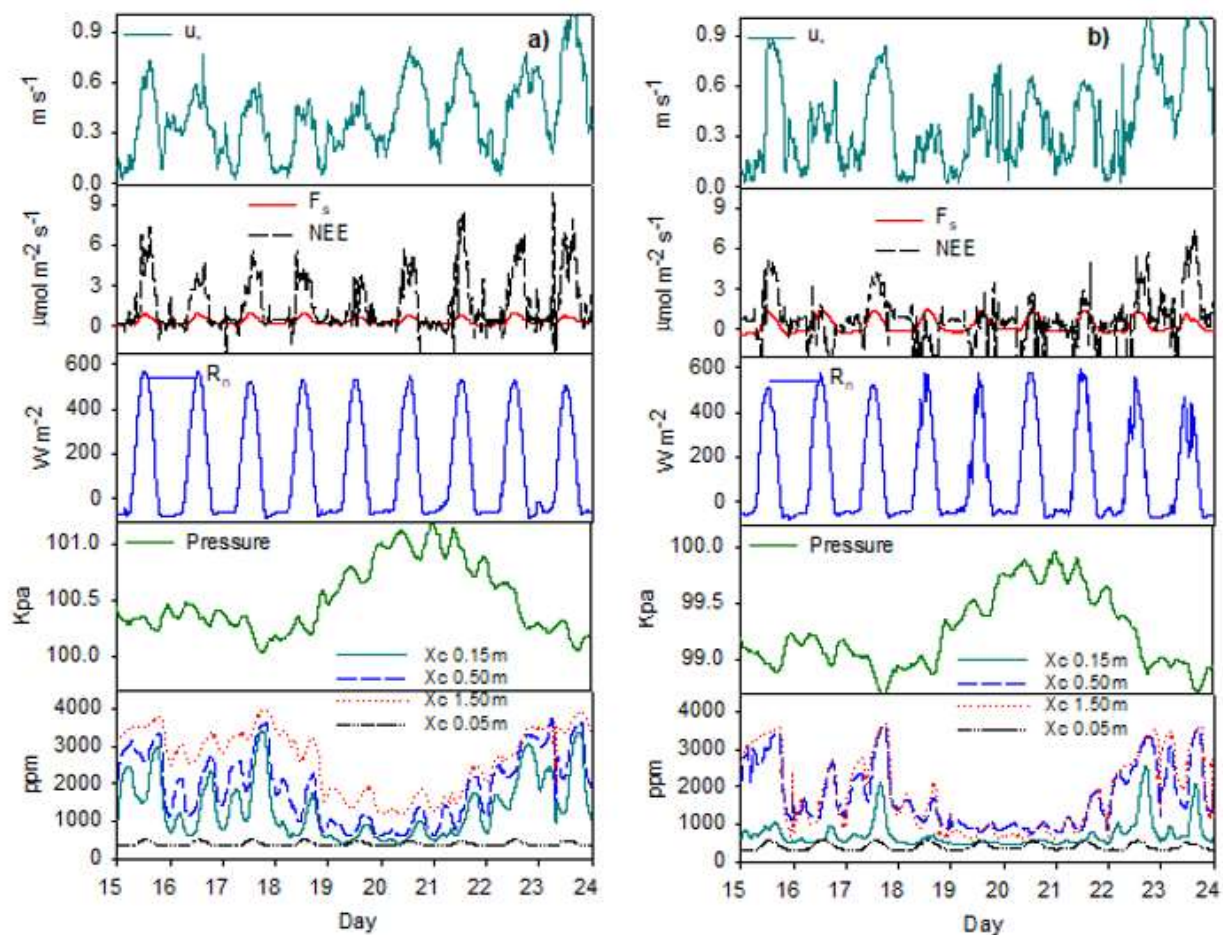
Figure 3. *Average half-hour time series of friction velocity (u_*), net ecosystem exchange (NEE), CO_2 fluxes at 0.05m (F_s), net radiation (R_n) atmospheric pressure and soil CO_2 molar fraction (χ_c) at 0.05m, 0.15 m, 0.50 m and 1.50 m depth during nine consecutive days (15/08/2015-23/8/2015) in Amoladeras (a) and Balsa Blanca (b) experimental sites.*
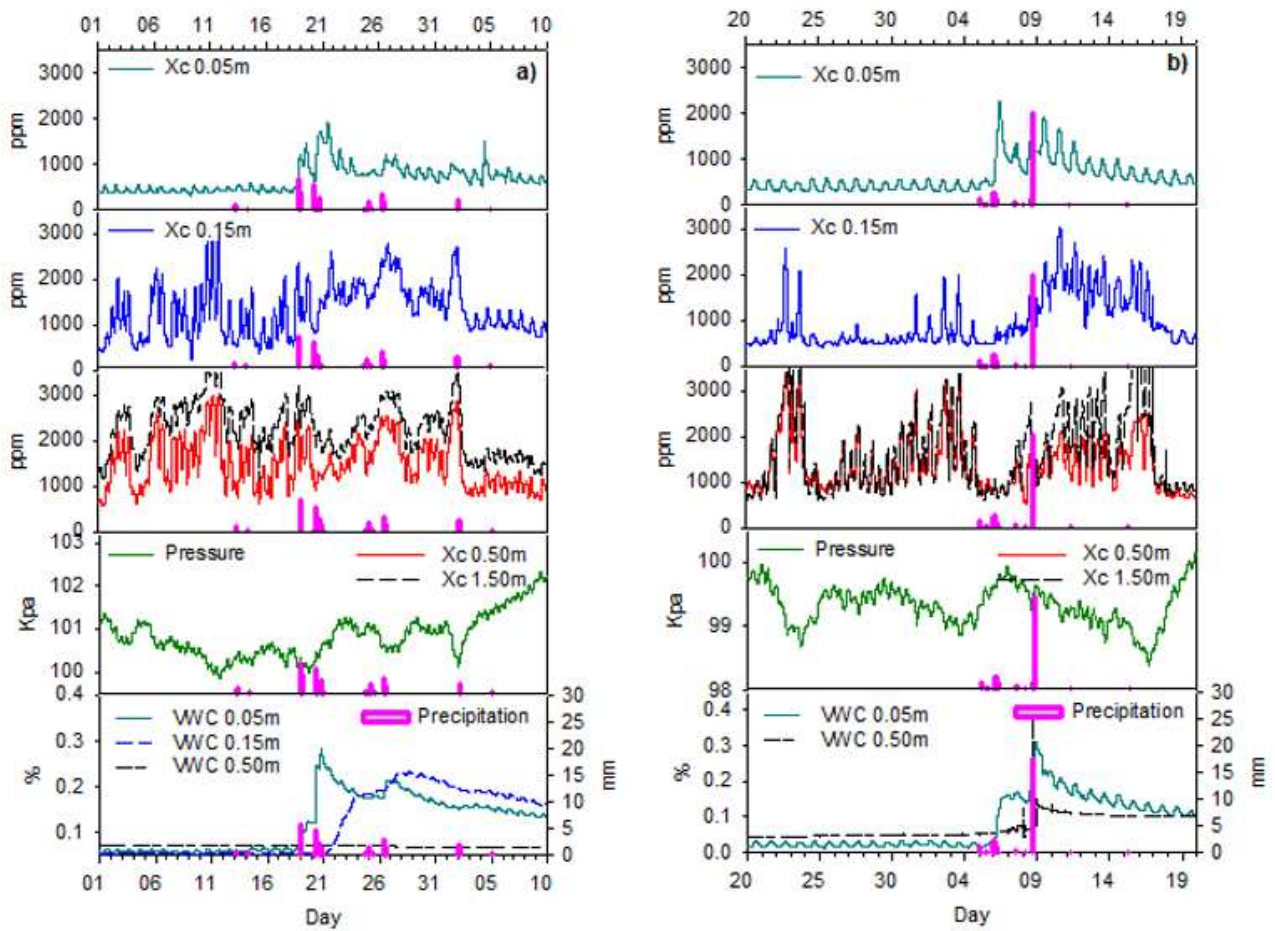
Figure 4. *Average half-hour time series of atmospheric pressure (kPa), precipitation, volumetric water content at 0.05 m, 0.15 m and 0.50 m (VWC) and soil CO_2 molar fraction (χ_c) at 0.05m, 0.15 m, 0.50 m and 1.50 m depth in Amoladeras (a) and Balsa Blanca (b) experimental sites during the periods 01/10/2015-10/11/2015 in AM and 20/08/2015-19/09/2015 in BB when a rain pulse occurred.*

3.3 DYNAMICS OF SOIL CO2 MOLAR FRACTION AT DAILY AND SYNOPTIC SCALE

During the whole study period, we detected a daily pattern in u_*, R_n, NEE, F_s and χ_c at surface. The χ_c daily pattern remains during pulse precipitation when soil respiration increases (Figures 3 and 4). Precipitation events in our experimental sites are produced during the first rains after the dry season (September–October; Figure 4) or after a big rain event (>15mm). During this intense or large rain events, χ_c increases sharply after watering and returns to similar previous values of χ_c progressively over several days (Figure 4). When precipitation events occur, χ_c at 0.05 m can raise up to 1500 ppm during periods of less than 12 hours (e.g. September 6 [th]; Figure 4).

At subsurface and deep soil, there was a sub-daily and synoptic pattern (from 3 to 8 days approximately) in p and χ_c, even during the first precipitation events at the end of the dry season, with inverse correlation between both variables (Figure 3). At the synoptic scale (oscillation in p induced by the passage of high- and low-pressure systems and fronts), p changes lasted from 3 to 8 days approximately. However, at daily scale there were two cycles per day, and the first generally had a lower amplitude than the second. At 0.15 m, only large rain events (>15 mm) triggered a χ_c increase in the daily pattern that also correlated with p variations. Regarding χ_c, daily fluctuations up to 2000 ppm CO_2 occurred during periods of less than 6 hours (e.g. August 17th; Figure 3). At all depths, χ_c was generally higher in AM (Figures 2, 3 and 4). On the other hand, χ_c showed similar values at 0.50 m and 1.50 m in BB (Figures 3 and 4), while in AM an increment in χ_c with depth was more evident.
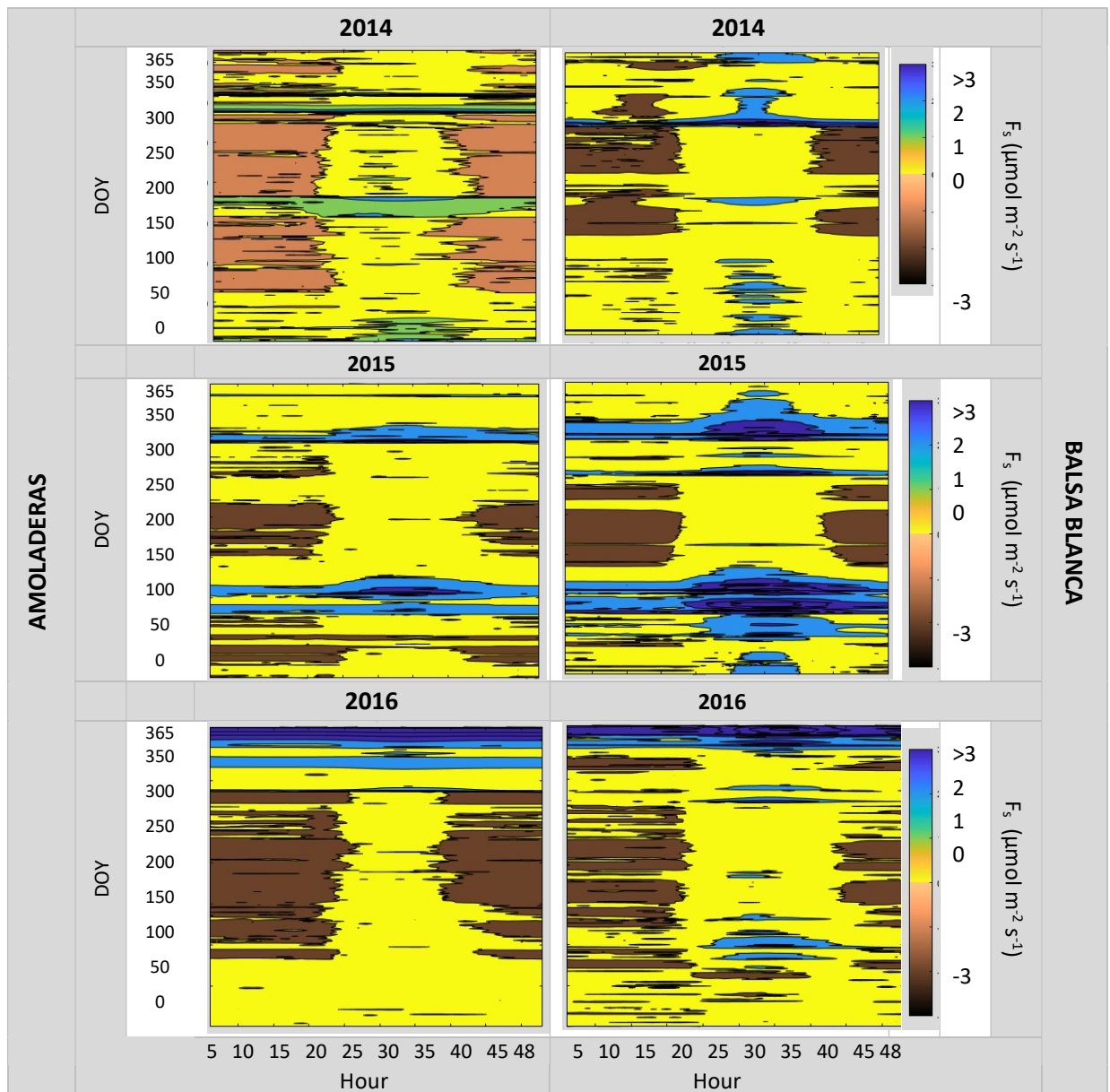
Figure 5. *Time series of half-hour values of soil CO₂ efflux in the horizontal profile at 0.05 m in Amoladeras (left) and Balsa Blanca (right) experimental sites during years 2014–2016. Brown areas denotes carbon uptake while yellow to blue areas denotes carbon release.*
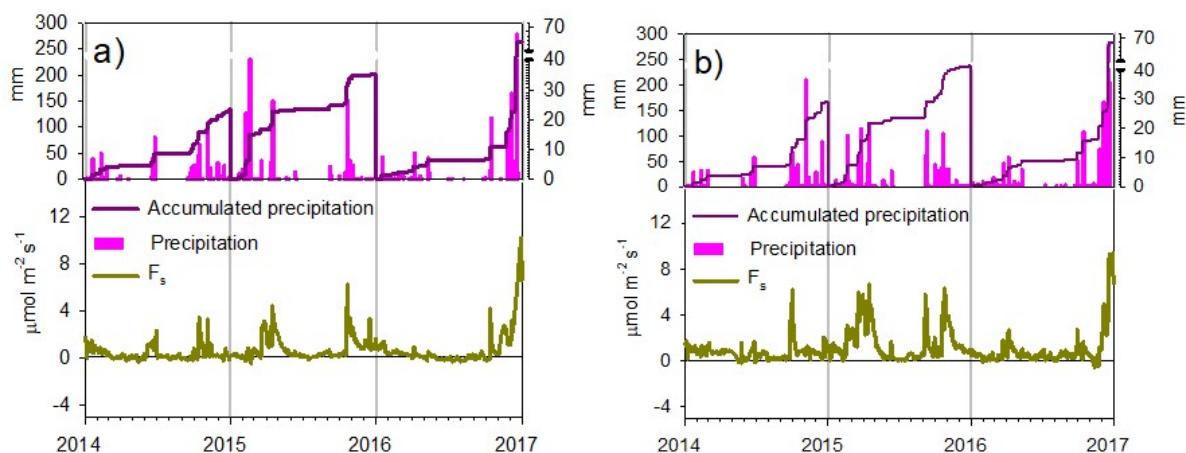
Figure 6. *Daily-averaged values of soil CO_2 efflux (F_s) at 0.05 m depth, daily precipitation and cumulative precipitation in Amoladeras (a) and Balsa Blanca (b) experimental sites during the study period (January 2014–December 2016). Negative values denote carbon uptake by the soil, and a positive value denotes a carbon emission to the atmosphere.*
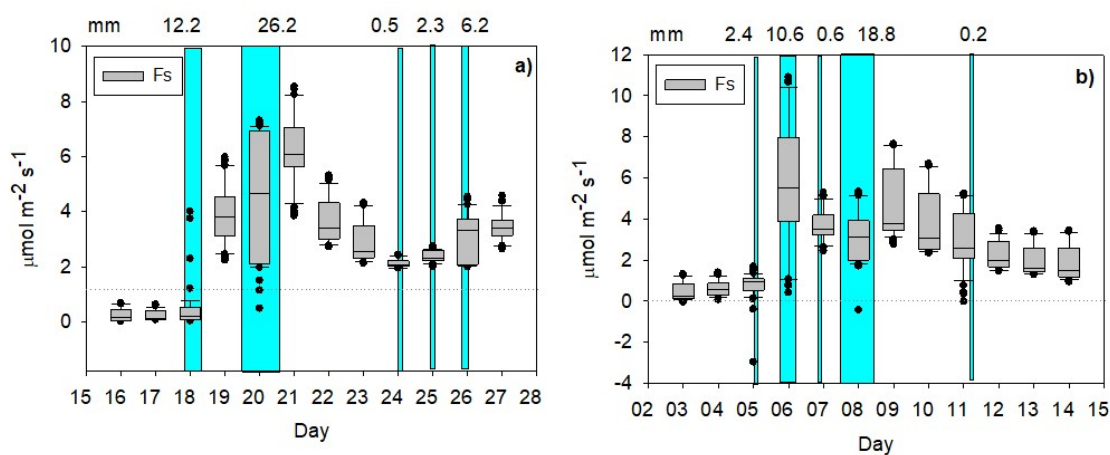
Figure 7. *Box-and-whisker plots of soil CO_2 efflux (F_s) at 0.05 m during twelve consecutives days with a rain pulse starting in day 4 in Amoladeras (a) and Balsa Blanca (b) experimental sites. The periods on the figures are 16/10/2015-27/10/2015 in AM and 03/09/2015-14/09/2015 in BB.*

A negative value denotes carbon uptake by the soil, and a positive value denotes a carbon source into the atmosphere. Blue bars denote precipitation events and the quantity of rainfall is indicated on the top of the figures. The middle line of box plot indicates the median; the upper and lower box bounds are the 25th and 75th percentiles. The error bars mark the 5th and 95th percentiles of the distributions.

3.4 SOIL FLUX DESCRIPTION

The empirical transfer model (k_s) obtained for our experimental sites can be written as:

$$k_s = D_a \, [0.0011 \, (\varphi - \theta)]^2 - 0.0044(\varphi - \theta) + 0.4611 \, ; \text{for AM (eq. 6)}$$

$$k_s = D_a \, [1.9870 \, (\varphi - \theta)]^2 - 0.7892 \, (\varphi - \theta) + 0.4714 \, ; \text{for BB (eq. 7)}$$

The empirical transfer models showed a $R^2 = 0.39$ and $R^2 = 0.41$ and RMSE = 0.007 and RMSE = 0.044 for AM and BB respectively.

Soil CO_2 effluxes (F_s) at 0.05m showed a clear annual irregular pattern influenced by rain pulse events (Figures 6 and 7). At daily scale, we detected a daily pattern in soil flux that correlates with χ_c at 0.05m, u_* and R_n. In general F_s was higher in BB (Figures 5 and 6). During most of the year, the fluxes were positives denoting carbon release to the atmosphere. However, several periods were found with negative values (carbon uptake by the soil) during night between March and July in AM and BB where nocturnal carbon uptake was around - 0.5 $\mu molCO_2$ m^{-2} s^{-1}. Was in AM when more periods with negative nocturnal fluxes were found. On average daily F_s was 0.66 ± 1.26 $\mu molCO_2$ m^{-2} s^{-1} in AM and 1.07 ± 1.57 $\mu molCO_2$

m^{-2} s^{-1} in BB. In periods not affected by rain pulses, minimum values were close to 0.3 $\mu molCO_2$ m^{-2} s^{-1} and maximum values were around 1-2 $\mu molCO_2$ m^{-2} s^{-1} in AM and 2-3 $\mu molCO_2$ m^{-2} s^{-1} in BB. However, immediately after the first rains after the dry season (September–October; Figure 6), or after a big rain event (>15 mm), the F_s increased quickly up to 8 $\mu molCO_2$ m^{-2} s^{-1} in AM and 10 $\mu molCO_2$ m^{-2} s^{-1} in BB and returns to similar previous values progressively over several days (~8 days; Figure 6). The annual cumulative CO_2 release was positive in AM and BB for the whole study period. The year with the highest cumulative F_s was 2015 with an annual emission of 310 g C m^{-2} $year^{-1}$ in AM and 564 g C m^{-2} $year^{-1}$ in BB. Emissions during 2014 and 2016 was respectively in AM 146 and 300 g C m^{-2} $year^{-1}$, and in BB, 284 and 368 g C m^{-2} $year^{-1}$. Comparison between F_s and NEE is shown in Table 1.

	Soil efflux (g C m^{-2} $year^{-1}$)			NEE (g C m^{-2} $year^{-1}$)
	2014	**2015**	**2016**	
AMOLADERAS	146	310	300	196 ± 40 (2009-2015; López-Ballesteros et al., 2018)
BALSA BLANCA	284	564	368	100 ± 40 (2006-2009; Rey et al., 2012) −23 ± 20 (2009-2015; López-Ballesteros et al., 2018)

Table 1. *Comparison between Net Ecosystem Exchange (NEE) published and soil efflux during the study period in Amoladeras and Balsa Blanca experimental sites.*

3.5 WAVELET ANALYSIS

We used the continuous wavelet transform (CWT) to explore the spectral characteristics of χ_c and VWC at different depths by decomposing into time–frequency space. With this technique we can describe the temporal variability of χ_c and VWC and how they vary in time. The areas (green, yellow and dark red respectively from low to high power values) inside the contour lines represent the dominant modes of variability with statistical significance ($p < 0.05$). Results in VWC and χ_c at 0.05 m shows a high power in the one-day band in almost all the period of study in BB and during the dry season in AM. Furthermore, the different precipitation events had different spectral signatures in the temporal correlation in both VWC and χ_c. The VWC have high power between a time-period of 1-to 30-days when some precipitation events occur. This pattern was observed in the χ_c continuous wavelet power spectra between a time-period of 1 to 8-days. This relation changes in depth because although precipitation events had effect in the VWC wavelet power, these peaks are barely reflected in the the spectral signature of the χ_c wavelet at the subsurface soil (0.15 m). Only the successional precipitation events occurred during December 2016 (>163 mm from DOY 1069 to 1096) had a spectral signature in χ_c in the 32-days days period in both BB and AM, and the precipitation events of DOY 448 (March 24th 2015, 24 mm) and DOY 616 (September 8th 2015, 18.5 mm) had a spectral signature of 8 to 64-days and 32-days respectively in BB. Finally, at the deep soil (0.50 m), changes in VWC only had effect on χ_c at annual scale considering the commonalities features in the wavelet power spectral signature.
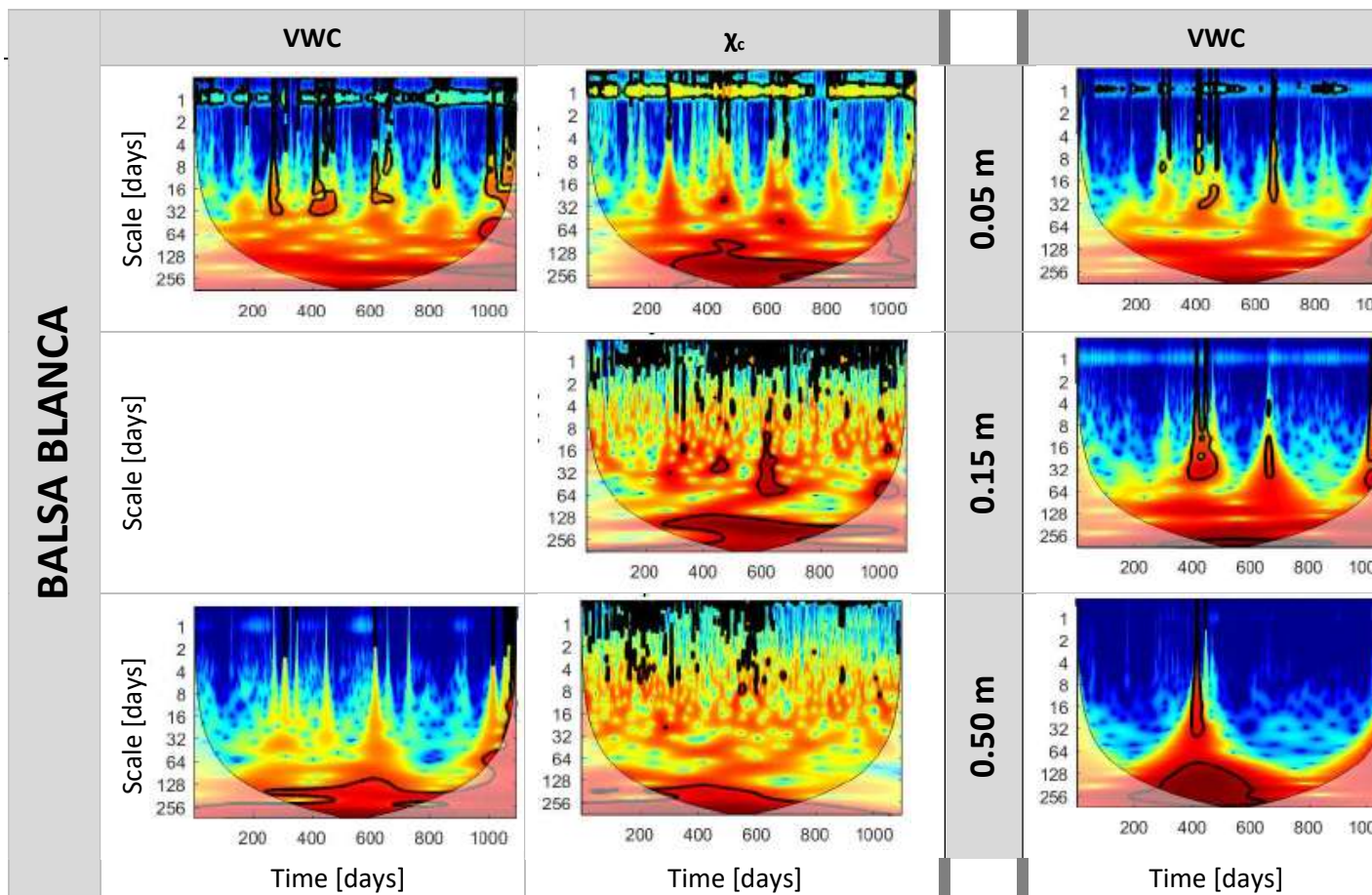
Figure 8. *Continuous wavelet power spectra using the continuous wavelet transform of soil water co* *fraction (χ_c) at three depths: 0.05 m (shallow), 0.15 m (interphase) and 0.50 m (deep) in Balsa Bla* *sites during three years (2014-2015-2016). The color codes for power values are from yellow (low* *Black contour lines represent the 5% significance level and the shaded area indicates the cone of inf* *influenced by edge effects.*

We used wavelet coherence analysis (WCA) to describe the temporal variability and test the temporal correlation between χ_c and ancillary variables related with biotic (T_{soil} and VWC) and abiotic (p and u_*) processes in BB and AM (Figure 9). The yellow areas inside the contour lines represent high local temporal correlation between both series at one specific scale with statistical significance ($p < 0.05$). The analysis in the surface layer (0.05 m) show that χ_c had a strong temporal correlation with the ancillary variables related with biotic processes (T_{soil} and VWC) at periodicities ranging from 0.5 day to ~1.5 days throughout the study period in AM in BB. There were also significant temporal correlations at higher periods related with precipitation events in both T_{soil} and VWC. This is especially relevant in the case of VWC, where precipitation events produce that the temporal influence of VWC on χ_c overrides the influence of T_{soil}, p and u_*. This temporal influence, from ~8 until ~60 days, was determined by the type of precipitation event. It was also remarkable, how the effect of T_{soil} at monthly, seasonal (> 128-days) and annual scale (> 256-days) was much more relevant in 2016, especially in AM. In relation with the variables related with abiotic processes (p and u_*), it was appreciable a daily and an annual temporal coherence more constant for BB than for AM. The temporal correlation between χ_c and u_* was higher and appreciable from a lower temporal scale (0.5~0.75) that the temporal correlation between χ_c and p. The effect of T_{soil} and VWC above χ_c was higher in BB, the ecosystem with the lower degradation status.

The causality relation of T_{soil}, VWC and u_* forcing variations in χ_c, was reduced with depth. The analysis in the interphase layer (0.15 m) shown strong spectral coherence between variations of T_{soil} or VWC and changes in χ_c at daily scale. However, this temporal correlation at daily scale was perfectly correlated in BB while in AM was less extensive and weaker in some periods, with both variables particularly correlated during dry

season. By other side, in BB there was a strong spectral coherence between variations of T_{soil} or VWC and changes in χ_c at seasonal (> 128-days) and annual scale (> 256-days), while in AM, was only appreciable and weaker in VWC. In relation with the abiotic variables, there was a daily strong spectral coherence in AM between u_* and χ_c. In BB this effect was also appreciable at daily and annual scale. Finally, the WCA shown that the temporal influence of p on χ_c overrides the influence of T_{soil}, VWC and u_*. At 0.15 m, p had a strong temporal correlation with χ_c at periodicities ranging from 0.5 day to ~30 days throughout the study period in AM in BB. This effect was weaker in BB, but also appreciable at seasonal and annual scale.

The analysis in the deep layer (1.50 m) was similar to the analysis in the interphase layer (0.15 m) with slightly differences between them. Variables T_{soil}, VWC and u_* shows strong spectral coherence with χ_c at annual scale, while the daily correlation was not significant (was not a reliable indication of causality) but presented in the wavelet. Probably, these extensive significant regions were very unlikely that this was simply by chance. By other side, the temporal correlation between p and χ_c was stronger and appreciable throughout all the study period at periodicities ranging from 0.5 day to ~30 days (daily, synoptic and monthly scale), and also at annual scale (> 256-days) in BB and AM. The WCA shown also that the temporal influence of p on χ_c overrides the influence of T_{soil}, VWC and u_*.

AMOLADERAS
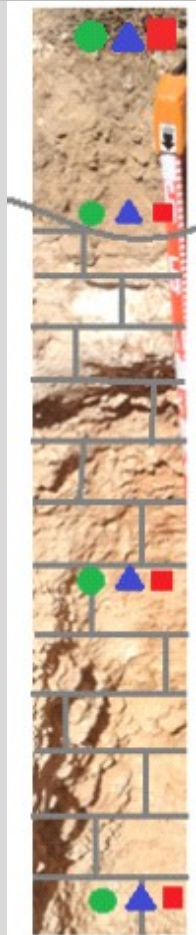
		VWC	T_soil	p
0.05 m	Shallow horizon	Period [days]		
0.15 m	Interphase layer	Period [days]		
1.50 m	Deep layer	Period [days]		
		Time [days]	Time [days]	Time [days]
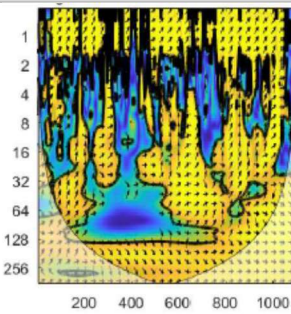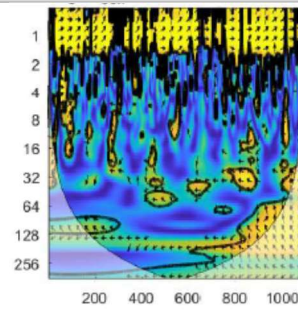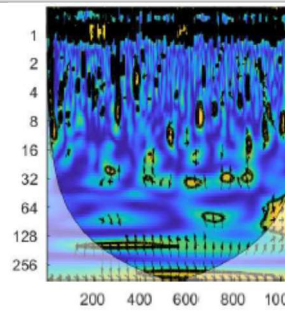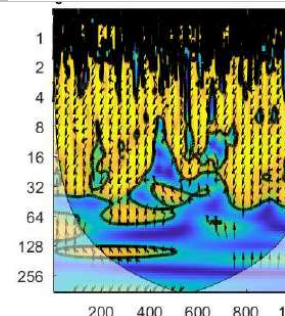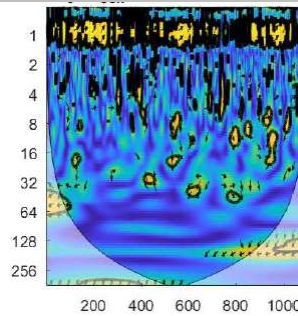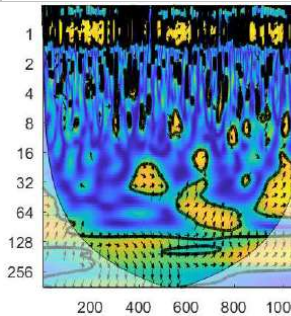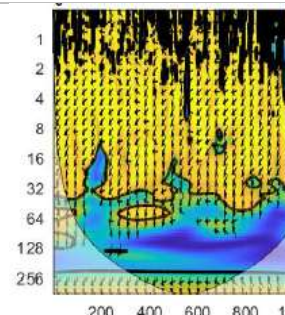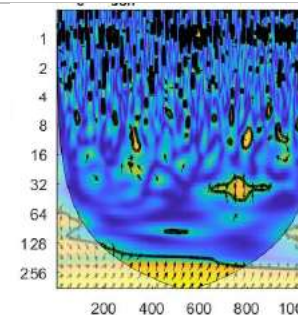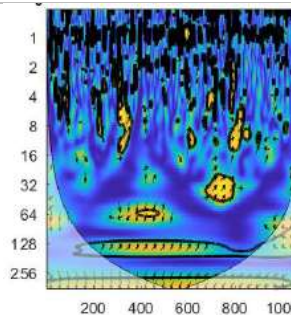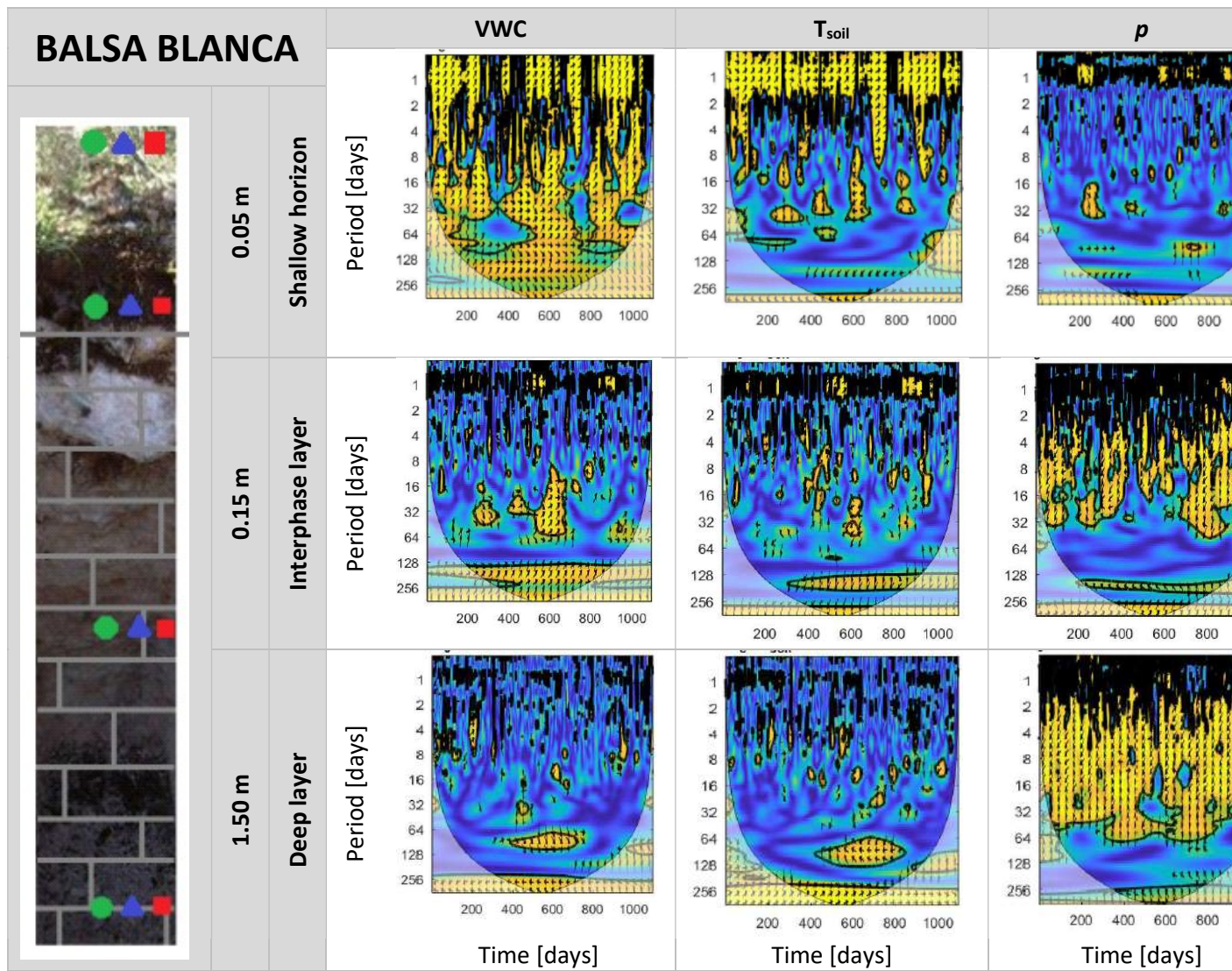
Figure 9. *Average 1-hour wavelet coherence analysis (WCA) to test the influence of soil water content (VWC), soil temperature (T_{soil}), atmospheric pressure (p) and friction velocity (u_*) on soil CO_2 molar fraction at three depths: 0.05 m (shallow), 0.15m (interphase) and 1.50 m (deep) in Amoladeras and Balsa Blanca experimental sites during three years (2014-2015-2016). Yellow areas with black contour lines represent a high significant temporal correlation with 5% significance level. Values ranges between 0 and 1, where 1 indicates the highest temporal correlation (and 0 for no correlation) between variables. Shaded area represents the cone of influence, where correlation is not influenced by edge effects.*

4. DISCUSSION

Through the analysis of edaphic variables at different soil depths forming the vadose zone surface, subsurface and deep soil together with the analysis of ancillary environmental variables, a decoupling in the soil CO_2 dynamic at different soil depths was found. How biotic and abiotic factors dominate the CO_2 dynamic and transport processes along the soil surface and the rest of the vadose zone is described below.

In the surface layer (0.05 m), the wavelet analysis show χ_c had a strong temporal correlation with the ancillary variables related with biotic processes (T_{soil} and VWC) at periodicities ranging from 0.5 day to ~1.5 days throughout the study period in AM in BB. This behaviour was supported by the well-known strong relation between soil CO_2 production from autotrophic (plants) and heterotrophic (microbes) biological sources with water availability in water-limited ecosystems (Curiel Yuste et al., 2007). The temporal influence of soil moisture in the soil surface layer overshadows the influence of T_{soil} and dominated the soil CO_2 dynamic (Figure 9). The presence of precipitation events had larger implications for the temporal influence of VWC and T_{soil} on χ_c at scales ranging from ~8 up to ~64-days, but also at seasonal (> 128-days) and annual scales (> 256-days). This supports the fact that temperature was only relevant in these ecosystems when the most limiting factor, the soil moisture, was available for metabolic processes (Leon et al., 2014; Almagro et al., 2009). E.g. during the rainiest year with lower soil moisture variability and lower water stress, the T_{soil} temporal influence was appreciable at higher temporal scales (monthly, seasonal and annual scale) much more that during 2014 and 2015, especially in AM.

The CWT analyses demonstrate that the temporal influences of VWC on χ_c determined by the type of precipitation event. It can be seen as

differences in the spectral signature of χ_c in the surface layer and subsurface layer derived for the different precipitation events (Figure 8). Results in VWC and χ_c at 0.05 m showed a high power in the one-day band in almost all the period of study in BB and during the dry season in AM. Furthermore, when some precipitation events occurred, the VWC had high power between a time-period of 1-to 30-days that were as well observed in the χ_c continuous wavelet power spectra at 0.05 m between a time-period of 1 to 8-days. This clearly common features in the wavelet power of the two-time series denoted a causality between χ_c and VWC. According to previous studies, the magnitude of the effect of each rain pulse was conditioned by the antecedent soil moisture (Almagro et al., 2009; Ogle et al., 2015; Shen et al., 2008), precipitation magnitude (Huxman et al., 2004; Potts et al., 2006), and the available organic matter supply for microbial respiration previously broken down by photodegradation (Austin & Vivanco 2006; Ma et al., 2012). Our results support the paradigm that the distribution and intensity of precipitation pulses influenced annual F_s. This relation changes in depth because although precipitation events had effect in the VWC wavelet power, these peaks were barely reflected in the the spectral signature of the χ_c wavelet at the subsurface soil. Only the successional precipitation events occurred during December 2016 (>163 mm from DOY 1069 to 1096) during March 24th 2015 (24 mm) and September 8th 2015 (18.5 mm) had effects on χ_c at 0.15 m. Thus, only large rain events (>15 mm) triggered a χ_c increase in the daily pattern at the subsurface soil (0.15 m; Cuezva et al., 2011; Jassal et al., 2005). These large events supposed the 5% of occurrence in AM and the 6% in BB during the period of study.

As was commented previously, depending on the timing, a small rain event could liberate more CO_2 than a subsequent large rain event (Xu & Baldocchi, 2004). The precipitation pulses at the beginning of each growing season for 2015 (i.e., September–October) were showed in figures 4 and 7.

They used to be large precipitation events (>15 mm; López-Ballesteros et al., 2017) but also small precipitation events (Rey et al., 2017; Schwinning & Sala, 2004) and were very relevant at ecosystem scale (Hastings et al., 2005; Huxman et al., 2004; Reynolds et al., 2004; Vargas et al., 2012). These events were the first rains after a long drought and mark the transition phase between dry and growing season in Mediterranean ecosystems (Cleverly et al., 2013; Lázaro et al., 2001). In our ecosystems, they resulted in an abrupt F_s increasing (up to 8 $\mu molCO_2\,m^{-2}\,s^{-1}$ in AM and 10 $\mu molCO_2\,m^{-2}\,s^{-1}$ in BB) followed by a prolonged exponential decay as the soil dries (Huxman et al., 2004; Jarvis et al., 2007; Xu & Baldocchi, 2004) between a time-period of 1-up to 16-days in AM and 1 up to 8-days in BB (figures 4 and 7). This effect on F_s has been attributed to the Birch effect (Birch, 1958; Jarvis et al., 2007). Affected by the precipitation event, litter that experienced antecedent photodegradation was rapidly dissolved by water and available for re-hydrated dormant microbes which tended to enhance respiration pulses (Ma et al., 2012). Soil microbial activity can be initiated within minutes of rewetting (García-Pichel & Belnap, 1996) breaking down the soil micro-aggregates that protect soil organic carbon, and stimulating their growth, metabolic activity, and reproduction (Austin & Ballaré, 2010; Austin & Vivanco, 2006; Brandt et al., 2009). The progressive decline of F_s, after the first peak following a rain pulse, was related to the depletion of water in soil pores as well as the reduction in soil labile organic matter (Huxman et al., 2004; Jarvis et al., 2007; Xu & Baldocchi, 2004). In addition to these biotic mechanisms, precipitation in semiarid and arid ecosystems has been shown to release the CO_2 bound to soil carbonates (Emmerich, 2003), and the infiltration of rainwater may displace CO_2 that accumulates in soil pore spaces during dry periods (Huxman et al., 2004).

Correlations between soil χ_c and p or u_* through the different soil layers showed in the WCA demonstrates the presence of abiotic non-

diffusive transport processes in the vadose zone CO_2 dynamic. The processes related with non-diffusive transport are pressure pumping (Massman et al., 1997; Mohr, et al., 2016; Roland et al., 2015), pressure tides (Clements & Wilkening, 1974; Kimball & Lemon, 1970; Glaser et al., 2004; Comas et al., 2011) and subterranean ventilation (Kowalski et al., 2008; Serrano-Ortiz et al., 2010). The wind velocity (or friction velocity) is the main trigger of ventilation (Flechard et al., 2007; Maier et al., 2010; Redeker et al., 2015), while changes in p is the main trigger of pressure pumping (Mohr et al., 2016; Takle et al., 2004) and pressure tides (Moya et al., 2019; Kuang et al., 2013; Le Blancq, 2011). At surface, during the whole study period, we detected a daily pattern in u_*, R_n, NEE, F_s and χ_c at surface layer. Figure 3 shows this daily pattern during nine consecutive days (15/08/2015-23/8/2015) during dry season in BB and AM. The positive fluxes observed in NEE were similar to the pattern described during ventilation events (Kowaski et al., 2008; Sánchez-Cañete et al.,2011): daily emissions at ecosystem scale during daytime, related with u_* and in some way also with R_n, both, important variables that triggers turbulence (Ganot et al., 2014; López-Ballesteros et al., 2017). Furthermore, ventilation events had been detected in the past in the experimental sites of BB (Rey et al., 2012) and AM (López-Ballesteros et al., 2017), with AM having the higher ventilation potential (López-Ballesteros et al., 2018).

These non-diffusive processes had different influence on χ_c through the different soil layers. The effect of biologic factors and u_* diminished with depth while the causality relation of p forcing variations in χ_c incresed (Figure 9). At surface, the temporal correlation between χ_c and u_* was higher and appreciable from a lower temporal scale (0.5~0.75) that the temporal correlation between χ_c and p. At 0.15 m the WCA showed that the temporal influence of p on χ_c overrides the influence of T_{soil}, VWC and u_*. At deep profile the influence of T_{soil}, VWC and u_* was only relevant at

annual scale while p had a strong temporal correlation with χ_c at periodicities ranging from 0.5 day to ~30 days throughout the study period at 0.15 m, and also at annual scale (> 256-days) at 1.50 m. In the same way, pressure tides are demonstrated that are produced at different low frequency scales implicating clear semidiurnal (Lindzen, 1979; Sánchez-Cañete et al., 2013a), diurnal (Kimball & Lemon, 1970; Le Blancq, 2011), synoptic (from 3 to 8 days; Auer et al., 1996; Clements & Wilkening, 1974; Elberling et al., 1998; Sánchez-Cañete, et al., 2013), quasi-monthly and monthly (Guoqing, 2005; Moya et al., 2019) temporal coherence. Sub-daily and synoptic patterns (from 3 to 8 days approximately) in p and χ_c at surbsurface and deep soil were shown in figure 3. Changes in p induced daily fluctuations in χ_c up to 2000 ppm CO_2 occurred during periods of less than 6 hours (e.g. August 17th; Figure 3). Changes in p conditions induced the expansion or contraction of the air stored in soil pores within the vadose zone. Pressure fluctuations penetrated deep into the soil vertical profile and the soil air expanded upward in conditions of falling p or is compressed downward under rising p (Redeker et al., 2015; Sánchez-Cañete et al., 2013a). The p influence was stronger in the deepest layer (Figure 8), where χ_c was higher and there was a lower influence of T_{soil} and VWC.

In the scientific literature there is a large variety of denominations associated to the non-diffusive transport processes: e.g. atmospheric or barometric pressure effect (Clements & Wilkening 1974; Elberling, 1998); atmospheric pumping (Nilson et al; 1991) or wind pumping (Fukuda, 1955; Weeks, 1994). This existing denomination heterogeneity is associated with the unclear distinction between pressure pumping, pressure tides and subterranean ventilation processes. Some authors have shown a positive relationship between pressure pumping and ventilation (Mohr et al., 2016; Nachshon et al., 2012; Redeker et al., 2015), due to the correlation presented between pressure fluctuations at high frequencies (e.g. 0.1 Hz) and wind

speed (Maier et al., 2010; Redeker et al., 2015; Takle et al., 2004). In contrast, pressure tides or atmospheric tides has been addressed as oscillations produced at low frequency scales (Kuang et al., 2013; Le Blancq, 2011; Lindzen, 1979; Massmann & Farrier, 1992). By other side, although pressure tides penetrate deep (>>10 m; Auer et al., 1996; Elberling et al., 1998) into the soil vertical profile with very little attenuation (Maier et al., 2010; Massmann & Farrier, 1992; Takle et al., 2004), the wind-induced gas transport produced by high-frequency pressure fluctuations, could penetrate up to 0.50 m in deep soil (Flechard et al., 2007; Nachson et al., 2012; Takle et al., 2004;), but are known to undergo strong attenuation with soil depth (Massman et al., 1997; Redeker et al., 2015; Takle et al., 2004). This is especially relevant in the artificially models e.g. Pourbakhtiar et al., (2017) established the critical depth of attenuation between 0.15 and 0.25 m layer applying a multi-dimensional gas transport model. Probably, pressure tides are produced in the sub-surface at low frequencies by large-scale atmospheric dynamics, while pressure pumping and ventilation are produced at high frequencies and limited to the shallower layer. This different capacity of permeability could create a possible decoupling between the surface layer, affected by ventilation, pressure pumping and pressure tides; and deeper layers that would be affected only by pressure tides. The subsurface layer would act as an interphase and being affected by pressure tides, pressure pumping and ventilation. This assumption could explain the different influence of u_* and p on χ_c in the WCA through the different soil layers.

The decoupling found, would imply functional differences at ecosystem scale between this non-diffusive transport processes. Our measurements suggest that atmospheric pressure fluctuations cause continuous changes in the CO_2 storage and the vertical transport (Comas et al., 2011; Glaser et al., 2004), showing significant seasonal, daily and

monthly patterns of variation (Redeker et al., 2015; Sánchez-Cañete., 2013). But it is important to note that there are no evidences that changes detected in the amount of CO_2 storage in the different soil layers provokes the release of this greenhouse gas to the atmosphere. However, ventilation is related with the CO_2 flux emissions detected at ecosystem level in our experimental sites (López-Ballesteros et al., 2018; Sánchez-Cañete et al., 2013a). This would imply that CO_2 transported between layers driven by pressure tides not produce directly changes in the net carbon balance in the ecosystem. In contrast, adventive transport driven by wind, induced CO_2 emission in the soil surface (Bowling & Massman, 2011; Kowalski et al. 2008; Takle et al., 2004). However, considering the WCA, pressure tides would contributes transporting vertically from deeper layers part of the CO_2 emitted later by pressure pumping and ventilation. Vertical transport produced by pressure tides, would explain the no detection of a decreasing concentration of χ_c at the surface layer found in other ecosystems (Hirsch et al., 2004; Sánchez-Cañete et al., 2011) during ventilation events.

A precise value for the diffusion coefficient has critical importance when using Fick's law to estimate soil CO_2 efflux from soil CO_2 concentrations (Laemmel et al., 2017; Roland et al., 2015). Potential effects of non-diffusive transport processes are not considered in the tradicionally soil respiration models. Experiments comparing in situ measurement methods and respiration ex situ models have demonstrated substantial deviation between observed and modeled diffusivities with soil carbon effluxes exceeeding the diffusion fluxes calculated by the gradient method up to 40% (Bowling & Massman, 2011; Massman et al., 1995), from 20 to 60-70% (Clements & Wilkening; 1974; Pourbakhtiar et al., 2017); by a factor of 2-4 (Kimball & Lemon; 1970; Maier et al., 2012) or by a factor of 5−10 (Takle 2004). For our experimental sites, we calculated soil CO_2 transfer coefficient (k_s) from soil CO_2 flux chamber in situ measurements

to get reliable estimations of soil CO_2 fluxes during whole the period (Sánchez-Cañete et al., 2017).

In the experimental sites, the calculated soil CO_2 efflux (F_s) for the years 2014 to 2016 show considerable interannual variability. During most of the year, F_s were positives denoting carbon release to the atmosphere (Figure 6). These positive F_s emissions were related with biotic and abiotic factors as demonstrates the WCA analysis, being precipitation events the main driver of emissions. In Balsa Blanca, precipitation pulses represented only 7% of dry season length but provoked approximately 40% of the carbon emitted during the dry seasons over 2009–2013 (López-Ballesteros et al., 2016). During summer, environmental conditions (water scarcity) tend to reduce the metabolic activity of living plant roots, soil microorganisms and soil fauna. López-Ballesteros et al., (2018) calculated the ventilate emissions in AM, getting that most part of the CO_2 emissions during May-September were produced by ventilation events. Furthermore, they found that VE was the main factor related with the great difference in annual C budgets between AM and BB sites (Table 1). The observed negative nocturnal F_s detected between March and July in AM and BB were related with abiotic factors by Hamerlynck et al., (2013) which related the negative F_s to processes of carbonate dissolution. This process also may happen in BB and AM where there is petrocalcic horizons (i.e., caliche) too.

As similar results were found in both experimental sites (they are located 23 km apart from each other) in the dependency found between VWC, T_{soil}, p and u_* with χ_c through the different soil layers, these similarities suggest that the same ecosystem behavior was extensible to the whole area affected by the same climate and soil type. However, some differences found between study sites may be relevant. In general, AM χ_c was more influenced by p and u_* changes in the subsurface and deep profile than in BB (Figure 5), while the influence of VWC and T_{soil} in the surface

layer was higher in BB. In relation with F_s, it was significantly higher and seems to be more responsive to rainfall events in BB. These differences would be related with the different degradation status present between ecosystems. The higher fraction of bare soil, the lower content in SOC and the coarser structure are "degradation indicators" showed by AM (López-Ballesteros et al., 2018; Rey et al., 2011). The deteriorated soil physical conditions, would increase in the interconnectivity between the soil medium and the atmosphere, and enhanced vertical transfer and storage capacity of soil CO_2-rich air from subsoil (Oyonarte et al., 2012). Differences in the VWC time recovery to base level after large precipitation events also suggest that the soil in AM favors drainage and is more porous than in BB, enhancing CO_2 storage and vertical transport. Hence, if these ecosystems are sources or sinks of CO_2 is likely to depend of the soil degradation status and the perturbations that leading to desertification could have important negative impacts in the carbon budget in this kind of ecosystems (Mouat & Lancaster, 2006).

CONCLUSIONS

Through the three year analysis of the CO_2 molar fraction and environmental variables (soil temperature, soil water content, pressure and friction velocity) in the vadose zone of two experimental sites, a clear functional decoupling were found between soil layers. The sensors were located at 0.05 m (surface layer), 0.15 m (subsurface layer), 0.50 m and 1.50 m (deep layer) depth. A wavelet analysis revealed that CO_2 concentration at surface layer was controlled by soil temperature, soil water content, pressure pumping and ventilation, being rain pulses events the most important factor controlling the carbon dynamic. The subsurface layer acted as an interphase layer affected by soil temperature, soil water content, pressure tides, pressure pumping and ventilation. Here, the rain influence only triggered variations in the CO_2 molar fraction in the daily pattern when large rain events (>15 mm) occur. The CO_2 concentrations in the deeper soil were influenced mainly by pressure tides. The physical decoupling found between pressure tides, pressure pumping and ventilation suggest that ventilation and pressure pumping only can emitted the CO_2 storage in the surface and subsurface layer while pressure tides would not be directly related with CO_2 emissions and its role in the ecosystem carbon dynamic would be related with the CO_2 vertical transport facilitating that deep CO_2 would be vented by pressure pumping and ventilation. Finally, two in-situ models were calculated using soil CO_2 flux chamber measurements to get reliable estimations of surface soil CO_2 effluxes. Thus, over whole study period (2014-2016) the annual soil CO_2 efflux was 254 ± 92 g C m^{-2} year^{-1} in Amoladeras and 405 ± 156 g C m^{-2} year^{-1} in Balsa Blanca.

Besides the global monitoring networks, few studies have been designed to monitor continuously the CO_2 exchanges from the soil and

coherent and continuous databases of soil CO_2 effluxes still do not exist. The consideration of abiotic process and the impact in the ecosystem carbon dynamic is often ignored, and most of the investigations was limited to a depth of few centimetres. The soils considered in this study stored large quantity of CO_2 in the vadose zone available to be vented. The carbon dynamic in semi-arid ecosystems has characteristics that make them unique due to the reduced biological activity and the relevance of non-diffusive transport processes. This study reinforces the importance of abiotic factors and mainly the soil moisture in predicting soil CO_2 efflux in arid regions. In semiarid sites similar to the sites studied here, we recommend that the experimental design in future experiments related to biological parameters (e.g. flux estimations, microbiological measurements, etc) should be focused on the first 0.15 m of soil, paying special attention in the first 0.05 m because this soil layer is the most affected by small precipitation events. In contrast, if the element of interest are the pressure tides, pressure pumping or ventilation, we recommend taking in account the whole vadose zone.

CHAPTER 3. ECOSYSTEM CO2 EMISSIONS DRIVEN BY WIND ARE PRODUCED IN DRYLANDS AT GLOBAL SCALE

Moya Jiménez, M. R., Sánchez-Cañete, E. P., Kowalski, A. S., Serrano-Ortiz, P., López-Ballesteros, A., Oyonarte, C., Domingo, F. Ecosystem CO_2 emissions driven by wind are produced in drylands at global scale.

ABSTRACT

Subterranean ventilation (VE) is a non-diffusive transport process that provokes the abrupt transfer of CO_2-rich air (previously stored) through water-free soil pores and cracks from the vadose zone to the atmosphere, under high-turbulence conditions. Although VE may occur in arid and semi-arid regions, which are unsung players in the global carbon cycle, little research has been focused on the role of VE CO_2 emissions in land-atmosphere CO_2 exchange. This study shows clear empirical evidence of globally occurring VE. To identify VE events, we used *in situ* quality-controlled eddy-covariance open data of carbon fluxes and ancillary variables from 145 sites in different open land covers (grassland, cropland, shrubland, savanna and barren) across the globe. The analyzed database was selected from FLUXNET2015, AmeriFlux, OzFlux and AsiaFlux networks. In order to standardize the analysis process, an algorithm was designed to detect CO_2 emissions produced by VE at all sites considered in this study. Its main requirement is the presence of considerable correlation between the friction velocity (i.e. turbulence) and CO_2 emissions. The 34% of the sites analyzed reported the occurrence of VE events. This vented CO_2 was found mainly in arid ecosystems (84%) and sites with hot and dry periods. Despite some limitations, this research demonstrates that VE CO_2 emissions occur globally. Future research should seek a better understanding of its drivers and the improvement of partition models, in order to reduce uncertainties and infer their contribution to the global net ecosystem carbon balance.

1. INTRODUCTION

The eddy covariance (EC) technique is a powerful tool (Aubinet et al., 2012; Baldocchi, 2014). Its use helps the scientific community to reach a better understanding of the Earth's climate system, an outstanding scientific challenge in the global change context (Reich, 2010; Solomon et al., 2007). With the EC technique, net fluxes of carbon dioxide (CO_2) and other trace gases, water and energy fluxes, can be measured at the ecosystem level over timescales of a half-hour or less with minimal disturbance to the underlying medium (Baldocchi et al., 2001). Despite some limitations inherent to the technique (i.e. its application is generally restricted to periods when atmospheric conditions are turbulent), annual integrations of CO_2 exchange have been demonstrated feasible (Wofsy et al., 1993) and the use of the EC towers has spread around the world.

With a growing number of EC towers worldwide, a set of regional (Aubinet et al., 1999; Isaac et al., 2016; Novick et al., 2018; Reich, 2010; Yu et al., 2006) and global networks (Pastorello et al., 2020) of EC flux measurement stations has been established. They provide an infrastructure for compiling, storing, and distributing open data of carbon, water, energy fluxes and related meteorological conditions to the scientific community. Examples of regional networks are AmeriFlux in the United States of America, CarboEurope in Europe; AsiaFlux in Asia, OzFlux in Australia or ChinaFlux in China. FLUXNET is considered a network of networks, and integrates information of many of the experimental sites included in these regional networks together. With more than eight hundred active and historic flux measurement sites distributed across most of the world´s climatic zones, FLUXNET is considered one of the largest environmental experiments in the world (Baldocchi et al., 2012). Despite its broad coverage, FLUXNET network has spatial observational gaps (Baldocchi,

2008; Bell et al., 2012; D. Schimel et al., 2015; Xiao et al., 2008). Thus, although arid and semiarid lands comprise approximately 40% of the global terrestrial surface (Reynolds et al., 2007) and play an important role in the global carbon (C) cycle (Ahlström et al., 2015; Lal, 2004), little is known about their functional behavior.

The flux tower community interprets CO_2 fluxes measured using EC technique as Net Ecosystem Exchange (NEE; Aubinet et al., 1999; Baldocchi, 2003). The NEE is generally defined as the difference between autotrophic uptake (gross primary production, GPP) and respiratory (autotrophic and heterotrophic) emission components (ecosystem respiration, R_{eco}; Falge et al., 2002; Valentini et al., 2000). However, other processes different from GPP and R_{eco} are included in the concept of the Net Ecosystem Carbon Balance (NECB). As defined by Chapin III et al., (2006), NECB is the net rate of organic plus inorganic C accumulation in an ecosystem, from all sources and sinks, regardless of the temporal and spatial scale at which it is estimated. In water-limited ecosystems, there is evidence of other processes, besides GPP and R_{eco}, that can significantly contribute to the NECB, at least on short time scales (Emmerich, 2003; Mielnick et al., 2005; Serrano-Ortiz et al., 2010); these include photodegradation (Rutledge et al., 2010), geochemical weathering (Hamerlynck et al., 2013), and subterranean ventilation (Kowalski et al., 2008).

Subterranean ventilation (VE) is a non-diffusive transport process that provokes the abrupt transfer of CO_2-rich air from the vadose zone to the atmosphere under drought and high-turbulence conditions (Kowalski et al., 2008). To make VE a significant component of the NECB, several conditions may co-occur. Firstly, vadose zone has to be well-aerated. A high quantity of soil pores and fractures interconnected with the atmosphere are needed in order to enable non-diffusive transport between vadose zone and

atmosphere (Pérez-Priego et al., 2013; Sánchez-Cañete et al., 2013a; Serrano-Ortiz et al., 2010). Furthermore, the soil pores must have low water content to allow gas flow. This condition commonly occurs during daytime and especially during the dry season coinciding with the dormancy period when water scarcity and high temperatures constrain biological activity (Cuezva et al., 2011; Risk et al., 2002; Roland et al., 2013; Sanchez-Cañete et al., 2011); during night time atmospheric stability, water deposition and vapor adsorption near the soil surface may inhibit ventilation. Secondly, high atmospheric turbulence conditions are indispensable to penetrate the vadose zone and produce the abrupt emissions of CO_2 from the vadose zone to the atmosphere via non-diffusive transport (Kowalski et al., 2008; Subke et al., 2003; Takle et al., 2004). For this reason, the wind velocity (or friction velocity) is the main trigger of this phenomena (Flechard et al., 2007; Maier et al., 2010; Redeker et al., 2015). Thirdly, the air located in the vadose zone must be significantly CO_2 rich (a high storage term is needed). In this sense, the concept of lateral transport has to be considered (Bourges et al., 2001; Chapin III et al., 2006; López-Ballesteros et al., 2017). Many of these conditions are inherent of drylands.

Recent publications using the EC technique have demonstrated that VE can temporarily dominate land-atmosphere CO_2 exchange in some Mediterranean ecosystems (López-Ballesteros et al., 2017; Pérez-Priego et al., 2013). However, most of this research analyzes the importance of VE at a local scale, while its relevance at global scale is still unknown.

The general aim of this study is to assess the relevance of VE at the global scale by analyzing flux data provided by FLUXNET and other related regional networks. Our main hypothesis is that VE events occur in water-limited ecosystems worldwide and is not a negligible process at the global scale. To test our hypothesis, we designed an algorithm, based on

previous scientific evidence, to systematically detect VE events in the 145 open ecosystems selected for this study. Therefore, our objectives are: 1) to detect daytime VE-driven CO_2 emissions in different ecosystems distributed around the world, 2) to assess the patterns of VE-driven emissions, 3) to investigate driving processes and triggers, and 4) to highlight the relevance of VE at the global scale.

2. MATERIAL AND METHODS

2.1   DATABASE SELECTION

To identify VE events we used *in situ*, quality-controlled eddy-covariance observations of carbon fluxes and ancillary data from FLUXNET and main regional EC networks that are available as open data to the science community. The datasets used in this study include the FLUXNET2015 database (https://fluxnet.fluxdata.org), the AmeriFlux database (http://ameriflux.lbl.gov), the OzFlux database (http://www.ozflux.org.au) and the AsiaFlux database (http://www.asiaflux.net).

Flux sites selection was limited to non-forested open ecosystems (Bond, 2019). Thus, only grasslands (GRA), savannas (SAV), woody savannas (WSA), open shrublands (OSH), closed shrublands (CSH) barrens or sparsely vegetates (BSV) and croplands (CRO) land covers were analyzed   (https://fluxnet.org/data/badm-data-templates/igbp-classification/). This selection yielded 588 site-years of EC data measured at 145 sites around the world. The sites selected were also categorized by climate using Köppen classification (KGCC; Rubel & Kottek, 2010) and the world dryland areas dataset (UNEP-WCMC; Sorensen, 2007). The latter is based on spatial analysis between the World Wildlife Fund terrestrial ecoregions (WWF-US; 2004) and aridity zones (CRU/UEA; UNEPGRID, 1991) according to United Nations Convention to Combat Desertification (UNCCD) and Convention on Biological Diversity (CBD) definitions.

The basic instrumentation of EC technique consists of a sonic anemometer (to measure 3-D wind velocity and virtual temperature at high frequency), an infrared gas analyzer (to measure CO_2 and water vapor densities at high frequency) and complementary sensors to measure other

meteorological ancillary variables at the flux site (e.g. air temperature, relative humidity, net radiation, precipitation). The flux and meteorological half-hourly data used in this analysis corresponded to quality-controlled data directly measured (i.e. minimum processing level). Therefore, we excluded post-processed gap-filled data (Papale & Valentini, 2003; Reichstein et al., 2005) from our analysis.

2.2 DATA PROCESSING METHODS

A novel algorithm was designed to automatically detect VE-driven CO_2 emissions among the analyzed flux data. Our algorithm employs the following criteria: (1) VE events are directly related with high turbulence conditions. Hence, an u_*-filtering threshold was applied to reject flux data during non-turbulent periods and to avoid the inclusion of measurement errors and spikes in the analysis; (2) there is no nocturnal VE due to soil re-humification; and (3) variability in air temperature and soil moisture had to be insufficient to explain variations of net CO_2 emissions (i.e. incompatible with ecophysiological interpretation of fluxes, such as the Birch effect at the end of the dry season).

The algorithm was applied to five-day intervals over one-year for each selected site. In accordance with our design criteria, these data were filtered according to the following constraints: only daytime [shortwave radiation incoming (SW_IN) or photosynthetic photon flux density incoming (PPFD_IN) > 50 W m^{-2}], positive fluxes [net ecosystem exchange (NEE) or carbon dioxide flux (F_c) > 0 $\mu molCO_2$ m^{-2} s^{-1}], mean air temperature (TA) absolute difference between day 1st and 5th < 3 °C, mean soil water content (SWC) absolute difference between day 1st and 5th < 1%, null precipitation (P > 0.00001) and with high-turbulence conditions (u_* >

0.2 m s^{-1}) data were used. Furthermore, only data with a maximum of 10% of gaps in the period selected and CO_2 fluxes (F_c) with maximum quality (flag qc = 0) were used. Partial Spearman correlation coefficients were computed over each five-day period filtered between F_c ($\mu molCO_2$ m^{-2} s^{-1}) and ancillary data: air temperature, vapor pressure deficit, soil temperature, atmospheric pressure, soil water content, photosynthetic photon flux density incoming, incoming shortwave radiation and friction velocity. Only five-day intervals with a partial Spearman correlation coefficient between F_c and u$_*$ above 0.2 and $p < 0.05$ were considered as VE events. The software Matlab was used for statistical analyses (Matlab, R2017a; MathWorks, Natick, Massachusetts, USA).

The algorithm was applied several times to each dataset with the following criteria: 1) for site-specific databases lasting from one to four years, the algorithm was applied to the whole database; 2) for site-specific databases lasting from five to six years, the algorithm was applied to the first four consecutive years; 3) for site-specific database lasting more than six years, the algoritm was appied to the first four non-consecutive years. In the ecosystems where our algorithm detected VE-driven CO_2 emissions, only one year was selected in order to simplify results and facilitates its representation. The year finally selected from each database corresponded to the year when our algorithm detected more VE events. The list of FLUXNET and regional EC networks sites used in this study with respective basic information is provided in the supporting information (tables S1, S2 and S3).

3. RESULTS

Of the 145 sites analyzed in our study, we found that 34% of them (50 sites) presented VE-driven CO_2 emissions according to the established criteria (Figure 1). Of these, 84% of them (42 of 50) are located in drylands, in accordance with the United Nations Convention to Combat Desertification (UNCCD) definition of Drylands (UNEP-WCMC; Sorensen, L. 2007). These VE-driven CO_2 emissions were frequent among the different dryland ecosystem types, occurring in half (3 of the 6) of arid drylands, 56% (24 of 43) of semiarid drylands, 57% (13 of 23) of dry subhumid drylands, and 64% (18 of 28) of additional dryland areas.

West Australia and the western USA are the main regions where this anomalous CO_2 emissions are produced. However, data availability conditioned this proportion. From the ecosystems analyzed in Europe 30% of them (6 of 20) gave positive results with half of these being located in SE Spain. In Asia 42% (5 of 12) of the experimental sites analyzed showed positive results with half of them concentrated on the Tibetan Plateau. In the USA and Mexico 34% (32 of 93) of the experimental sites analyzed gave positive results. These places are located in the lower part of USA, in the middle and in the west coast. Finally, in Australia 32% (6 of 19) of the experimental sites analyzed gave positive results. These places are located in the middle and east part of the country. Unluckily due to the lack of data availability in South America and Africa, there are no positive events detected in South America and only one ecosystem was found in South Africa of three places analyzed (30%).

a)

US-Rms US-SFP
US-Twt US-A74 US-Wjs US-IB1
US-SCg US-Ne1 US-SO4 US-Kon
US-Whs   US-Ctn US-AR2
                US-ARM US-IB2
US-SCw US-Fwf
US-SRG US-Var US-Bo1
US-SRM MX-Lpa US-Seg US-Bo2
US-AR1 US-SCd US-LWW
US-Aud US-Wkg

BE-Lon
FR-Gri IT-Bci
ES-Ln2 ES-Lju
ES-Amo

RU
CN-H

ZA-Kru

| arid; P/PET 0.05 - 0.20 |
| semiarid; P/PET 0.20 - 0.50 |
| dry subhumid; P/PET 0.50 - 0.65 |
| additional areas included in CBD definition |
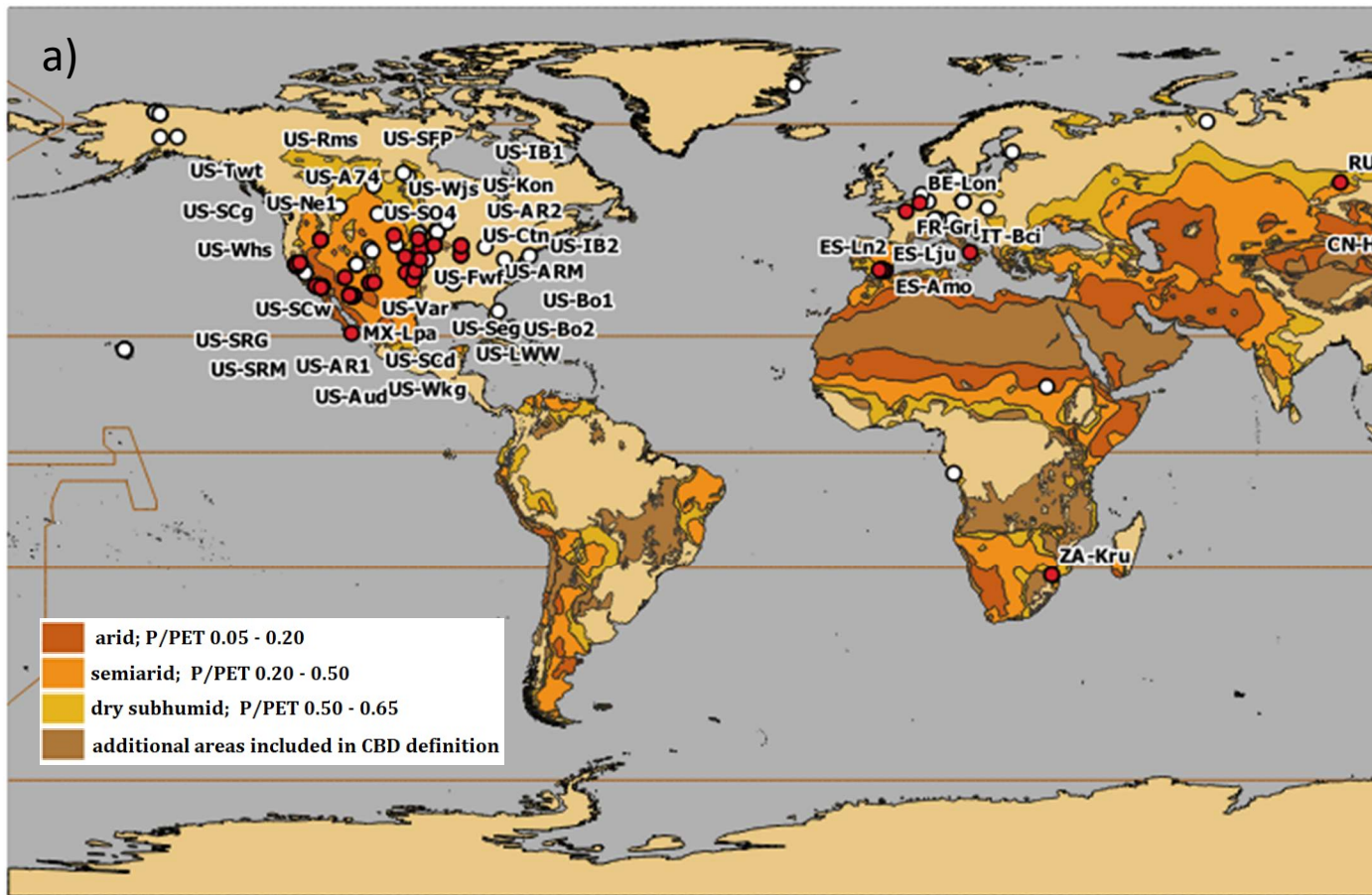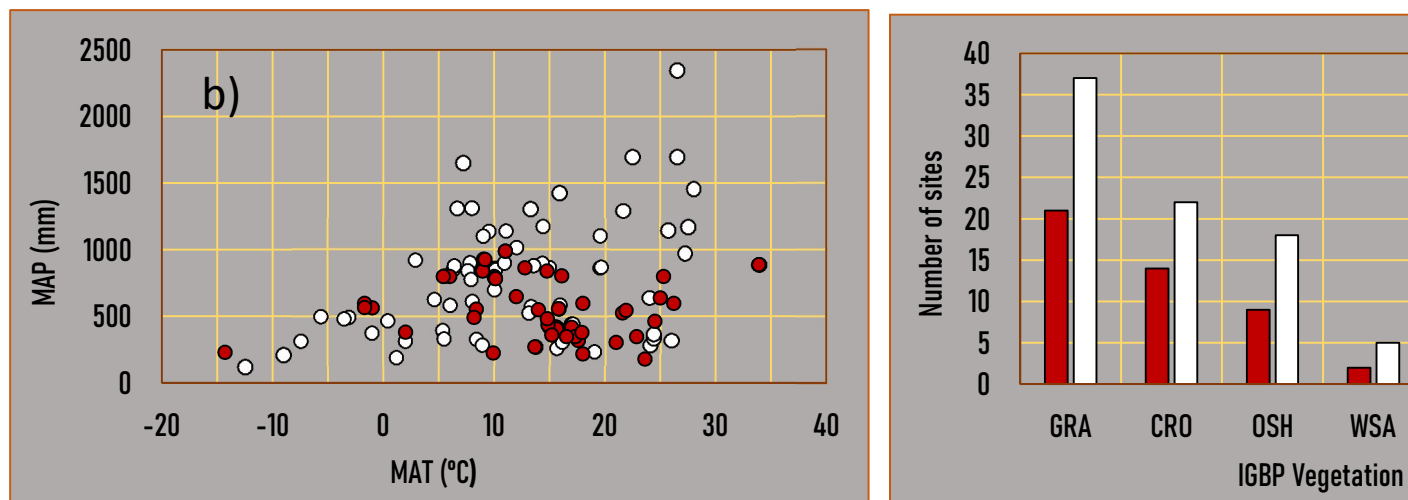
Figure 1. a) *World map distribution of FLUXNET2015, AmeriFlux, European Eddy Fluxes Cl*
analyzed in this study with distinction of experimental sites with (site marker in red) and without (site
emissions detected by our algorithm. On the map, the world dryland areas dataset classification (UN
according to dryness index PET/P (potential evapotranspiration/precipitation). Codes of sites wi
been included; b) Distribution of analyzed sites with (red) and without (white) VE emissions along
and mean annual precipitation (MAP) gradients; c) Number of analyzed sites with (red) and withou
IGBP land cover classification (grassland, GRA; savanna, SAV; woody savanna, WSA; open shrubla
barren or Sparsely Vegetated, BSV; and cropland, CRO).

The mean annual precipitation was below 1000 mm in all the experimental sites with VE events detected (Figure 1, b). The mean annual temperature ranges between -1 and 26 °C, although two ecosystems (Ru-Cok with -14.3 °C and US-A74 33.9 °C) far exceeded this range. The ecosystem types where more VE events were detected corresponded to grasslands, croplands, and open shrublands, in that order. From the rest of ecosystems analyzed, only one (in savannas and barrens or sparsely vegetates sites) and two places (in woody savannas and closed shrublands sites) showed VE events. More details for each experimental site can be found in the supporting information (S1, S2 and S3).

Figure 2 shows a selection of four experimental sites with VE events detected by our algorithm. This selection was chosen to exemplify the driving processes and patterns of VE events detected by our algorithm. US-Ctn is a grassland located in United States classified as cold arid steppe (BSk); ZA-Kru is a savanna located in South Africa classified as hot arid steppe (BSh); ES-Amo is an open shrubland located in Spain and classified as a cold arid steppe (BSk); and, AU-Dap is a grassland located in Australia and classified as equatorial with dry winter (Aw). Although these are ecosystems located in faraway regions, the ecosystem's dynamic is very similar between them. The sites described reveal a seasonal variability with two contrasting CO_2 exchange behaviours during two predominant periods: the growing and dry season. During growth periods, these sites act as net daily carbon sinks (not shown). However, during dry periods (when plants are dormant), these sites act as net carbon sources (Figure 2). Both, SWC, F_c and u_* shows a daily pattern. The parallelism in the daily pattern occurrence and magnitude of the CO_2 emissions (positive F_c) from the vadose zone towards the atmosphere were related with the intensity of the atmospheric turbulence in the surface (u_* value). Also, these emissions were

produced when SWC was very low. US-CTN and AU-DAP were in their 20th percentiles of annual soil moisture, and ES-AMO and ZA-KRU were in their 30th percentiles. The US-Ctn figure shows the "pre-emission" period and when ventilation events start, while in ES-AMO, ZA-Kru and AU-Dap the graph shows days when the ventilation events are presented also in previous days (not shown in the figure). When the SWC reached its percentile 30 in US-CTN our filter detects the first five-day periods of emissions (DOY 180-184). Although there are few days with turbulent conditions (high u_*) during night (DOY 150 in ZA-Kru and 178-179 in US-Ctn), all VE detected occurred always during daytime. The length of the emissions periods varies between years. For the selected year, the length of the emission periods was 258 days in ES-Amo (DOY 97-355), 47 days in US-Ctn (DOY 175-222), 149 days in AU-DaP (DOY 158-307), and 249 days in ZA-Kru (DOY 54-303).

VE events detected in the four experimental sites selected were directly correlated with u_* and the shortwave incoming radiation SW_IN (Figure 3). The value of the F_c-u_* partial correlation or the F_c-SW_IN partial correlation varies among the different VE events detected; however, the median was similar among ecosystems (between 0.44 and 0.55 the F_c-u_* correlation and 0.45-0.67 the F_c-SW_IN correlation). During these periods there were also positive and negative correlations with other variables measured in the ecosystems: air temperature (TA), vapor pressure deficit (VPD), atmospheric pressure (PA), soil temperature (TS), or/and soil water content (SWC). However, these correlations were more heterogeneous among ecosystems, weaker and not always significant.
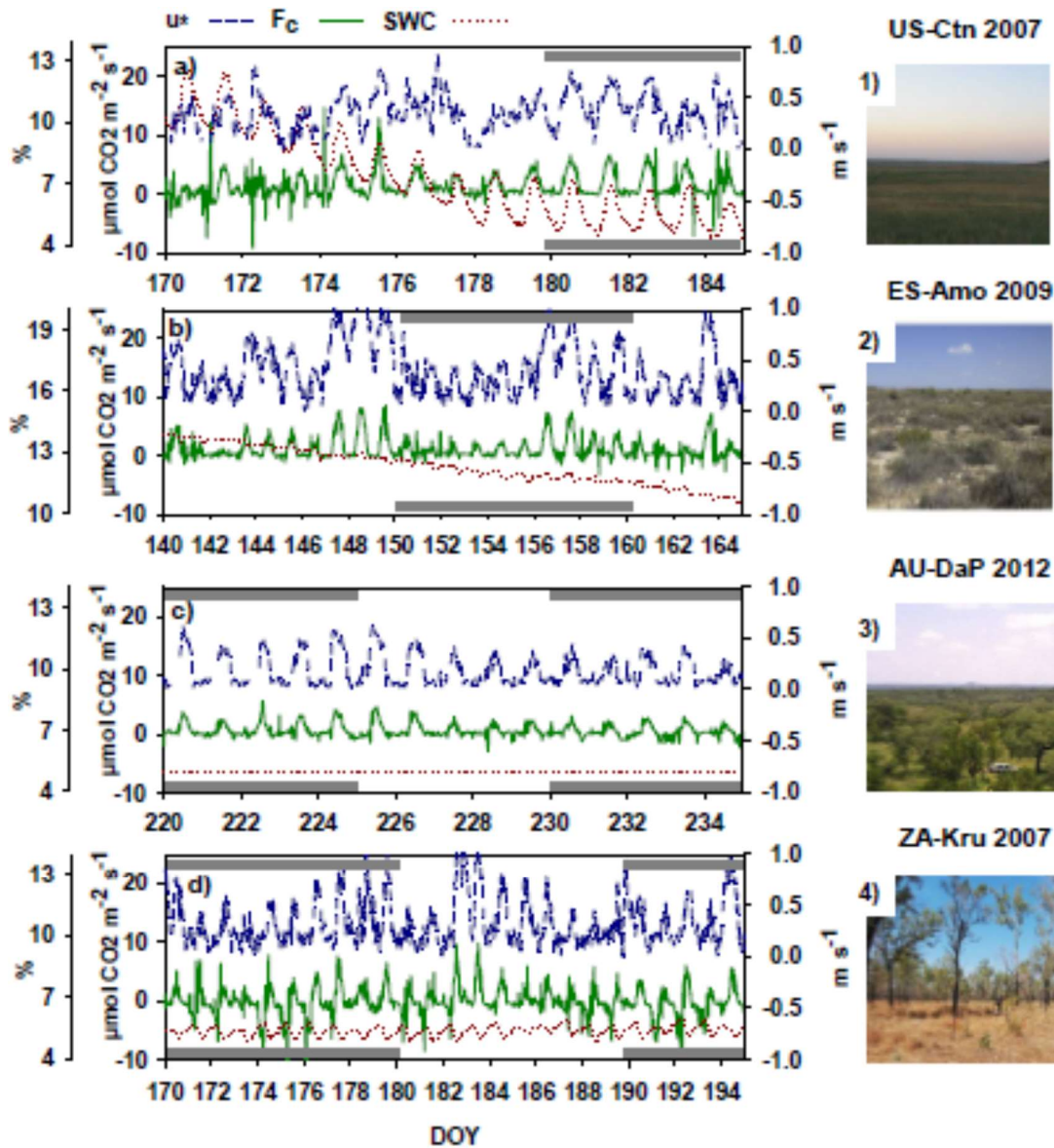
Figure 2. *Average half-hour time series of friction velocity (u_*; m s⁻¹) CO₂ fluxes (Fc; µmolCO₂ m⁻² s⁻¹) and soil water content (SWC;%) in: a.1) US-Ctn (Cottonwood, grassland, United States, AmeriFlux, 2007); b.2) ES-Amo (Amoladeras, open shrubland, Spain, FLUXNET, 2009); c.3) AU-DaP (Daly River Savanna, grassland, Australia, FLUXNET, 2012); d.4) ZA-Kru (Skukuza, savanna, South Africa, FLUXNET, 2007) experimental sites. A negative Fc denotes carbon uptake by the ecosystem, and a positive Fc denotes a carbon source into the atmosphere. Grey bars at the top and bottom of each figure*

denote the five-day periods for which VE events were detected via our algorithm. Photos from https://fluxnet.org/
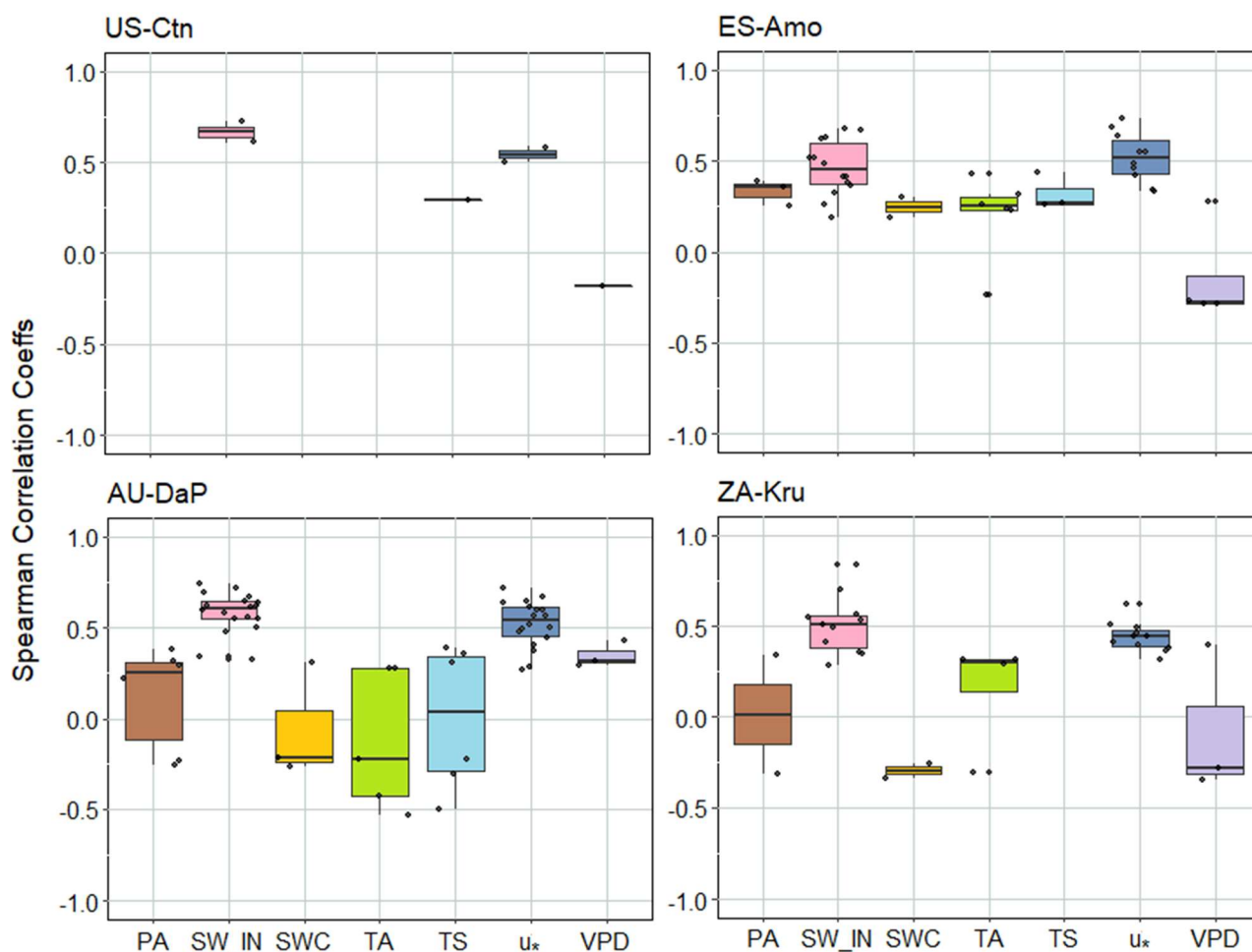
Figure 3. *Box-and-whisker plots of Spearman coefficients obtained from partial correlation between CO_2 fluxes (F_c) and friction velocity (u_*), air temperature (TA), vapor pressure deficit (VPD), atmospheric pressure (PA), soil temperature (TS), soil water content (SWC) or shortwave radiation incoming (SW_IN) in the five-day periods when VE-driven CO_2 emissions were detected at ZA-Kru, ES-Amo, US-Ctn and AU-Dap sites. Data shown have a p-value < 0.05.*
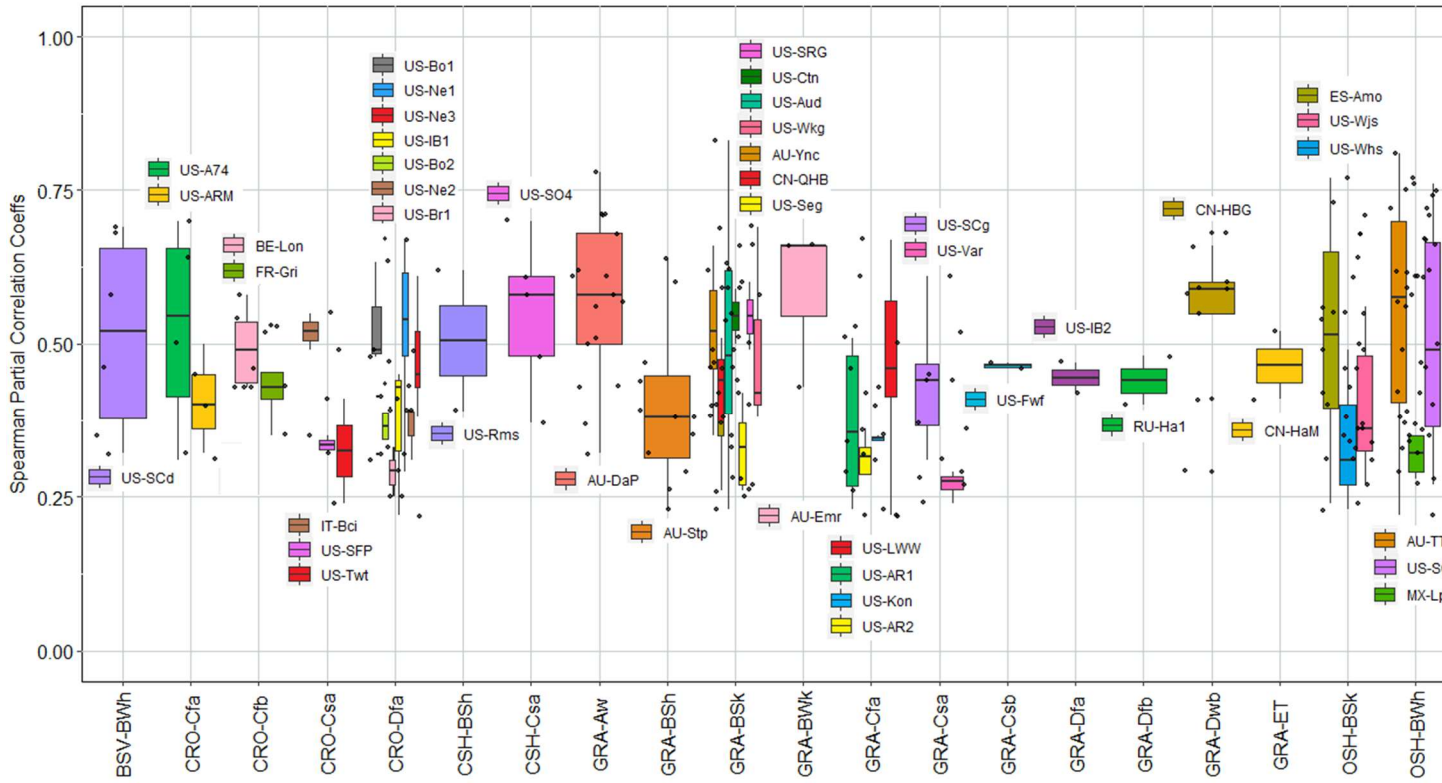
Figure 4. *Box-and-whisker plots of Spearman coefficients obtained from partial correlation betw... velocity (u∗) for all the flux sites where five-day VE events were detected by our algorithm. Sites are... cover (IGBP)] and Köppen climate classification (KGCC). Data shown have a p-value < 0.05.*

In the 50 sites with VE-driven CO_2 emissions, 300 VE-events were detected according to the established criteria by our algorithm. The Spearman correlation coefficients obtained from partial correlation between F_c and u_* was found similar in the climatic zones that showed VE events. They range between 0.2 and 0.8 with a median value around 0.5 (Figure 4). The climatic zones with the highest Spearman correlation coefficients were BWh (hot desert climate), BSk (cold steppe climate) and Aw (equatorial savannah with dry winter), while BSk, CSa (warm temperate climate with hot and dry summer), Cfa (warm temperate climate, fully humid with hot summer) and Dfa (Snow climate, fully humid with hot summer) showed the lowest Spearman correlation coefficients. Regarding VE occurrence frequency, BSk (28%) and BWh (18%) are the climatic zones with more VE events detected, and Csb (warm temperate climate with warm and dry summer; 0.7%) and Dfb (snow climate, fully humid with warm summer; 1.3%) the climatic zones with less VE events detected.

By region, the 50% of the Australian sites analyzed showed the highest coefficient median (AU-Emr [GRA-BWk], CN-HBG [GRA-DWb], AU-DaP [GRA-Aw], US-SO4 [CSH-Csa] and AU-TTE [OSH-BWh]). While the sites with the lowest coefficient median are located in USA and Mexico (US-Whs [OSH-BSk], MX-Lpa [OSH-BWh], US-Var [GRA-Csa], US-AR2 [GRA-Cfa], US-Twt [CRO-Csa], US-SPF [CRO-Csa] and US-BR1 [CRO-Dfa]). By land cover, GRA, and OSH are the ecosystem types with the highest and lowest partial Spearman correlation coefficients, respectively. Details of the Spearman correlation coefficients obtained for each experimental site analyzed are described in the supporting information S1.

4. DISCUSSION

Experimental sites with CO_2 emissions that could be mainly produced by subterranean ventilation (VE) were common and spread around the world. Based on previous scientific evidence, we designed an algorithm, to systematically detect VE events. After analyzing 145 open ecosystems (Bond, 2019) selected from main EC networks, 34% of them showed VE events (Figure 1a, and tables S1 and S2). The IGBP selection criteria was successful considering that 84% were located in drylands (Figure 1a) in accordance with the UNCCD definition of Drylands (UNEP-WCMC; Sorensen, 2007). The detection of VE events was quite balanced among the different kinds of drylands presented (50% in arid, 56% in semiarid, 57% in dry subhumid and 64% in the additional dryland areas).

The occurrence and magnitude of the CO_2 emissions (positive F_c) from the vadose zone towards the atmosphere were directly related with the intensity of the atmospheric turbulence in the surface (u_* value; Figures 2 and 3). No evident differences in the Spearman coefficients obtained from partial correlation between F_c and u_* were found among the climatic zones that showed VE events, since the similar ranges obtained for all analyzed climate-IGBP categories between 0.2 and 0.8 with a median value around 0.5 (Figure 4). Larger eddies promoted by high atmospheric turbulence conditions can penetrate within the vadose zone and produce an abrupt emission of CO_2-rich air from the vadose zone to the atmosphere via non-diffusive transport (Kowalski et al., 2008; Subke et al., 2003; Takle et al., 2004). At night, although there are days with turbulent conditions (DOY 150 in ZA-Kru and 178-179 in US-Ctn), VE events were not detected. As pointed out by other authors, at night-time water deposition and vapor adsorption near the soil surface may inhibit ventilation (Agam & Berliner, 2006; Cuezva et al., 2011; Kosmas et al., 2001; Verhoef et al., 2006). Our

results suggest that our algorithm can efficiently detect CO_2 emissions produced by VE.

Most VE events were detected during dry conditions, with SWC values below the 30th percentile of site-specific annual soil moisture. Such behaviour can be clearly observed in US-CTN site (Figure 2, a), where the first five-day period of emissions (DOY 180-184) was detected when the SWC decreased down its 30th percentile during day-time and over the dry season. Due to the lack of water inputs, the interconnectivity between vadose zone and the atmosphere can allow for an effective gas transport across the land surface (Cuezva et al., 2011; Risk et al., 2002; Roland et al., 2013; Sanchez-Cañete et al., 2011). This dryness condition can correspond to an inherent feature of the ecosystem (i.e. US-Ctn, AU-DaP or ES-AMO) or to a climate extreme, such as a drought event (i.e. ZA-Kru). It is also remarkable how the mean annual precipitation is a limiting factor above 1000 mm in all the experimental sites with VE events detected (Figure 1, b).

The shortwave incoming radiation (SW_IN) also constitutes an important meteorological variable involved in the VE CO_2 emissions detected (Figure 3) probably because solar heating is an important mechanism that triggers turbulence (López-Ballesteros et al., 2017; Stull, 1988). In relation with the VPD determinant, López-Ballesteros et al., 2017 found VE CO_2 efflux at high turbulence and specific VPD conditions.

In relation with the F_c-pressure correlation, several processes would be involved. Pressure pumping (Massman et al., 1997; Mohr, et al., 2016; Roland et al., 2015), pressure tides (Clements & Wilkening, 1974; Kimball & Lemon, 1970; Le Blancq, 2011) and VE are non-diffusive transport processes affected by atmospheric pressure changes at different temporal scales. For them, a well-aerated soil (Pérez-Priego et al., 2013; Sánchez-Cañete et al., 2013a), dry conditions and high atmospheric turbulence

conditions are indispensable to produce the subsoil CO_2 emissions. For this reason, there is no clear distinction between pressure pumping, pressure tides and VE. Some authors have shown a positive relationship between pressure pumping and ventilation (Mohr et al., 2016; Nachshon et al., 2012; Redeker et al., 2015), due to the correlation presented between pressure changes and wind perturbations at high frequencies (Maier et al., 2010; Redeker et al., 2015; Takle et al., 2004). However, other authors (Moya et al., 2019; Sánchez-Cañete et al., 2013a) found a temporal and spatial decoupling between VE and pressure tides. Pressure tides were produced in the sub-surface at low frequencies by large-scale atmospheric dynamics (Elberling et al., 1998; Guoqing, 2005; Lindzen, 1979), while VE is produced at high frequencies and limited to the shallower horizon (Redeker et al., 2015; Takle et al., 2004).

Production and transport of CO_2 may be lagged in time in ecosystems affected by VE (Chapin III et al., 2006). Due to water dependency, in ecosystems affected by VE, flux measurements reveal two contrasting CO_2 exchange behaviours during two predominant periods: the growing and dry seasons (López-Ballesteros et al., 2017; Pérez-Priego et al., 2013; Serrano-Ortiz et al., 2014). During growing periods, sufficient soil moisture enables autotrophic and heterotrophic biological activity and inhibits VE by lowering vadose zone and atmosphere interconnectivity. However, during dry periods, the low soil moisture provokes that biological processes involved in the production and consequent emission of CO_2 may occasionally play a secondary role leading VE to become determinant in annual NECB while allowing a more efficient gas transport between soil/vadose zone and the atmosphere. For example, in Figure 3, the effect of TA, VPD, PA, TS and SWC were more heterogeneous among ecosystems, weaker, and not always significant, compared to SW_ IN and

u_*, which suggests the predominance of VE over GPP or R_{eco} during drier periods.

Based on our results (Figures 2 and 3), ecosystems affected by the VE process, tended to act as CO_2 sinks during their growing seasons and CO_2 sources during their dry seasons. What is more, this study suggests that the high interannual variability of F_c in ES-Amo and ZA-Kru could be a consequence of the frequency and intensity of VE events. ES-Amo acted an annual net source of CO_2 with ranging from +163 g C m-2 yr^{-1} to +324 g C m^{-2} yr^{-1} over 2009-2015 (López-Ballesteros et al., 2017), whereas ZA-Kru varied from −138 to +155 g C m^{-2} yr^{-1} over 2000-2005 (Archibald et al., 2009). Differences in the F_c balance among years depended on the length and severity of the dry season, which was determined by the magnitude and timing of precipitation events (Gilmanov et al., 2006; Luo et al., 2007; Ma et al., 2007; Meyers, 2001; Pereira et al., 2007). Therefore, the duration of dry conditions might correlate with VE-driven CO_2 emissions, and could be the most important factor determining the variability in the annual ecosystem C balance.

The VE magnitude would be also related to the volume and concentration of CO_2 stored in the vadose zone available to be vented. Although we did not find any relation between site-specific soil type and occurrence of VE events (data not shown), a minimum gas permeability of the soil matrix is needed to make VE happen (Figure 2; Pérez-Priego et al., 2013; Sánchez-Cañete et al., 2013a). In this sense, vadose zone systems containing caves, macropores and fissures usually coincide with carbonated parent soil material, which can temporally store large amounts of CO_2 below ground (Decarlo & Caylor, 2020; Emmerich, 2003; Serrano-Ortiz et al., 2010). A vadose zone with significantly CO_2-rich air is also presented in some drylands with low soil organic carbon (SOC) production. For example, in ES-AMO, the CO_2 vented is higher than variations of in situ

SOC pools presented in the ecosystem (López-Ballesteros et al., 2017). In these ecosystems, the vadose zone is beyond the ecosystem conceptual boundaries and the released CO_2 might be lagged in space (Bourges et al., 2001; Chapin III et al., 2006). The observation of the underground CO_2 concentrations measurements is useful to prove the occurrence of VE processes (Sanchez-Cañete et al., 2011). Unfortunately, there is scarce information available on CO_2 dynamics below the soil surface and they are barely presented in the databases analyzed.

The co-existence of other processes involved in the NECB, acting together with VE, is far from sufficient to explain the large magnitude of the daytime CO_2 emissions detected by our algorithm (Figures 2 and table S1). For instance, some estimations of CO_2 fluxes corresponding to photodegradation of senescent organic matter correspond to very low CO_2 effluxes (Austin & Ballaré, 2010; Austin & Vivanco, 2006; Brandt & Adair, 2012), i.e. 0.015 μmol m^{-2} s^{-1} in microcosms in lab under natural solar radiation (Brandt et al., 2009) and 0.179 μmol m^{-2} s^{-1} in annual grasslands during the dry season (Rutledge et al., 2010), respectively. Likewise, short-term estimates of geochemical weathering and calcite precipitation are estimated to correspond to very low CO_2 effluxes (Goddéris et al., 2006; Hamerlynck et al., 2013; Roland et al., 2013) of ca. 0.05 μmol m^{-2} s^{-1} (Serrano-Ortiz et al., 2010). Finally, the production of geogas is associated with seismicity and volcanic and geothermal systems (Burton et al., 2013; Etiope et al., 1999; Lewicki et al., 2003; Mörner & Etiope, 2002), however, to know how this process interacts with VE we need further investigation.

Finally, the EC databases used in this study presented some limitations in order to provide more in-depth information on the global VE relevance. These limitations include: 1) the presence of long-term gaps in many databases made it difficult to calculate the contribution of VE at the annual scale; 2) the limited length of the time series (the majority of EC flux

sites analyzed are usually limited to only 3–5 years of measurements) could be an issue (Schimel et al., 2015; Sulkava et al., 2011; Sundareshwar et al., 2007) to determine the effect of VE in the interannual variation in the ecosystem C balance; 3) the heterogeneity among databases (absence of some variables collected and differences in data quality) and the lack of information and/or parameter misspecification in the metadata made it difficult to establish relations between VE and other variables across the different types of ecosystems; and 4) the spatial representativeness in the EC databases (D. Schimel et al., 2015; Sulkava et al., 2011; Sundareshwar et al., 2007) was not sufficient to capture the natural variability of climatological and biological conditions in some geographical regions. FLUXNET and regional network sites are mainly located in ecosystems with annual temperatures between 5 and 17 °C, annual rainfall between 600 and 1250 mm, and latitudes above 30º N (Vargas et al., 2013). Furthermore, longer datasets are limited to temperate and boreal ecosystems (Chu et al., 2017; Pastorello et al., 2017; Pastorello et al., 2020). Thus, regions more vulnerable to environmental or climate change are still underrepresented (Bell et al., 2012). Many of these regions are drylands or prone to desertification (Emmerich, 2003; Eswaran et al., 2000; Huenneke et al., 2002; Schlesinger et al., 1990), which makes VE potentially relevant now and even more so in the future (Ahlström et al., 2015).

These issues create uncertainties that severely limit our ability to better understand VE processes and make confident estimations of the contribution of VE in the global terrestrial carbon balance. Nevertheless, the results achieved in this work are very relevant because the presence of VE have been identified in many arid and semiarid lands which constitute the largest biome in the world (Schimel, 2010).

CONCLUSIONS

The present study is a step toward to better understanding the processes involved in the global C cycle. After analyzing eddy-covariance open data observations of carbon fluxes and ancillary data from 145 common semiarid ecosystem types from FLUXNET and its main regional networks, we can confirm that subterranean ventilation CO_2 emissions occur globally.

The occurrence and magnitude of the CO_2 emissions from the vadose zone towards the atmosphere were directly related to changes in friction velocity (indicator of atmospheric turbulence), the triggering variable. The soil water content and annual rainfall were found as limiting factors. Only when the soil water content declines to values below the 30 percentile of site-specific annual soil moisture, could the interconnectivity between vadose zone and the atmosphere allow for an effective gas transport across the land surface. These subterranean ventilated CO_2 emissions occurred in dry ecosystems, but also in ecosystems where dryness was not an inherent feature of the ecosystem. It varied from days to weeks, and occurred only during daytime. The Spearman coefficients obtained from partial correlation between u_* and CO_2 fluxes was found to be similar across the different climatic zones analyzed. Finally, depending on the length and severity of the dry season, ventilation events could determine the variability in the annual ecosystem C balance in these ecosystems as a sink or source of CO_2.

Our results suggest that our algorithm can efficiently detect CO_2 emissions produced by VE and constitutes a useful tool to its detection to be used in future research. Global warming and anthropogenic disturbance will increase the rate of drying in ecosystems leading to more frequent and intense drought events. This drying could provoke an ecosystem

degradation favoring a greater exposure of subsoil CO_2 to ventilation and affecting negatively in the trend of global carbon sequestration. Understanding the occurrence of processes, feedbacks and driving factors that modulate the carbon (C) source capacity of natural ecosystems due to ventilation events is needed to advance towards more robust model projections for future climate as well as more adequate design of mitigation policies.

SUPPLEMENTARY MATERIAL

Site ID	Year	Periods detected	F_c potential	F_c-u_* corr	% gaps	
AU-DaP	2012	155-164, 170-189, 195-199, 210-224, 230-234, 240-269, 275-279, 285-294, 300-304	3.25 ± 0.69	0.57 ± 0.13	65	Jason Beringer, Lindsay Hutley (200... 10.18140/FLX/1440123
AU-Emr	2013	260-264,275-279,285-289	3.21 ± 0.69	0.58 ± 0.14	53	Ivan Schroder, Steve Zegelin, Tehar... Emerald, DOI: 10.18140/FLX/144019...
AU-RDF	2013	135-139, 160-169	2.45 ± 0.57	0.40 ± 0.08*	80	Jason Beringer, Lindsay Hutley (201... Northern Territory, DOI: 10.18140/F...
BE-Lon	2014	10-14, 25-34, 50-54, 60-64, 285-289	2.34 ± 1.03	0.49 ± 0.06	66	Anne De Ligne, Tanguy Manise, Chr... Heinesch (2004-2014) FLUXNET201...
CN-HaM	2002	45-49, 55-59	3.66 ± 0.90	0.47 ± 0.08*	44	Yanhong Tang, Tomomichi Kato, M... Alpine Tibet site, DOI: 10.18140/FLX...
ES-Amo	2009	100-104,150-159,165-194, 200-209, 215-249,335-344	4.86 ± 1.63	0.52 ± 0.15	37	Francisco Domingo Poveda, Ana Lóp... Serrano Ortiz, Mª Rosario Moya Jim... 2012) FLUXNET2015 ES-Amo Amola...
ES-Lju	2009	170-179,205-209,235-244	2.61 ± 1.92	0.46 ± 0.16	48	Erique Pérez Sánchez Cañete, Penél... Domingo Poveda, Oscar Pérez Prieg... 2013) FLUXNET2015 ES-LJu Llano de...
ES-Ln2	2009	150-154,165-199,205-209,215-219,230-249,265-269	4.52 ± 1.03	0.43 ± 0.16	66	Andrew Kowalsky (2009-2009) FLUX... 10.18140/FLX/1440226
FR-Gri	2006	265-279	6.46 ± 1.89	0.44 ± 0.07	63	Pauline Buysse, Brigitte Durand, Je... Larmanou, Pierre Cellier, Benjamin... 10.18140/FLX/1440162
IT-Bci	2008	260-269	6.52 ± 1.51	0.44 ± 0.07	67	Vincenzo Magliulo, Paul Di Tommas... Vitale, Antonio Manco (2004-2014)... 10.18140/FLX/1440166
RU-Cok	2003	140-144, 150-154	1.38 ± 0.08	0.42 ± 0.21*	78	Han Dolman, Michiel van der Molen... Dean, Ko van Huissteden, Trofim M... DOI: 10.18140/FLX/1440182
RU-Ha1	2004	275-280,285-289	1.72 ± 0.22	0.44 ± 0.05*	66	Luca Belelli, Dario Papale, Riccardo... steppe, DOI: 10.18140/FLX/144018...
US-AR1	2011	50-54, 75-79,180-184,220-224, 235-239, 320-324	3.50 ± 1.82	0.37 ± 0.13	39	Dave Billesbach, James Bradford, M... USDA UNL OSU Woodward Switchgr...
US-AR2	2010	200-204,220-224,240-244,260-264	3.38 ± 1.07	0.30 ± 0.06	35	Dave Billesbach, James Bradford, M... USDA UNL OSU Woodward Switchgr...

US-ARM	2003	155-159,160-164, 230-234	5.55 ± 0.59	0.41 ± 0.09	57	Sebastien Biraud (2003-2012) FLUXN... Lamont, DOI: 10.18140/FLX/1440060
US-IB2	2008	95-99,320-324,355-359	1.62 ± 0.46	0.45 ± 0.04*	41	Roser Matamala (2004-2011) FLUXN... Batavia (Prairie site), DOI: 10.18140/...
US-LWW	1998	95-99, 190-199,205-214,220-224, 230-234	8.07 ± 2.47	0.47 ± 0.15	53	Tilden Meyers (1997-1998) FLUXNET... 10.18140/FLX/1440077
US-Ne1	2003	10-14,35-39,45-49,185-189,195-199,325-329	3.83 ± 1.37	0.52 ± 0.14	45	Andy Suyker (2001-2013) FLUXNET2... 10.18140/FLX/1440084
US-Ne2	2002	170-174,180-184,210-214	2.79 ± 0.51	0.36 ± 0.05	39	Andy Suyker (2001-2013) FLUXNET2... site, DOI: 10.18140/FLX/1440085
US-Ne3	2003	35-39,45-49,65-69,155-159,185-189	4.42 ± 0.68	0.48 ± 0.09	42	Andy Suyker (2001-2013) FLUXNET2... 10.18140/FLX/1440086
US-SRG	2011	160-164, 350-354	2.37 ± 1.17	0.55 ± 0.08*	40	Russell Scott (2008-2014) FLUXNET2... DOI: 10.18140/FLX/1440114
US-Twt	2011	65-69, 160-164	3.77 ± 2.30	0.32 ± 0.12*	67	Dennis Baldocchi (2009-2014) FLUX... 10.18140/FLX/1440106
US-Var	2013	160-164,180-184, 240-244,275-279	3.64 ± 1.05	0.27 ± 0.02	55	Dennis Baldocchi (2000-2014) FLUX... 10.18140/FLX/1440094
US-Whs	2014	40-44,145-149,165-169	1.53 ± 0.38	0.34 ± 0.13	52	Russ Scott (2007-2014) FLUXNET201... 10.18140/FLX/1440097
US-Wkg	2011	5-9, 55-59,65-69,310-314,350-354	1.50 ± 0.29	0.49 ± 0.13	62	Russell Scott (2004-2014) FLUXNET2... 10.18140/FLX/1440096
ZA-Kru	2007	65-69,75-79,125-129,155-159,160-164,170-179,190-194,200-204,270-274,330-334	7.36 ± 1.39	0.44 ± 0.08	56	Bob Scholes (2000-2013) FLUXNET2...
MX-Lpa	2006	40-44, 105-114, 180-184, 190-194,325-329	9.90 ± 6.77	0.37 ± 0.14	2	Walter Oechel AmeriFlux MX-Lpa La...
US-A74	2016	35-39,90-94,95-99,315-319	6.74 ± 1.97	0.53 ± 0.18	43	Lara Kueppers, Margaret Torn, Seba... DOI:10.17190/AMF/1436328
US-Aud	2005	15-19, 30-34, 45-49, 55-64, 95-99, 115-119, 125-129, 135-139, 150-174, 180-194, 330-334	4.89 ± 1.21	0.49 ± 0.17	12	Tilden Meyers AmeriFlux US-Aud Au...
US-Bo1	2006	55-59, 265-269, 300-304	7.13 ± 4.30	0.53 ± 0.08	23	Tilden Meyers AmeriFlux US-Bo1 Bo...
US-Bo2	2007	80-84, 130-134	4.74 ± 1.62	0.37 ± 0.06*	74	Carl Bernacchi AmeriFlux US-Bo2 Bo...
US-Br1	2009	305-314	1.60 ± 0.27	0.29 ± 0.06*	3	John Prueger, Tim Parkin AmeriFlux ... DOI:10.17190/AMF/1246038
US-Ctn	2007	180-184,210-214	7.13 ± 0.56	0.55 ± 0.06*	23	Tilden Meyers AmeriFlux US-Ctn Cot...

Site	Year	DOY ranges			N	Reference
US-Fwf	2009	310-314, 320-324	0.55 ± 0.17	0.47 ± 0.01*	2	Sabina Dore, Thomas Kolb AmeriFlux DOIi:10.17190/AMF/1246052
US-IB1	2007	75-79,110-114,135-139	4.23 ± 1.47	0.37 ± 0.13	18	Roser Matamala AmeriFlux US-IB1 F... (Agricultural site), DOI:10.17190/AM...
US-Kon	2010	100-104, 335-339	3.86 ± 2.67	0.34 ± 0.01*	33	Nathaniel Brunsell AmeriFlux US-Kor...
US-Rms	2015	200-204,185-189	2.68 ± 0.32	0.51 ± 0.16	28	Gerald Flerchinger AmeriFlux US-Rm... DOI:10.17190/AMF/1375202
US-SCd	2011	110-114, 140-144, 155-159, 180-184, 270-274, 335-339	3.55 ± 3.01	0.51 ± 0.16	7	Mike Goulden AmeriFlux US-SCd Sou... DOI:10.17190/AMF/1419505
US-SCg	2014	145-149,155-159,165-179, 185-194, 220-224	6.15 ± 2.34	0.44 ± 0.10	32	Mike Goulden AmeriFlux US-SCg Sou... DOI:10.17190/AMF/1419502
US-SCw	2012	130-134, 140-149, 155-159, 165-169, 180-189, 200-209, 220-224, 245-249.260-264,295-299,305-309, 320-324	4.01 ± 1.36	0.52 ± 0.17	3	Mike Goulden AmeriFlux US-SCw So... Woodland, doi:10.17190/AMF/1419...
US-Seg	2011	55-59,140-144,155-159,335-339,355-359	1.55 ± 0.54	0.33 ± 0.07	27	Marcy Litvak AmeriFlux US-Seg Sevil...
US-SFP	2008	100-104,280-284	4.13 ± 1.65	0.33 ± 0.03*	39	Tilden Meyers AmeriFlux US-SFP Sio...
US-SO4	2006	35-39, 225-229, 305-309, 320-324, 335-339	4.15 ± 2.87	0.55 ± 0.13	17	Walt Oechel AmeriFlux US-SO4 Sky ...
US-SRM	2006	5-9,10-14,35-39,40-44,135-139, 140-144,165-169,170-174,200-204	5.72 ± 5.89	0.37 ± 0.14	10	Marcy Litvak AmeriFlux US-Wjs Willa...
US-Wjs	2013	20-24,45-49,60-64,70-74, 80-84,100-104,120-124,135-149, 140-144, 145-149, 170-174	2.21 ± 0.65	0.40 ± 0.10	18	Marcy Litvak AmeriFlux US-Wjs Willa...
CN-HBG	2003	10-15, 20-25, 30-49, 290-294, 300-304, 345-349	2.92 ± 1.57	0.55 ± 0.12	9	Xinquan Zhao, Asiaflux, CN-QHB, Ha...
CN-QHB	2002	45-49, 55-59, 310-314	4.49 ± 1.35	0.40 ± 0.13	59	Yanhong Tang, AsiaFlux, CN-QHB, Qi...
AU-Stp	2010	155-164, 185-199, 225-234, 250-254, 260-264, 270-274, 335-339, 350-354	1.76 ± 1.07	0.40 ± 0.12	16	Jason Beringer, Lindsay Hutley (200... 10.18140/FLX/1440204
AU-TTE	2013	5-9 15-39, 45-49, 70-74, 80-84, 95-99, 120-129, 180-184, 200-204, 210-214, 240-244, 255-259, 295-269, 280-289, 295-299, 330-334	3.14 ± 1.32	0.55 ± 0.16	23	James Cleverly, Derek Eamus (2012... 10.18140/FLX/1440205
AU-Ync	2014	275-279, 285-294, 300-304, 340-344, 360-364	5.09 ± 1.91	0.52 ± 0.11	16	Jason Beringer, Jeffery Walker (201... 10.18140/FLX/1440208

Table S1. Sites with ventilation events. The table provides information for each ID site abo
year analyzed; the five-day periods (beginning and ending day of years) where our algor
emissions according to the established criteria; the average of the CO_2 fluxes (F_c) maximum
potential; $\mu molCO_2$ m^{-2} s^{-1}); the mean and standard deviation values of Spearman coef
correlation between Fc and friction velocity (u$_*$) over all VE events detected (F_c-u$_*$ corr) wit
with less than two periods of anomalous events ($p < 0.05$); an indication of uncertainty thro
of gaps in the F_c time series (% gaps); and the citation information.

Site ID	Site Country	IGBP	KGCC	Latitude	Longitude	MAT	MAP	Data Base	
AU-DaP	Australia	GRA	Aw	-14.159	131.388	25	801	Fluxnet	http
AU-Emr	Australia	GRA	BWk	-23.859	148.475	22	527	Fluxnet	http
AU-RDF	Australia	WSA	BWh	-14.564	132.478	26	600	Fluxnet	http
BE-Lon	Belgium	CRO	Cfb	50.552	4.746	10	800	Fluxnet	http
CN-HaM	China	GRA	ET	37.370	101.180	-1	565	Fluxnet	http
ES-Amo	Spain	OSH	BSk	36.834	-2.252	18	220	Fluxnet	http
ES-Lju	Spain	OSH	Csa	36.927	-2.752	16	400	Fluxnet	http
ES-Ln2	Spain	OSH	Csa	36.970	-3.476	6	800	Fluxnet	http
FR-Gri	France	CRO	Cfb	48.844	1.952	12	650	Fluxnet	http
IT-Bci	Italy	CRO	Csa	40.524	14.957	18	600	Fluxnet	http
RU-Cok	Russia	OSH	Dfc	70.829	147.494	-14	232	Fluxnet	http
RU-Ha1	Russia	GRA	Dfc	54.725	90.002	2	384	Fluxnet	http
US-AR1	United States	GRA	Cfa	36.427	-99.420	14	550	Fluxnet	http
US-AR2	United States	GRA	Cfa	39.636	-99.598	15	419	Fluxnet	http
US-ARM	United States	CRO	Cfa	36.606	-97.489	15	843	Fluxnet	http
US-IB2	United States	GRA	Dfa	41.841	-88.241	9	930	Fluxnet	http
US-LWW	United States	GRA	Cfa	34.960	-97.979	16	805	Fluxnet	http
US-Ne1	United States	CRO	Dfa	41.165	-96.477	10	790	Fluxnet	http
US-Ne2	United States	CRO	Dfa	41.165	*-96.470*	10	789	Fluxnet	http
US-Ne3	United States	CRO	Dfa	41.180	-96.439	10	784	Fluxnet	http
US-SRG	United States	GRA	BSk	31.908	-110.839	17	420	Fluxnet	http
US-Twt	United States	CRO	Csa	38.109	-121.653	16	421	Fluxnet	http
US-Var	United States	GRA	Csa	38.413	-120.951	16	559	Fluxnet	http
US-Whs	United States	OSH	BSk	31.744	-110.052	18	320	Fluxnet	http
US-Wkg	United States	GRA	BSk	31.737	-109.942	16	407	Fluxnet	http
ZA-Kru	South Africa	SAV	BSh	-25.020	31.497	22	547	Fluxnet	http
MX-Lpa	Mexico	OSH	BWh	24.129	-110.438	24	182	AmeriFlux	http:

US-A74	United States	CRO	Cfa	36.809	-97.549	34	889	AmeriFlux	http:
US-Aud	United States	GRA	BSk	31.591	-110.510	15	438	AmeriFlux	http:
US-Bo1	United States	CRO	Dfa	40.006	-88.290	11	991	AmeriFlux	http:
US-Bo2	United States	CRO	Dfa	40.009	-88.290	11	991	AmeriFlux	http:
US-Br1	United States	CRO	Dfa	41.975	-93.691	9	842	AmeriFlux	http:
US-Ctn	United States	GRA	BSk	43.950	-101.847	10	228	AmeriFlux	http:
US-Fwf	United States	GRA	Csb	35.445	-111.772	8	557	AmeriFlux	http:
US-IB1	United States	CRO	Dfa	41.859	-88.241	9	929	AmeriFlux	http:
US-Kon	United States	GRA	Cfa	39.082	-96.560	13	867	AmeriFlux	http:
US-Rms	United States	CSH	BSh	43.065	-116.749	5	800	AmeriFlux	http:
US-SCd	United States	BSV	BWh	33.652	-116.372	23	350	AmeriFlux	http:
US-SCg	United States	GRA	Csa	33.737	-117.695	17	350	AmeriFlux	http:
US-SCw	United States	OSH	BWh	33.605	-116.453	17	350	AmeriFlux	http:
US-Seg	United States	GRA	BSk	34.362	-106.702	14	273	AmeriFlux	http:
US-SFP	United States	CRO	Csa	43.241	-96.902	8	494	AmeriFlux	http:
US-SO4	United States	CSH	Csa	33.385	-116.641	15	484	AmeriFlux	http:
US-SRM	United States	WSA	BSk	31.821	-110.866	18	380	AmeriFlux	http:
US-Wjs	United States	OSH	BSk	34.426	-105.862	15	361	AmeriFlux	http:
CN-HBG	China	GRA	Dwb	37.482	101.200	-2	600	AsiaFlux	http:
CN-QHB	China	GRA	BSk	37.607	101.332	-2	567	AsiaFlux	http
AU-Stp	Australia	GRA	BSh	-17.151	133.350	25	640	OzFlux	http
AU-TTE	Australia	OSH	BWh	-22.287	133.640	21	305	OzFlux	http
AU-Ync	Australia	GRA	BSk	-34.989	146.291	25	465	OzFlux	http

Table S2. Sites with ventilation events. The table provide information about the main chara
with information for each ID site about (in order of appearance): land cover IGBP classific
classification (KGCC), latitude, longitude, mean annual temperature (MAT; °C); mean ann
network to which the database belongs and associated DOI.

Site ID	Site Country	IGBP	KGCC	Latitude	Longitude	MAT	MAP	Data Base	
AT-Neu	Austria	GRA	Cfb	47.117	11.318	6	852	Fluxnet	http:
AU-Ade	Australia	WSA	Aw	-13.077	131.118	28	1460	Fluxnet	http:
AU-DaS	Australia	SAV	Aw	-14.159	131.388	27	976	Fluxnet	http:
AU-Dry	Australia	SAV	Aw	-15.259	132.371	28	1170	Fluxnet	http:
AU-GWW	Australia	SAV	-	-30.191	120.654	19	240	Fluxnet	http:
CA-NS6	Canada	OSH	Dfc	55.917	-98.964	-3	495	Fluxnet	http:
CA-NS7	Canada	OSH	Dfc	56.636	-99.948	-4	483	Fluxnet	http:
CA-SF3	Canada	OSH	Dfc	54.092	-106.005	0	470	Fluxnet	http:
CG-Tch	Congo	SAV	Aw	-4.289	11.656	26	1150	Fluxnet	http:
CH-Cha	Switzerland	GRA	Dwb	47.210	8.410	10	1136	Fluxnet	http:
CH-Fru	Switzerland	GRA	Cfb	47.116	8.538	7	1651	Fluxnet	http:
CH-Oe1	Switzerland	GRA	Cfb	47.286	7.732	9	1100	Fluxnet	http:
CN-Du2	China	GRA	Dwb	42.047	116.284	2	319	Fluxnet	http:
CN-Du3	China	GRA	Dwb	42.055	116.281	-	-	Fluxnet	http:
CZ-BK2	Czech Rep.	GRA	Dfb	49.494	18.543	7	1316	Fluxnet	http:
DE-Gri	Germany	GRA	Cfb	50.950	13.513	8	901	Fluxnet	http:
DE-Kli	Germany	CRO	Cfb	50.893	13.522	8	842	Fluxnet	http:
DE-RuS	Germany	CRO	Cfb	50.866	6.447	10	700	Fluxnet	http:
DK-Eng	Denmark	GRA	Cfb	55.691	12.192	8	613	Fluxnet	http:
DK-ZaH	Denmark	GRA	ET	74.473	-20.550	-9	211	Fluxnet	http:
ES-LgS	Spain	OSH	Csa	37.098	-2.966	6	800	Fluxnet	http:
FI-Jok	Finland	CRO	Dfb	60.899	23.513	5	627	Fluxnet	http:
IT-Noe	Italy	CSH	Csa	40.606	8.152	16	588	Fluxnet	http:
IT-Tor	Italy	GRA	Dfc	45.844	7.578	3	920	Fluxnet	http:
NL-Hor	Netherlands	GRA	Cfb	52.240	5.071	10	800	Fluxnet	http:

PA-SPs	Panama	GRA	Am	9.314	-79.631	27	2350	Fluxnet	http;
RU-Sam	Russia	GRA	Dfd	72.374	126.496	-13	124	Fluxnet	http;
RU-Vrk	Russia	CSH	Dfc	67.055	62.940	-6	501	Fluxnet	http;
SD-Dem	Sudan	SAV	BWh	13.283	30.478	26	320	Fluxnet	http;
US-Cop	United States	GRA	BSk	38.090	-109.390	-	-	Fluxnet	http;
US-Goo	United States	GRA	Cfa	34.255	-89.874	16	1426	Fluxnet	http;
US-KS2	United States	CSH	Cfa	28.609	-80.672	22	1294	Fluxnet	http;
US-Lin	United States	CRO	-	36.357	-119.842	-	-	Fluxnet	http;
US-Sta	United States	OSH	Bsh	41.397	-106.802	5	-	Fluxnet	http;
US-Ton	United States	WSA	Csa	38.432	-120.966	16	559	Fluxnet	http;
US-Tw2	United States	CRO	Csa	38.105	-121.643	16	421	Fluxnet	http;
US-Wi6	United States	OSH	Dfb	46.625	-91.298	-	-	Fluxnet	http;
CA-Let	Canada	GRA	Dfb	49.709	-112.940	5	398	AmeriFlux	http;
US-A32	United States	GRA	Cfa	36.819	-97.820	34	889	AmeriFlux	http;
US-An1	United States	OSH	Dfc	68.990	-150.280	-	-	AmeriFlux	http;
US-An2	United States	OSH	Dfc	68.950	-150.210	-	-	AmeriFlux	http;
US-An3	United States	OSH	Dfc	68.930	-150.270	-	-	AmeriFlux	http;
US-ARb	United States	GRA	Cfa	35.550	-98.040	10	860	AmeriFlux	http;
US-ARc	United States	GRA	Cfa	35.546	-98.040	-	-	AmeriFlux	http;
US-Bi2	United States	CRO	Csa	38.109	-121.535	16	338	AmeriFlux	http;
US-Bkg	United States	GRA	Cfa	44.345	-96.836	6	586	AmeriFlux	http;
US-Bn3	United States	OSH	Dsc	63.923	-145.744	-	-	AmeriFlux	http;
US-Br3	United States	CRO	Dfa	41.975	-93.694	9	847	AmeriFlux	http;
US-CaV	United States	GRA	Cfb	39.063	-79.421	8	1317	AmeriFlux	http;
US-Ced	United States	CSH	Cfa	39.838	-74.379	11	1138	AmeriFlux	http;
US-Cop	United States	GRA	BSk	38.090	-109.390	-	-	AmeriFlux	http;
US-Goo	United States	GRA	Cfa	34.255	-89.874	16	1426	AmeriFlux	http;
US-CRT	United States	CRO	Dfa	41.628	-83.347	10	849	AmeriFlux	http;

US-Dia	United States	GRA	Csa	37.677	-121.530	16	265	AmeriFlux	http;
US-Dk1	United States	GRA	Cfa	35.971	-79.093	14	1170	AmeriFlux	http;
US-EML	United States	OSH	ET	63.878	-149.254	-1	378	AmeriFlux	http;
US-FPe	United States	GRA	BSk	48.308	-105.102	5	335	AmeriFlux	http;
US-FR2	United States	WSA	Cfa	29.949	-97.996	19	864	AmeriFlux	http;
US-FR3	United States	CSH	Cfa	29.940	-97.990	20	869	AmeriFlux	http;
US-ICh	United States	OSH	ET	68.607	-149.296	-7	318	AmeriFlux	http;
US-ICt	United States	OSH	ET	68.606	-149.304	-7	318	AmeriFlux	http;
US-KFS	United States	GRA	Cfa	39.056	-95.191	12	1014	AmeriFlux	http;
US-KUT	United States	GRA	Dfa	44.995	-93.186	8	777	AmeriFlux	http;
US-Pon	United States	CRO	Cfa	36.767	-97.133	15	866	AmeriFlux	http;
US-Rls	United States	CSH	Bsh	43.144	-116.736	8	333	AmeriFlux	http;
US-Ro1	United States	CRO	Cfa	44.714	-93.090	6	879	AmeriFlux	http;
US-Ro2	United States	CRO	Cfa	44.729	-93.089	6	879	AmeriFlux	http;
US-Ro3	United States	CRO	Cfa	44.722	-93.089	6	879	AmeriFlux	http;
US-Ro4	United States	GRA	Dfa	44.678	-93.072	6	879	AmeriFlux	http;
US-Ro5	United States	CRO	Dfa	44.691	-93.058	6	879	AmeriFlux	http;
US-Ro6	United States	CRO	Dfa	44.695	-93.058	6	879	AmeriFlux	http;
US-Rws	United States	OSH	BSk	43.168	-116.713	9	290	AmeriFlux	http;
US-SCs	United States	OSH	Csa	33.734	-117.696	-	-	AmeriFlux	http;
US-SdH	United States	GRA	Dsb	42.069	-101.407	-	-	AmeriFlux	http;
US-Ses	United States	OSH	BSk	34.335	-106.744	14	275	AmeriFlux	http;
US-Shd	United States	GRA	Cfa	36.933	-96.683	14	898	AmeriFlux	http;
US-Snd	United States	GRA	Csa	38.037	-121.754	16	358	AmeriFlux	http;
US-Sne	United States	GRA	Csa	38.037	-121.755	16	311	AmeriFlux	http;
US-SO2	United States	CSH	Csa	33.374	-116.623	14	553	AmeriFlux	http;
US-SO3	United States	CSH	Csa	33.377	-116.623	13	576	AmeriFlux	http;
US-SuM	United States	CRO	Aw	20.798	-156.454	24	287	AmeriFlux	http;

US-SuS	United States	CRO	Aw	20.785	-156.404	24	334	AmeriFlux	http;
US-SuW	United States	CRO	Aw	20.825	-156.491	24	366	AmeriFlux	http;
US-Wdn	United States	OSH	Bsh	40.784	-106.262	3	-	AmeriFlux	http;
US-Wi7	United States	OSH	Dfb	46.649	-91.069	-	-	AmeriFlux	http;
US-Wlr	United States	GRA	Cfa	37.521	-96.855	14	881	AmeriFlux	http;
CN-HFK	China	CRO	Cfa	37.607	101.332	13	1306	AsiaFlux	http;
CN-KBU	China	GRA	BSk	47.214	108.737	1	196	AsiaFlux	http;
CN-YCS	China	CRO	Cwa	36.833	116.570	13	528	AsiaFlux	http;
NZ-Bfm	New Zealand	CRO	-	-43.593	171.928	11	900	OzFlux	http; beac
Boyagin	Australia	WSA		-32.477	116.939	17	445	OzFlux	http; nd/b
AU-Gin	Australia	WSA	Csa	-31.376	115.714	24	641	OzFlux	http;
AU-How	Australia	SAV	Aw	-12.494	131.152	27	1700	OzFlux	http;
AU-Lit	Australia	SAV	-	-13.179	130.795	-	-	OzFlux	http; nd/lit
AU-Nim	Australia	GRA	Cfb	-36.216	148.553	23	1700	OzFlux	http; nimm
AU-Rgf	Australia	CRO	Csa	-32.506	116.967	17	446	OzFlux	http; ridge
AU-Sam	Australia	CRO	-	-27.388	152.878	20	1102	OzFlux	http; samf

Table S3. Sites without ventilation events. The table provide information about the main sites with information for each ID site about (in order of appearance): land cover IGBP classif classification (KGCC), latitude, longitude, mean annual temperature (MAT; °C); mean an network to which the database belongs and associated DOI.

MATLAB CODE FOR FLUXNET, AMERIFLUX AND ASIAFLUX DATABASES

```matlab
clear
clc

[data]=csvread('D:\file.csv');

%% We divide the file by years
% Leap years=2000,2004,2008,2012,2016 are n=17568.
[m,n]=size(data);
m1=17520;
data2003=data(1:m1,1:n);
m11=m1+1;
m2=17568+17520;
data2004=data(m11:m2,1:n);
m21=m2+1;
m3=17568+17520+17520;
data2005=data(m21:m3,1:n);
m31=m3+1;
m4=17520+17568+17520+17520;
data2006=data(m31:m4,1:n);
clearvars m1 m11 m2 m21 m3 m31 m4

%% The column of each variable varies between databases
clc
variable1=data2003(:,42);    %Ustar
variable1name=textdata(:,42)
variable2=data2003(:,77);    %NEE_VUT
variable2name=textdata(1,77)
variable3=data2003(:,35);   %precipitación
variable3name=textdata(1,35)
variable4=data2003(:,79);   %QC NEE.
variable4name=textdata(1,79);
variable5=data2003(:,31);   % TA air temperature
variable5name=textdata(1,31)
variable6=data2003(:,6);    % VPD
variable6name=textdata(1,6)
variable7=data2003(:,27);   % PA
variable7name=textdata(1,27)
variable8=data2003(:,43);   % NETRADiation.
variable8name=textdata(1,43)
variable9=data2003(:,49);   % TS
variable9name=textdata(1,49)
variable10=data2003(:,51);  % SWC
variable10name=textdata(1,51)
variable11=data2003(:,47);  % C02
variable11name=textdata(1,47)
variable13=data2003(:,12);  % SW_IN
variable13name=textdata(1,12)

%% Doy column is prepared aside.
[doyB]=xlsread('D \Doyb');      % Leap year
[doy]=xlsread('D:\Doy');

%%
%For QC values other tan O I use NaN instead.
```

```matlab
[i,j]=find(variable4~=(0));
variable2(i,:)=[NaN];


%% I use NaN instead -9999

missval=find(variable1==-9999); missval2=find(variable2==-9999);
missval3=find(variable3==-9999); missval4=find(variable4==-9999);
missval5=find(variable5==-9999); missval6=find(variable6==-9999);
missval7=find(variable7==-9999); missval8=find(variable8==-9999);
missval9=find(variable9==-9999); missval10=find(variable10==-9999);
missval11=find(variable11==-9999); missval13=find(variable13==-9999);

variable1(missval,:)=NaN; variable2(missval2,:)=NaN;
variable3(missval3,:)=NaN; variable4(missval4,:)=NaN;
variable5(missval5,:)=NaN; variable6(missval6,:)=NaN;
variable7(missval7,:)=NaN; variable8(missval8,:)=NaN;
variable9(missval9,:)=NaN; variable10(missval10,:)=NaN;
variable11(missval11,:)=NaN;variable13(missval13,:)=NaN;

clearvars missval missval2 missval3 missval4 missval5 missval6
missval7 missval8 missval9 missval10 missval11 missval12 missval13
missval14 missval15

clc

%% The algorithm of detection

for o=1:360

s = o(mod(o, 5) == 0);        %each five days
for m=s
USTAR=variable1; NEE_VUT=variable2; PRECIPITAC=variable3;
TA=variable5; VPD=variable6; PA=variable7; NETRAD=variable8;
TS=variable9; SWC=variable10; CO2=variable11; SW_IN=variable13;
%doy=doyB; %Use instead for Leap year
doyy=doy;

    m;
     t=m+5;
     [n,j]=find((doy<=m)|(doy>=t));

USTAR(n,:)=[]; NEE_VUT(n,:)=[]; PRECIPITAC(n,:)=[]; TA(n,:)=[];
VPD(n,:)=[]; PA(n,:)=[]; NETRAD(n,:)=[]; TS(n,:)=[]; SWC(n,:)=[];
SW_IN(n,:)=[]; CO2(n,:)=[];
%doyBB(n,:)=[];
doyy(n,:)=[];

  [k,j]=find((SW_IN<50)|(NEE_VUT<0)|(PRECIPITAC>0.00001)|(USTAR<0.2));
%Only daytime [shortwave radiation incoming (SW_IN) or photosynthetic
photon flux density incoming (PPFD_IN) > 50 W m-2], positive fluxes
[net ecosystem exchange (NEE) or carbon dioxide flux [Fc] > 0 µmolCO2
m-2 s-1], and with high-turbulence conditions [u* > 0.2 m s-1] data
were used
USTAR(k,:)=[]; NEE_VUT(k,:)=[]; PRECIPITAC(k,:)=[]; TA(k,:)=[];
VPD(k,:)=[]; PA(k,:)=[]; NETRAD(k,:)=[]; TS(k,:)=[]; SWC(k,:)=[];
CO2(k,:)=[]; SW_IN(k,:)=[];
%doyBB(k,:)=[];
doyy(k,:)=[];
```

```
    mm=m+1;
    tt=t-1;
     [nn,j]=find((doyy<=m)|(doyy>=mm));
     SWC_day1=SWC;
     SWC_day1(nn,:)=[];
     [nnn,j]=find((doyy<=tt)|(doyy>=t));
     SWC_day5=SWC;
     SWC_day5(nnn,:)=[];
    difSWC=abs(nanmean(SWC_day5)-nanmean(SWC_day1));
    if (1>=difSWC)      % only mean soil water content (SWC) absolute
difference between day 1st and 5th < 1 %.

     [nn,j]=find((doyy<=m)|(doyy>=mm));
     TA_day1=TA;
     TA_day1(nn,:)=[];
     [nnn,j]=find((doyy<=tt)|(doyy>=t));
     TA_day5=TA;
     TA_day5(nnn,:)=[];
    difTA=abs(nanmean(TA_day5)-nanmean(TA_day1));
    if (3>=difTA)       %only mean air temperature (TA) absolute
difference between day 1st and 5th < 3 °C.

x=[NEE_VUT USTAR TA VPD PA TS SWC SW_IN];   %five days matrix

 isnanx=isnan(x);
 [rho,pval]=partialcorr(x,'Type','Spearman','Rows','complete');
rho;
pval;


U_NEE_correl=rho(2,1);
U_NEE_pvalor=pval(2,1);


if (U_NEE_correl>=0.2)&&(U_NEE_pvalor<=0.05);

 % Here are only the values of u* and NEE that had passes all the
filters and with significant correlation. I establish a minimum of
0.2.

 % To show the data of interest

[N,X]=size(USTAR);
N
YEAR=2003
DAY_1=m
DAY_5=t-1
x
rho
pval


U_NEE_correl
U_NEE_pvalor



end
end
end
end
```

MATLAB CODE FOR OZFLUX DATABASE (NET.CDF FILES)

```matlab
%% Open toolbox mexnc and snctools
addpath(genpath('C:\Program Files\MATLAB\R2017a\toolbox\mexnc'))
addpath(genpath('C:\Program Files\MATLAB\R2017a\toolbox\snctools'))
cd('C:\file\')
variables = nc_getall ('file_year_level.nc')

%%
nc_dump('file_year_level.nc')  %metadata

names =
{'Day','Fc','Fc_QCFlag','Fld','Flu','Fm','Fsd','Fsu','Hour','Minute','
Second','Month','Precip','Sws','Ta','Ts','Wd_CSAT','Ws_CSAT','Year','p
s','ustar','ustar_QCFlag','xlDateTime'};
%names = {'Ah','xlDateTime'};

for i=1:length(names)
   c.(char(names(i))) = nc_varget('RDMF_2012_L3.nc',names{i});
end


%%
Day=c.Day; Month=c.Month; Hour=c.Hour; Minute=c.Minute;
Second=c.Second; Year=c.Year; xlDateTime = c.xlDateTime;
Fc=c.Fc; ustar=c.ustar; Precip=c.Precip; Swc=c.Sws; Ta=c.Ta; Ts=c.Ts;
Pa=c.ps; Sw_in=c.Fsd;

%DateVector = [Year,Month,Day,Hour,Minute,Second];
%%
t1 = datetime(Year(1),Month(1),Day(1),Hour(1),Minute(1),Second(1));
t2 =
datetime(Year(end),Month(end),Day(end),Hour(end),Minute(end),Second(en
d));
t = (t1:(1/(24*2)):t2)';
date=datevec(t);
daten = datenum(t);
doy=daten-datenum(2012,1,1,0,0,0);   %2012 is the year selected in
that case

%% I use NaN instead -9999

missval=find(Fc==-9999); missval2=find(ustar==-9999);
missval3=find(Precip==-9999); missval4=find(Swc==-9999);
missval5=find(Ta==-9999);
missval6=find(Ts==-9999); missval7=find(Pa==-9999);
missval8=find(Sw_in==-9999);

Fc(missval,:)=NaN; ustar(missval2,:)=NaN; Precip(missval3,:)=NaN;
Swc(missval4,:)=NaN; Ta(missval5,:)=NaN; Ts(missval6,:)=NaN;
Pa(missval7,:)=NaN;  Sw_in(missval8,:)=NaN;
%%


%% The algorithm of detection
```

```matlab
for o=1:360


s = o(mod(o, 5) == 0);      %each five days
for m=s


USTAR=ustar;FC=Fc;PRECIP=Precip; TA=Ta; PA=Pa; TS=Ts; SWC=Swc;
SW_IN=Sw_in; doyy=doy;


    m;
     t=m+5;
     [n,j]=find((doy<=m)|(doy>=t));


USTAR(n,:)=[]; FC(n,:)=[]; PRECIP(n,:)=[]; TA(n,:)=[];
PA(n,:)=[]; TS(n,:)=[]; SWC(n,:)=[]; SW_IN(n,:)=[]; doyy(n,:)=[];


[k,j]=find((SW_IN<50)|(FC<0)|(PRECIP~=0));
%Only daytime [shortwave radiation incoming (SW_IN) or photosynthetic
photon flux density incoming (PPFD_IN) > 50 W m-2], positive fluxes
[net ecosystem exchange (NEE) or carbon dioxide flux [Fc] > 0 µmolCO2
m-2 s-1], and with high-turbulence conditions [u* > 0.2 m s-1] data
were used
USTAR(k,:)=[]; FC(k,:)=[]; PRECIP(k,:)=[]; TA(k,:)=[];
PA(k,:)=[]; TS(k,:)=[]; SWC(k,:)=[]; SW_IN(k,:)=[]; doyy(k,:)=[];


    mm=m+1;
    tt=t-1;
     [nn,j]=find((doyy<=m)|(doyy>=mm));
     SWC_day1=SWC;
     SWC_day1(nn,:)=[];
     [nnn,j]=find((doyy<=tt)|(doyy>=t));
     SWC_day5=SWC;
     SWC_day5(nnn,:)=[];
    difSWC=abs(nanmean(SWC_day5)-nanmean(SWC_day1));
    if (1>=difSWC)    % only mean soil water content (SWC) absolute
difference between day 1st and 5th < 1 %.


     [nn,j]=find((doyy<=m)|(doyy>=mm));
     TA_day1=TA;
     TA_day1(nn,:)=[];
     [nnn,j]=find((doyy<=tt)|(doyy>=t));
     TA_day5=TA;
     TA_day5(nnn,:)=[];
    difTA=abs(nanmean(TA_day5)-nanmean(TA_day1));
    if (3>=difTA)
%only mean air temperature (TA) absolute difference between day 1st
and 5th < 3 °C.


x=[FC USTAR TA PA TS SWC SW_IN doyy];


isnanx=isnan(x);


 [rho,pval]=partialcorr(x,'Type','Spearman','Rows','complete');
rho;
pval;



if (U_NEE_correl>=0.2)&&(U_NEE_pvalor<=0.05);
```

```matlab
 % Here are only the values of u* and NEE that had passes all the
filters and with significant correlation. I establish a minimum of
0.2.

 % To show the data of interest

[N,X]=size(USTAR)
N
YEAR=Year(1)
DAY_1=m
DAY_5=t-1
x
rho
pval


U_NEE_correl=rho(2,1)
U_NEE_pvalor=pval(2,1)




end
end
end
end
```

GENERAL CONCLUSSIONS

1. Pressure tides played a dominant role in regulating CO_2 storage and vertical transport in Balsa Blanca and Amoladeras. Changes in atmospheric pressure conditions induced the expansion or contraction of the air stored in soil pores within the vadose zone, inducing a natural "soil breathing phenomenon". The effect of pressure tides was stronger in deep.

2. Pressure tides produced changes in soil CO_2 concentration at semidiurnal, diurnal, synoptic and monthly time-scales. The monthly pattern supposed the first published insights in the relation between lunar forcing and subterranean CO_2 fluctuations.

3. Proximity to the coast, could influence the atmospheric pressure tide effect on soil CO_2 molar fraction (χ_c) and explain the higher range of variation in the χ_c in AM, as well as the higher pressure tidal effect in comparison with BB. Fluctuations in the water table could change the volume of the vadose zone and could influence in the depth of air penetration.

4. Biotic and abiotic processes involved in transport and exchange with the atmosphere differed between soil layers producing discontinuities. The χ_c at 0.05 m depth was controlled by soil moisture, soil temperature, pressure pumping and ventilation, being rain pulses events the most important factor controlling the carbon dynamic. The χ_c in the deeper layers (0.5 and 1.5 m), by other side, was influenced mainly by pressure tides. The subsurface layer (0.15 m) acted as an interphase layer and was affected by all the environmental factors studied.

5. The influence of soil water content on χ_c at 0.05 m was determined by the type of precipitation event. The magnitude of the effect of each rain pulse was conditioned by the antecedent soil moisture, precipitation

magnitude, and the available organic matter supply for microbial respiration. With small precipitation events, the slow water infiltration only permeates into the soil surface (0.05 m) and the soil subsurface (0.15 m) layers. During a large precipitation event or events of intense rain (>15 mm) water could descend up to 1.5 m in the same day (data not shown). Only large rain events (>15 mm) triggered a χ_c increase in the daily pattern at the subsurface soil (0.15 m).

6. The physical decoupling found between pressure tides, pressure pumping and ventilation suggest that pressure tides would not be related with CO_2 emissions and its role in the ecosystem carbon dynamic would be related with the CO_2 vertical transport facilitating to be vented by pressure pumping and ventilation.

7. Petrophysical properties of soil medium, such as permeability and connectivity, are pivotal factors in the abiotic factors influence above the soil CO_2 dynamics. Land degradation can also potentially enhance interconnectivity between vadose zone and atmosphere.

8. Over the whole study period (2014-2016), the annual cumulative soil CO_2 efflux was positive in Amoladeras (AM) and Balsa Blanca (BB). The average soil CO_2 efflux was 254 ± 92 g C m^{-2} year^{-1} in AM and 405 ± 156 g C m^{-2} year^{-1} in BB, being BB the ecosystem with the lower degradation status.

9. Subterranean ventilation (VE) was demonstrated be relevant at global scale. Experimental sites with CO_2 emissions that could be mainly produced by VE were common and spread around the world. The 34% of the sites analyzed (145 sites) reported the occurrence of VE events. This vented CO_2 was found mainly in arid ecosystems (84%) and sites with hot and dry periods. These findings will suppose the first publication about this issue at global scale.

10. The occurrence and magnitude of the CO_2 emissions produced by VE were directly related with the intensity of the atmospheric turbulence in the surface. No evident differences were found between the ecosystem CO_2 flux and the friction velocity (indicator of turbulence) relationship among the climatic zones that showed VE events.

11. Most VE events were detected during dry conditions, with soil water content values below the 30th percentile of site-specific annual soil moisture. This dryness condition can correspond to an inherent feature of the ecosystem or to a climate extreme, such as a drought event.

12. The ventilation detection algorithm can efficiently detect CO_2 emissions produced by VE and constitutes a useful tool to its detection to be used in future researches.

CONCLUSIONES GENERALES

1. Las mareas de presión juegan un papel fundamental en regular el almacenamiento del CO_2 del suelo y el transporte vertical en Balsa Blanca y Amoladeras. Los cambios en la presión atmosférica inducen la expansión y contracción del aire almacenado en los poros del suelo de la zona vadosa lo que produce un fenómeno natural de "respiración del suelo". El efecto de las mareas de presión es mayor a más profundidad.

2. Las mareas de presión producen cambios en el CO_2 del suelo a escala semidiurna, diurna, sinóptica y mensual. El patrón de variación mensual supone el primer indicio publicado de la influencia de la luna en la variación de CO_2 subterráneo.

3. La proximidad a la costa podría influir en el efecto de marea de presión en la fracción molar del CO_2 del suelo (χ_c) y explicar el hecho de que el rango de variación en χ_c y el efecto de este fenómeno sea mayor en Amoladeras. Las fluctuaciones en el nivel freático alteran el volumen de zona vadosa y podrían influir en la profundidad de penetración del aire.

4. Los procesos bióticos y abióticos vinculados en el transporte e intercambio de CO_2 con la atmósfera varían en las diferentes profundidades del suelo produciendo discontinuidades. La χ_c a 0.05 m es controlada por la humedad y temperatura del suelo, el bombeo por presión y ventilación, siendo los pulsos de lluvia el factor más importante en controlar la dinámica del CO_2. La χ_c en profundidad (0.50 y 1.50 m), por otro lado, es influenciado principalmente por las mareas de presión. La capa sub-superficial (0.15 m) actúa como una interfase y es influida por todos los procesos estudiados.

5. La influencia del contenido del agua del suelo en χ_c a 0.05 m es determinada por el tipo de evento de precipitación. La magnitud del efecto de cada pulso de lluvia es condicionada por la humedad previa, la

magnitud del pulso y la materia orgánica disponible para la respiración microbiana del suelo. Con pequeños pulsos de lluvia, la baja capacidad de infiltración del agua solo penetra en la capa superficial (0.05 m) y sub-superficial (0.15 m) del suelo. Durante los grandes pulsos de lluvia (>15 mm) el agua puede llegar a descender hasta 1.50 m en el mismo día. Sólo los grandes pulsos de lluvia (> 15 mm) desencadenan un incremento del contenido de CO_2 en el patrón diario en el perfil sub-superficial (0.15 m).

6. El desacoplamiento físico encontrado entre las mareas de presión, el bombeo por presión y la ventilación sugieren que las mareas de presión pueden no estar relacionadas con las emisiones de CO_2 del suelo y que su papel en la dinámica de C del ecosistema está relacionada con el transporte vertical de CO_2 facilitando que éste sea ventilado por bombeo por presión y ventilación en superficie.

7. Las propiedades petrofisicas del medio, así como su permeabilidad y conectividad son factores determinantes en la influencia de los factores abióticos en la dinámica del CO_2 del suelo. La degradación del suelo también podría aumentar potencialmente la interconectividad entre la zona vadosa y la atmósfera.

8. A lo largo de todo el período de estudio (2014-2016), el flujo de CO_2 anual emitido es positivo en Amoladeras (AM) y Balsa Blanca (BB). El flujo de CO_2 promedio fue de 254 g C m^{-2} año^{-1} en AM y 405 g C m^{-2} año^{-1} en BB, siendo BB el ecosistema que se encuentra en menor estado de degradación.

9. La ventilación subterránea (VE) es relevante a escala global. Los sitios experimentales con emisiones de CO_2 que pueden ser producidas principalmente por VE son comunes y están repartidos a lo largo del planeta. El 34% de los sitios analizados (145 sitios) reportaron la ocurrencia de eventos de VE. Estos eventos se encontraron principalmente en ecosistemas áridos (84%) y sitios con períodos secos y

cálidos. Estos resultados supondrán la primera publicación que demuestran la presencia de la VE a escala global.

10. La ocurrencia y magnitud de las emisiones de CO_2 producidas por VE están directamente relacionadas con la intensidad de la turbulencia atmosférica en superficie. No se han encontrado diferencias evidentes en la relación de flujo de CO_2 del ecosistema y la velocidad de fricción (indicador de turbulencia) a lo largo de las zonas climáticas que muestran eventos de VE.

11. La mayoría de eventos de ventilación se detectaron durante condiciones de sequedad, con valores de humedad del suelo por debajo del percentil 30th de la humedad específica de cada sitio. Esta condición de sequedad puede responder a una característica inherente del ecosistema o a un fenómeno extremo, como un evento de sequía.

12. El algoritmo de detección de VE puede detectar de forma eficaz las emisiones de CO_2 producidas por eventos de ventilación y constituyen una herramienta útil para su detección en investigaciones futuras.

LIST OF ABREVIATIONS AND ACRONYMS

AI   Aridity Index

AM   Amoladeras experimental site

BB   Balsa Blanca experimental site

CBD   Convention on Biological Diversity

CWT   Continuous Wavelet Transform

DOY   Day of the year

EC   Eddy Covariance

GPP   Gross Primary Production

IGBP   International Geosphere-Biosphere Programme

IPCC   Intergovernmental Panel on Climate Change

IR   Infrared

IRGA   Infrared Gas Analyzer (IRGA)

KGCC   Köppen climate classification

MA   Millennium Ecosystem Assessment

MAGNA   Mapa Geológico Nacional

MAT   Mean annual temperature

MAP   Mean annual precipitation

NEE   Net Ecosystem Exchange

NECB   Net Ecosystem Carbon Balance

P   Precipitation

PA	Atmospheric pressure
PAR	Photosynthetically Active Radiation
PET	Potential Evapotranspiration
SOC	Soil Organic Carbon
SW_IN	Shortwave radiation incoming
SWC	Soil Water Content
TA	Air temperature
TS	Soil temperature
UNCCD	United Nations Convention to Combat Desertification
UNEP	United Nations Environment Programme
VE	Subterranean Ventilation
VPD	Vapor Pressure Defficit
VWC	Volumetric Soil Water Content
WCA	Wavelet Coherency Analysis
WCMC	World Conservation Monitoring Centre
WRB	World Reference Base for Soil Resources

LIST OF SYMBOLS

C	Carbon
CO_2	Carbon dioxide
k_s	Gas transfer coefficient
$F_{chamber}$	Soil CO_2 flux measured with a portable soil CO_2 flux chamber
F_s	Soil CO_2 efflux
F_C	Ecosystem CO_2 efflux
N_2	Nitrogen
p	Atmospheric pressure
R_{eco}	Ecosystem respiration
R_n	Net radiation
T_{soil}	Soil temperature
u_*	Friction velocity
ρ	CO_2 density
χ_c	Soil CO_2 molar fraction

BIBLIOGRAPHY

Agam, N., & Berliner, P. R. (2006). Dew formation and water vapor adsorption in semi-arid environments—A review. *Journal of Arid Environments, 65*(4), 572–590. https://doi.org/10.1016/j.jaridenv.2005.09.004

Ahlström, A., Raupach, M. R., Schurgers, G., Smith, B., Arneth, A., Jung, M., … Zeng, N. (2015). The dominant role of semi-arid ecosystems in the trend and variability of the land CO2 sink. *Science, 348*(6237), 895–899. https://doi.org/10.1126/science.aaa1668

Alados, C. L., Pueyo, Y., Barrantes, O., Escós, J., Giner, L., & Robles, A. B. (2004). Variations in landscape patterns and vegetation cover between 1957 and 1994 in a semiarid Mediterranean ecosystem. *Landscape Ecology, 19*(5 LB-Alodos2004), 543–559. https://doi.org/doi: 10.1023/B:LAND.0000036149.96664.9a

Albertsen, M. 1979. Carbon dioxide balance in the gas-filled part of the unsaturated zone, demonstrated at a podzol. Zeitschrift f¨ur Pflanzenernahrung & Bodenkunde, 142, 39–56.

Alessandri, A., De Felice, M., Zeng, N., Mariotti, A., Pan, Y., Cherchi, A., … Artale, V. (2014). Robust assessment of the expansion and retreat of Mediterranean climate in the 21st century. *Scientific Reports, 4*(1), 7211. https://doi.org/10.1038/srep07211

Almagro, M., López, J., Querejeta, J. I., & Martínez-Mena, M. (2009). Temperature dependence of soil CO2 efflux is strongly modulated by seasonal patterns of moisture availability in a Mediterranean ecosystem. *Soil Biology and Biochemistry, 41*(3), 594–605. https://doi.org/doi: 10.1016/j.soilbio.2008.12.021

Archibald, S. A., Kirton, A., Van der Merwe, M. R., Scholes, R. J., Williams, C. A., & Hanan, N. (2009). Drivers of inter-annual variability in Net Ecosystem Exchange in a semi-arid savanna ecosystem, South Africa. *Biogeosciences, 6,* 251–266. https://doi.org/10.5194/bg-6-251-2009

Arya, S.P., 1988. Introduction to Micrometeorology. Academic Press, San Diego, p. 303.

Aubinet, M, Grelle, A., Ibrom, A., Rannik, Ü., Moncrieff, J., Foken, T., … Vesala, T. (1999). *Estimates of the Annual Net Carbon and Water Exchange of Forests: The EUROFLUX Methodology* (A. H. Fitter & D. G. B. T.-A. in E. R. Raffaelli, eds.). https://doi.org/10.1016/S0065-

2504(08)60018-5

Aubinet, Marc, Vesala, T., & Papale, D. (2012). *Eddy covariance: a practical guide to measurement and data analysis* (Marc Aubinet, T. Vesala, & D. Papale, eds.). https://doi.org/10.1007/978-94-007-2351-1

Auer, L. H., Rosenberg, N. D., Birdsell, K. H., & Whitney, E. M. (1996). The effects of barometric pumping on contaminant transport. *Journal of Contaminant Hydrology, 24*(2), 145–166. https://doi.org/10.1016/S0169-7722(96)00010-1

Auffret, M. D., Karhu, K., Khachane, A., Dungait, J. A. J., Fraser, F., Hopkins, D. W., … Prosser, J. I. (2016). The Role of Microbial Community Composition in Controlling Soil Respiration Responses to Temperature. *PLOS ONE, 11*(10), e0165448. Retrieved from https://doi.org/10.1371/journal.pone.0165448

Austin, A., & Ballaré, C. (2010). Dual role of lignin in plant litter decomposition in terrestrial ecosystems. *Proceedings of the National Academy of Sciences of the United States of America, 107,* 4618–4622. https://doi.org/10.1073/pnas.0909396107

Austin, A. T., & Vivanco, L. (2006). Plant litter decomposition in a semi-arid ecosystem controlled by photodegradation. *Nature, 442*(7102), 555–558. https://doi.org/10.1038/nature05038

Baldini, J. U. L., L. M. Baldini, F. McDermott, and N. Clipson (2006), Carbon dioxide sources, sinks, and spatial variability in shallow temperate zone caves: Evidence from Ballynamintra Cave, Ireland, *Journal of Cave and Karst Studies,* 68(1), 4-11.

Baldocchi, D. (2003). Assessing the eddy covariance technique for evaluating carbon dioxide exchange rates of ecosystems: Past, present and future. *Global Change Biology, 9*(4), 479–492. https://doi.org/10.1046/j.1365-2486.2003.00629.x

Baldocchi, D. (2008). TURNER REVIEW No. 15. "Breathing" of the terrestrial biosphere: Lessons learned from a global network of carbon dioxide flux measurement systems. *Australian Journal of Botany,* Vol. 56, pp. 1–26. https://doi.org/10.1071/BT07151

Baldocchi, D. (2014). Measuring fluxes of trace gases and energy between ecosystems and the atmosphere – the state and future of the eddy covariance method. *Global Change Biology, 20*(12), 3600–3609. https://doi.org/10.1111/gcb.12649

Baldocchi, D., Falge, E., Gu, L., Olson, R., Hollinger, D., Running, S., … Wofsy, S. (2001). FLUXNET: A New Tool to Study the Temporal and Spatial Variability of Ecosystem-Scale Carbon Dioxide, Water

Vapor, and Energy Flux Densities. *Bulletin of the American Meteorological Society, 82*(11), 2415–2434. https://doi.org/10.1175/1520-0477(2001)082<2415:FANTTS>2.3.CO;2

Baldocchi, D., Reichstein, M., Papale, D., Koteen, L., Vargas, R., Agarwal, D., & Cook, R. (2012). The role of trace gas flux networks in the biogeosciences. *Eos, Transactions American Geophysical Union, 93*(23), 217–218. https://doi.org/10.1029/2012EO230001

Beer, C., Reichstein, M., Tomelleri, E., Ciais, P., Jung, M., Carvalhais, N., … Papale, D. (2010). Terrestrial Gross Carbon Dioxide Uptake: Global Distribution and Covariation with Climate. *Science, 329*(5993), 834 LP – 838. https://doi.org/10.1126/science.1184984

Bell, T. W., Menzer, O., Troyo-Diéquez, E., & Oechel, W. C. (2012). Carbon dioxide exchange over multiple temporal scales in an arid shrub ecosystem near La Paz, Baja California Sur, Mexico. *Global Change Biology, 18*(8), 2570–2582. https://doi.org/10.1111/j.1365-2486.2012.02720.x

Benavente, J., Vadillo, I., Carrasco, F., Soler, A., Liñán, C., & Moral, F. (2010). Air carbon dioxide contents in the vadose zone of a Mediterranean karst. *Vadose Zone Journal, 9*(1), 126–136. https://doi.org/10.2136/vzj2009.0027

Bloom, A. A., Exbrayat, J.-F., van der Velde, I. R., Feng, L., & Williams, M. (2016). The decadal state of the terrestrial carbon cycle: Global retrievals of terrestrial carbon allocation, pools, and residence times. *Proceedings of the National Academy of Sciences, 113*(5), 1285 LP – 1290. https://doi.org/10.1073/pnas.1515160113

Birch, H. F. (1958). The effect of soil drying on humus decomposition and nitrogen availability. *Plant and Soil, 10*(1), 9–31. https://doi.org/10.1007/BF01343734

Bond, W. J. (2019). *Open Ecosystems: ecology and evolution beyond the forest edge.* https://doi.org/10.1093/oso/9780198812456.001.0001

Bond-Lamberty, B., Bailey, V. L., Chen, M., Gough, C. M., & Vargas, R. (2018). Globally rising soil heterotrophic respiration over recent decades. *Nature, 560*(7716), 80–83. https://doi.org/10.1038/s41586-018-0358-x

Bourges, F., Mangin, A., & d'Hulst, D. (2001). Carbon dioxide in karst cavity atmosphere dynamics: The example of the Aven d'Orgnac (Ardèche). *Comptes Rendus de l'Académie Des Sciences - Series IIA - Earth and Planetary Science, 333*, 685–692. https://doi.org/10.1016/S1251-8050(01)01682-2

Bowling, D. R., & Massman, W. J. (2011). Persistent wind-induced enhancement of diffusive CO_2 transport in a mountain forest snowpack. *Journal of Geophysical Research: Biogeosciences, 116*(4). https://doi.org/doi: 10.1029/2011JG001722

Brandt, L. A., Bohnet, C., & King, J. Y. (2009). Photochemically induced carbon dioxide production as a mechanism for carbon loss from plant litter in arid ecosystems. *Journal of Geophysical Research: Biogeosciences, 114*(G2). https://doi.org/10.1029/2008JG000772

Burba, G. (2013). Eddy Covariance Method-for Scientific, Industrial, Agricultural, and Regulatory Applications. In *Book.*

Burke, I., Mosier, A., Hook, P., Milchunas, D., Barrett, J., Vinton, M., … Lauenroth, W. (2008). Soil Organic Matter and Nutrient Dynamics of Shortgrass Steppe Ecosystems. In *Ecology of the Shortgrass Steppe* (pp. 306–341). https://doi.org/10.1093/oso/9780195135824.003.0017

Burton, M., Sawyer, G., & Granieri, D. (2013). Deep Carbon Emissions from Volcanoes. *Reviews in Mineralogy and Geochemistry, 75, 323–354.* https://doi.org/10.2138/rmg.2013.75.11

Buyanovsky, G. A., and G. H. Wagner (1983), Annual cycles of carbon dioxide level in soil air, *Soil Science Society of America Journal, 47*(6), 1139-1145.

Canadell, J. G., & Schulze, E. D. (2014). Global potential of biospheric carbon management for climate mitigation. *Nature Communications, 5*(1), 5282. https://doi.org/10.1038/ncomms6282

Capolongo, D., Diodato, N., Mannaerts, C. M., Piccarreta, M., & Strobl, R. O. (2008). Analyzing temporal changes in climate erosivity using a simplified rainfall erosivity model in Basilicata (southern Italy). *Journal of Hydrology, 356*(1), 119–130. https://doi.org/10.1016/j.jhydrol.2008.04.002

Cazelles, B., Chavez, M., Berteaux, D., Ménard, F., Vik, J. O., Jenouvrier, S., & Stenseth, N. C. (2008). Wavelet analysis of ecological time series. *Oecologia, 156*(2 LB-Cazelles2008), 287–304. https://doi.org/doi: 10.1007/s00442-008-0993-2

Cazelles B, Hales S (2006) Infectious diseases, climate influences and nonstationarity. PLoS Med 3:1212–1213 (e328)

Chapin, F. S., Woodwell, G. M., Randerson, J. T., Rastetter, E. B., Lovett, G. M., Baldocchi, D. D., … Schulze, E.-D. (2006). Reconciling Carbon-cycle Concepts, Terminology, and Methods. *Ecosystems, 9*(7), 1041–1050. https://doi.org/10.1007/s10021-005-0105-7

Chatfield, C. (1989) The Analysis of Time Series: An Introduction. 4th Edition, Chapman and Hall, New York.

Chu, H., Baldocchi, D. D., John, R., Wolf, S., & Reichstein, M. (2017). Fluxes all of the time? A primer on the temporal representativeness of FLUXNET. *Journal of Geophysical Research: Biogeosciences, 122*(2), 289–307. https://doi.org/10.1002/2016JG003576

Ciais, P., Sabine, C., Bala, G., Bopp, L., Brovkin, V., Canadell, J., … Thornton, P. (2013). Contribution of working group I to the fifth assessment report of the intergovernmental panel on climate change. In V. B. and P. M. M. (eds.). [Stocker, T.F., D. Qin, G.-K. Plattner, M. Tignor, S.K. Allen, J. Boschung, A. Nauels, Y. Xia (Ed.), *Climate Change 2013: The physical science basis.* (pp. 465–570). https://doi.org/10.1017/CBO9781107415324.015

Clements, W. E., & Wilkening, M. H. (1974). Atmospheric pressure effects on 222Rn transport across the Earth-air interface. *Journal of Geophysical Research, 79*(33), 5025–5029. https://doi.org/doi: 10.1029/JC079i033p05025

Cleverly, J., Boulain, N., Villalobos-Vega, R., Grant, N., Faux, R., Wood, C., … Eamus, D. (2013). Dynamics of component carbon fluxes in a semi-arid Acacia woodland, central Australia. *Journal of Geophysical Research: Biogeosciences, 118*(3), 1168–1185. https://doi.org/10.1002/jgrg.20101

Comas, X., Slater, L., & Reeve, A. S. (2011). Atmospheric pressure drives changes in the vertical distribution of biogenic free-phase gas in a northern peatland. *Journal of Geophysical Research: Biogeosciences, 116*(4). https://doi.org/10.1029/2011JG001701

Corey, A. T., W. D. Kemper, and J. H. Dane (2010), Revised model for molecular diffusion and advection, *Vadose Zone Journal*, 9(1), 85-94, https://doi.org /doi: 10.2136/vzj2009.0082.

Cuezva, S., Fernandez-Cortes, A., Benavente, D., Serrano-Ortiz, P., Kowalski, A. S., & Sanchez-Moral, S. (2011). Short-term CO2 exchange between a shallow karstic cavity and the external atmosphere during summer: Role of the surface soil layer. *Atmospheric Environment, 45*(7), 1418–1427. https://doi.org/10.1016/j.atmosenv.2010.12.023

Curiel Yuste, J., Baldocchi, D. D., Gershenson, A., Goldstein, A., Misson, L., & Wong, S. (2007). Microbial soil respiration and its dependency on carbon inputs, soil temperature and moisture. *Global Change Biology, 13*(9), 2018–2035. https://doi.org/10.1111/j.1365-2486.2007.01415.x

Curiel Yuste, J., Janssens, I. A., Carrara, A., Meiresonne, L., & Ceulemans, R. (2003). Interactive effects of temperature and precipitation on soil respiration in a temperate maritime pine forest. *Tree Physiology*, *23*(18), 1263–1270. https://doi.org/10.1093/treephys/23.18.1263

D'Odorico, P., Bhattachan, A., Davis, K. F., Ravi, S., & Runyan, C. W. (2013). Global desertification: Drivers and feedbacks. *Advances in Water Resources*, *51*, 326–344. https://doi.org/10.1016/j.advwatres.2012.01.013

Daubechies, I. (1992). Ten Lectures on Wavelets. In *CBMS-NSF Regional Conference Series in Applied Mathematics*. https://doi.org/doi:10.1137/1.9781611970104

Davidson, E A, Belk, E., & Boone, R. D. (1998). Soil water content and temperature as independent or confounded factors controlling soil respiration in a temperate mixed hardwood forest. *Global Change Biology*, *4*(2), 217–227. https://doi.org/doi: 10.1046/j.1365-2486.1998.00128.x

Davidson, Eric A, Savage, K. E., Trumbore, S. E., & Borken, W. (2006). Vertical partitioning of CO_2 production within a temperate forest soil. *Global Change Biology*, *12*(6), 944–956. https://doi.org/10.1111/j.1365-2486.2005.01142.x

Davies-Barnard, T., Valdes, P. J., Singarayer, J. S., Wiltshire, A. J., & Jones, C. D. (2015). Quantifying the relative importance of land cover change from climate and land use in the representative concentration pathways. *Global Biogeochemical Cycles*, *29*(6), 842–853. https://doi.org/10.1002/2014GB004949

Decarlo, K. F., & Caylor, K. K. (2020). Effects of crack morphology on soil carbon flux dynamics in a dryland vertisol. *Geoderma*, *375*. https://doi.org/10.1016/j.geoderma.2020.114478

De Galdeano, C. S., Rodriguez-Fernandez, J., & Lopez-Garrido, A. C. (1985). A strike-slip fault corridor within the Alpujarra Mountains (Betic Cordilleras, Spain). *Geologische Rundschau*, *74*(3), 641–655. https://doi.org/10.1007/BF01821218

Denis, A., Lastennet, R., Huneau, F., & Malaurent, P. (2005). Identification of functional relationships between atmospheric pressure and CO_2 in the cave of Lascaux using the concept of entropy of curves. *Geophysical Research Letters*, *32*(5). https://doi.org/doi: 10.1029/2004GL022226

Drewitt, G. B., Black, T. A., Nesic, Z., Humphreys, E. R., Jork, E. M., Swanson, R., … Morgenstern, K. (2002). Measuring forest floor CO_2

fluxes in a Douglas-fir forest. *Agricultural and Forest Meteorology*, *110*(4), 299–317. https://doi.org/10.1016/S0168-1923(01)00294-5

Dong, L., J. Shimada, M. Kagabu, and H. Yang (2014), Barometric and tidal-induced aquifer water level fluctuation near the Ariake Sea, *Environmental Monitoring and Assessment*, 187(1), 4187, https://doi.org /doi: 10.1007/s10661-014-4187-6.

Dungait, J. A. J., Hopkins, D. W., Gregory, A. S., & Whitmore, A. P. (2012). Soil organic matter turnover is governed by accessibility not recalcitrance. *Global Change Biology*, *18*(6), 1781–1796. https://doi.org/10.1111/j.1365-2486.2012.02665.x

Duniway, M. C., Herrick, J. E., & Monger, C. (2007). *The High Water-Holding Capacity of Petrocalcic Horizons* (Vol. 71). https://doi.org/10.2136/sssaj2006.0267

Elberling, B., Larsen, F., Christensen, S., & Postma, D. (1998). Gas transport in a confined unsaturated zone during atmospheric pressure cycles. *Water Resources Research*, *34*(11), 2855–2862. https://doi.org/doi: 10.1029/98WR02037

Emmerich, W. E. (2003). Carbon dioxide fluxes in a semiarid environment with high carbonate soils. *Agricultural and Forest Meteorology*, *116*(1), 91–102. /https://doi.org/10.1016/S0168-1923(02)00231-9

Engelbrecht, F., Adegoke, J., Bopape, M. J., Naidoo, M., Garland, R., Thatcher, M., … Gatebe, C. (2015). Projections of rapidly rising surface temperatures over Africa under low mitigation. *Environmental Research Letters*, *10*(8), 16. https://doi.org/10.1088/1748-9326/10/8/085004

Esch, T., Heldens, W., Hirner, A., Keil, M., Marconcini, M., Roth, A., … Strano, E. (2017). Breaking new ground in mapping human settlements from space – The Global Urban Footprint. *ISPRS Journal of Photogrammetry and Remote Sensing*, *134*, 30–42. https://doi.org/10.1016/j.isprsjprs.2017.10.012

Eswaran, H., Reich, P., Kimble, J. M., Beinroth, F. H., Padmanabhan, E., & Moecharoen, P. (2000). Global carbon sinks. In B. S. and H. E. Rattan Lal, John M Kimble (Ed.), *Global Climate Change and Pedogenic Carbonates*. United States: Lewis Publishers.

Etiope, G., Beneduce, P., Calcara, M., Favali, P., Frugoni, F., Schiattarella, M., & Smriglio, G. (1999). Structural pattern and CO2–CH4 degassing of Ustica Island, Southern Tyrrhenian basin. *Journal of Volcanology and Geothermal Research*, *88*(4), 291–304. https://doi.org/10.1016/S0377-0273(99)00010-4

European Court of Auditors (ECA). (2018). *Desertfication in Europe. Background paper* (E. C. of Auditors, ed.). Luxembourg.

Falge, E., Baldocchi, D., Tenhunen, J., Aubinet, M., Bakwin, P., Berbigier, P., … Wofsy, S. (2002). Seasonality of ecosystem respiration and gross primary production as derived from FLUXNET measurements. *Agricultural and Forest Meteorology, 113*(1), 53–74. https://doi.org/10.1016/S0168-1923(02)00102-8

Fasullo, J. T., Otto-Bliesner, B. L., & Stevenson, S. (2018). ENSO's Changing Influence on Temperature, Precipitation, and Wildfire in a Warming Climate. *Geophysical Research Letters, 45*(17), 9216–9225. https://doi.org/10.1029/2018GL079022

Flechard, C. R., Neftel, A., Jocher, M., Ammann, C., Leifeld, J., & Fuhrer, J. (2007). Temporal changes in soil pore space CO_2 concentration and storage under permanent grassland. *Agricultural and Forest Meteorology, 142*(1), 66–84. https://doi.org/10.1016/j.agrformet.2006.11.006

Fang, C., and J. B. Moncrieff (1999), A model for soil CO_2 production and transport 1: Model development, *Agricultural and Forest Meteorology, 95*(4), 225-236, https://doi.org /doi:10.1016/S0168-1923(99)00036-2.

FAO (2009), Guía para la descripción de suelos (4ª edición), 99 pp., Roma.

Friend, A. D., Lucht, W., Rademacher, T. T., Keribin, R., Betts, R., Cadule, P., … Woodward, F. I. (2014). Carbon residence time dominates uncertainty in terrestrial vegetation responses to future climate and atmospheric CO_2. *Proceedings of the National Academy of Sciences, 111*(9), 3280 LP – 3285. https://doi.org/10.1073/pnas.1222477110

Fu, Q., & Feng, S. (2014). Responses of terrestrial aridity to global warming. *Journal of Geophysical Research: Atmospheres, 119*(13), 7863–7875. https://doi.org/10.1002/2014JD021608

Fukuda, H. (1955). Air and vapor movement in soil due to wind gustiness. *Soil Science, 79*(4). Retrieved from https://journals.lww.com/soilsci/Fulltext/1955/04000/AIR_AND_VAPOR_MOVEMENT_IN_SOIL_DUE_TO_WIND.2.aspx

Ganot, Y., Dragila, M. I., & Weisbrod, N. (2014). Impact of thermal convection on CO_2 flux across the earth–atmosphere boundary in high-permeability soils. *Agricultural and Forest Meteorology, 184*, 12–24. https://doi.org/10.1016/j.agrformet.2013.09.001

Garcia-Anton, E., S. Cuezva, A. Fernandez-Cortes, D. Benavente, and S. Sanchez-Moral (2014), Main drivers of diffusive and advective processes of CO2-gas exchange between a shallow vadose zone and the atmosphere, International Journal of Greenhouse Gas Control, 21, 113-129, https://doi.org /doi: 10.1016/j.ijggc.2013.12.006.

García-Fayos, P., & Bochet, E. (2009). Indication of antagonistic interaction between climate change and erosion on plant species richness and soil properties in semiarid Mediterranean ecosystems. *Global Change Biology, 15*(2), 306–318. https://doi.org/10.1111/j.1365-2486.2008.01738.x

Garcia-Pichel, F., & Belnap, J. (1996). Microenvironments and microescale productivity of cyanobacterial desert crust. *Journal of Phycology, 32*(5), 774–782. https://doi.org/10.1111/j.0022-3646.1996.00774.x

Gbeckor-Kove, N. (1989). *Lectures on drought, desertification, in drought and desertification. WMO, TDNo. 286, World Meteorological Organization, Geneva, Switzerland.*

Giannakopoulos, C., Le Sager, P., Bindi, M., Moriondo, M., Kostopoulou, E., & Goodess, C. M. (2009). Climatic changes and associated impacts in the Mediterranean resulting from a 2 °C global warming. *Global and Planetary Change, 68*(3), 209–224. https://doi.org/10.1016/j.gloplacha.2009.06.001

Gilmanov, T. G., Svejcar, T. J., Johnson, D. A., Angell, R. F., Saliendra, N. Z., & Wylie, B. K. (2006). Long-Term Dynamics of Production, Respiration, and Net CO2 Exchange in Two Sagebrush-Steppe Ecosystems. *Rangeland Ecology & Management, 59*(6), 585–599. https://doi.org/10.2111/05-198R1.1

Glaser, P. H., Chanton, J. P., Morin, P., Rosenberry, D. O., Siegel, D. I., Ruud, O., … Reeve, A. S. (2004). Surface deformations as indicators of deep ebullition fluxes in a large northern peatland. *Global Biogeochemical Cycles, 18*(1). https://doi.org/10.1029/2003GB002069

Goddéris, Y., François, L. M., Probst, A., Schott, J., Moncoulon, D., Labat, D., & Viville, D. (2006). Modelling weathering processes at the catchment scale: The WITCH numerical model. *Geochimica et Cosmochimica Acta, 70*(5), 1128–1147. https://doi.org/10.1016/j.gca.2005.11.018

González-Jaramillo, V., Fries, A., Rollenbeck, R., Paladines, J., Oñate-Valdivieso, F., & Bendix, J. (2016). Assessment of deforestation during the last decades in Ecuador using NOAA-AVHRR satellite data. *Erdkunde, 70,* 217–235. https://doi.org/10.3112/erdkunde.2016.03.02

Gonzalez, P., Neilson, R. P., Lenihan, J. M., & Drapek, R. J. (2010). Global

patterns in the vulnerability of ecosystems to vegetation shifts due to climate change. *Global Ecology and Biogeography, 19*(6), 755–768. https://doi.org/10.1111/j.1466-8238.2010.00558.x

Govindan, R. B., Raethjen, J., Kopper, F., Claussen, J. C., & Deuschl, G. (2005). Estimation of time delay by coherence analysis. *Physica A: Statistical Mechanics and Its Applications, 350*(2), 277–295. https://doi.org/10.1016/j.physa.2004.11.043

Grinsted, A., C. Moore, J., & Jevrejeva, S. (2004). Application of cross wavelet transform and wavelet coherence to geophysical time series. *Nonlinear Processes in Geophysics, 11*, 561–566. https://doi.org/doi: 10.5194/npg-11-561-2004

Goffin, S., C. Wylock, B. Haut, M. Maier, B. Longdoz, and M. Aubinet (2015), Modeling soil CO2 production and transport to investigate the intra-day variability of surface efflux and soil CO2 concentration measurements in a Scots Pine Forest (Pinus Sylvestris, L.), *Plant and Soil, 390*(1-2), 195-211, https://doi.org/ doi: 10.1007/s11104-015-2381-0.

Guoqing, L. (2005). 27.3-day and 13.6-day atmospheric tide and lunar forcing on atmospheric circulation. *Advances in Atmospheric Sciences, 22*(3 LB-Guoqing2005), 359–374. https://doi.org/doi: 10.1007/bf02918750

Hamerlynck, E. P., Scott, R. L., Sánchez-Cañete, E. P., & Barron-Gafford, G. A. (2013). Nocturnal soil CO2 uptake and its relationship to subsurface soil and ecosystem carbon fluxes in a Chihuahuan Desert shrubland. *Journal of Geophysical Research: Biogeosciences, 118*(4), 1593–1603. https://doi.org/10.1002/2013JG002495

Hanson, P. J., Edwards, N. T., Garten, C. T., & Andrews, J. A. (2000). Separating root and soil microbial contributions to soil respiration: A review of methods and observations. *Biogeochemistry, 48*(1), 115–146. https://doi.org/10.1023/A:1006244819642

Hastings, S. J., Oechel, W. C., & Muhlia-Melo, A. (2005). Diurnal, seasonal and annual variation in the net ecosystem CO2 exchange of a desert shrub community (Sarcocaulescent) in Baja California, Mexico. *Global Change Biology, 11*(6), 927–939. https://doi.org/10.1111/j.1365-2486.2005.00951.x

Hegerl, G. C., Brönnimann, S., Schurer, A., & Cowan, T. (2018). The early 20th century warming: Anomalies, causes, and consequences. *WIREs Climate Change, 9*(4), e522. https://doi.org/10.1002/wcc.522

Hicks Pries, C. E., Castanha, C., Porras, R. C., & Torn, M. S. (2017). The

whole-soil carbon flux in response to warming. *Science, 355*(6332), 1420 LP – 1423. https://doi.org/10.1126/science.aal1319

Hirano, T., Kim, H., & Tanaka, Y. (2003). Long-term half-hourly measurement of soil CO_2 concentration and soil respiration in a temperate deciduous forest. *Journal of Geophysical Research: Atmospheres, 108*(D20). https://doi.org/10.1029/2003JD003766

Hirsch, A. I., Trumbore, S. E., & Goulden, M. L. (2004). The surface CO_2 gradient and pore-space storage flux in a high-porosity litter layer. *Tellus B: Chemical and Physical Meteorology, 56*(4), 312–321. https://doi.org/10.3402/tellusb.v56i4.16449

Holmgren, M., Hirota, M., van Nes, E. H., & Scheffer, M. (2013). Effects of interannual climate variability on tropical tree cover. *Nature Climate Change, 3*(8), 755–758. https://doi.org/10.1038/nclimate1906

Hubb, J. (2012), The importance of water vapour measurements and corrections LI-COR Biosciences Inc. Application Note, 129, pp. 8.

Huenneke, L. F., Anderson, J. P., Remmenga, M., & Schlesinger, W. H. (2002). Desertification alters patterns of aboveground net primary production in Chihuahuan ecosystems. *Global Change Biology, 8*(3), 247–264. https://doi.org/10.1046/j.1365-2486.2002.00473.x

Hutley, L. B., Leuning, R., Beringer, J., & Cleugh, H. A. (2005). The utility of the eddy covariance techniques as a tool in carbon accounting: Tropical savanna as a case study. *Australian Journal of Botany, 53*(7), 663–675. https://doi.org/10.1071/BT04147

Huxman, T. E., Snyder, K. A., Tissue, D., Leffler, A. J., Ogle, K., Pockman, W. T., … Schwinning, S. (2004). Precipitation pulses and carbon fluxes in semiarid and arid ecosystems. *Oecologia, 141*(2), 254–268. https://doi.org/10.1007/s00442-004-1682-4

IPCC, 2019: Climate Change and Land: an IPCC special report on climate change, desertification, land degradation, sustainable land management, food security, and greenhouse gas fluxes in terrestrial ecosystems. (2019). In (eds.) P.R. Shukla, J. Skea, E. Calvo Buendia, V. Masson-Delmotte, H.-O. Pörtner, D. C. Roberts, P. Zhai, R. Slade, S. Connors, R. van Diemen, M. Ferrat, E. Haughey, S. Luz, S. Neogi, M. Pathak, J. Petzold, J. Portugal Pereira, P. Vyas, E. Huntley, K. Kissick, (Ed.), *2019 Intergovernmental Panel on Climate Change.*

Isaac, P., Cleverly, J., McHugh, I., van Gorsel, E., Ewenz, C., & Beringer, J. (2016). OzFlux Data: Network integration from collection to curation. *Biogeosciences Discussions*, (May), 1–41. https://doi.org/10.5194/bg-2016-189

Ivans, S., Hipps, L., Leffler, A. J., & Ivans, C. Y. (2006). Response of Water Vapor and CO2 Fluxes in Semiarid Lands to Seasonal and Intermittent Precipitation Pulses. *Journal of Hydrometeorology, 7*(5), 995–1010. https://doi.org/10.1175/JHM545.1

Janssens, I. A., Kowalski, A. S., & Ceulemans, R. (2001). Forest floor CO2 fluxes estimated by eddy covariance and chamber-based model. *Agricultural and Forest Meteorology, 106*(1), 61–69. https://doi.org/10.1016/S0168-1923(00)00177-5

Jarvis, P., Rey, A., Petsikos, C., Wingate, L., Rayment, M., Pereira, J., … Valentini, R. (2007). Drying and wetting of Mediterranean soils stimulates decomposition and carbon dioxide emission: the "Birch effect"†. *Tree Physiology, 27*(7), 929–940. https://doi.org/10.1093/treephys/27.7.929

Jassal, R., Black, A., Novak, M., Morgenstern, K., Nesic, Z., & Gaumont-Guay, D. (2005). IPCC, Intergovernmental Panel on Climate Change, 2000. In: Special Report: Land Use, Land-Use Change and Forestry: Summary for Policymakers. *Agricultural and Forest Meteorology, 130*(3), 176–192. https://doi.org/10.1016/j.agrformet.2005.03.005

Jenerette, G. D., Scott, R. L., & Huxman, T. E. (2008). Whole ecosystem metabolic pulses following precipitation events. *Functional Ecology, 22*(5), 924–930. https://doi.org/https://doi.org/10.1111/j.1365-2435.2008.01450.x

Jiao, J. J., and H. Li (2004), Breathing of coastal vadose zone induced by sea level fluctuations, Geophysical Research Letters, 31(11), L11502 11501-11504, doi: 10.1029/2004GL019572.

Jiao, J. J., and Z. Tang (1999), An analytical solution of groundwater response to tidal fluctuation in a leaky confined aquifer, Water Resources Research, 35(3), 747-751, doi: 10.1029/1998WR900075.

Jones, H. G. (1992), Plants and Microclimate: A Quantitative Approach to Environmental Plant Physiology, 2nd ed., Cambridge Univ. Press, New York.

Junta de Andalucía, C. d. M. A. y. O. d. T. (2013), Mapa de información general de aguas subterráneas de Andalucía, edited, Red de Información Ambiental de Andalucía (REDIAM).

Kelley, C. P., Mohtadi, S., Cane, M. A., Seager, R., & Kushnir, Y. (2015). Climate change in the Fertile Crescent and implications of the recent Syrian drought. *Proceedings of the National Academy of Sciences, 112*(11), 3241 LP − 3246. https://doi.org/10.1073/pnas.1421533112

Kimball, B. A., & Lemon, E. R. (1970). Spectra of air pressure fluctuations

at the soil surface. *Journal of Geophysical Research, 75*(33), 6771–6777. https://doi.org/doi: 10.1029/JC075i033p06771

Kimball, B. A., and E. R. Lemon (1971), Air turbulence effects upon soil gas exchange, *Soil Science Society of America Journal, 35*(1), 16-21, https://doi.org/doi: 10.2136/sssaj1971.03615995003500010013x.

King, J. Y., Brandt, L. A., & Adair, E. C. (2012). Shedding light on plant litter decomposition: Advances, implications and new directions in understanding the role of photodegradation. *Biogeochemistry, 111*(1–3), 57–81. https://doi.org/10.1007/s10533-012-9737-9

Köchy, M., Hiederer, R., & Freibauer, A. (2015). Global distribution of soil organic carbon – Part 1: Masses and frequency distributions of SOC stocks for the tropics, permafrost regions, wetlands, and the world. *Soil, 1*(1), 351–365. https://doi.org/10.5194/soil-1-351-2015

Kosmas, C., Marathianou, M., Gerontidis, S., Detsis, V., Tsara, M., & Poesen, J. (2001). Parameters affecting water vapor adsorption by the soil under semi-arid climatic conditions. *Agricultural Water Management, 48*(1), 61–78. https://doi.org/https://doi.org/10.1016/S0378-3774(00)00113-X

Koutroulis, A. G. (2019). Dryland changes under different levels of global warming. *Science of The Total Environment, 655*, 482–511. https://doi.org/https://doi.org/10.1016/j.scitotenv.2018.11.215

Kowalski, A. S., Serrano-Ortiz, P., Janssens, I. A., Sánchez-Moral, S., Cuezva, S., Domingo, F., … Alados-Arboledas, L. (2008). Can flux tower research neglect geochemical CO2 exchange? *Agricultural and Forest Meteorology, 148*(6), 1045–1054. https://doi.org/10.1016/j.agrformet.2008.02.004

Kuang, X., Jiao, J. J., & Li, H. (2013). Review on airflow in unsaturated zones induced by natural forcings. *Water Resources Research, 49*(10), 6137–6165. https://doi.org/doi: 10.1002/wrcr.20416

Kutzbach, L., Schneider, J., Sachs, T., Giebels, M., Nykänen, H., Shurpali, N. J., … Wilmking, M. (2007). CO2 flux determination by closed-chamber methods can be seriously biased by inappropriate application of linear regression. *Biogeosciences, 4*(6), 1005–1025. https://doi.org/10.5194/bg-4-1005-2007

Laemmel, T., Maier, M., Schack-Kirchner, H., & Lang, F. (2017). An in situ method for real-time measurement of gas transport in soil. *European Journal of Soil Science, 68*(2), 156–166. https://doi.org/doi:10.1111/ejss.12412

Lal, R. (2004). Carbon Sequestration in Dryland Ecosystems.

Environmental Management, 33(4), 528–544.
https://doi.org/10.1007/s00267-003-9110-9

Larcher, W. (2000). Temperature stress and survival ability of Mediterranean sclerophyllous plants. *Plant Biosystems - An International Journal Dealing with All Aspects of Plant Biology, 134*(3), 279–295. https://doi.org/10.1080/11263500012331350455

Lázaro, R., Rodrigo, F. S., Gutiérrez, L., Domingo, F., & Puigdefábregas, J. (2001). Analysis of a 30-year rainfall record (1967–1997) in semi–arid SE Spain for implications on vegetation. *Journal of Arid Environments, 48*(3), 373–395.
https://doi.org/10.1006/jare.2000.0755

Le Blancq, F. (2011). Diurnal pressure variation: the atmospheric tide. *Weather, 66*(11), 306–307. https://doi.org/doi: 10.1002/wea.857

Le Quéré, C., Andrew, R. M., Friedlingstein, P., Sitch, S., Hauck, J., Pongratz, J., … Zheng, B. (2018). Global Carbon Budget 2018. *Earth Syst. Sci. Data, 10*(4), 2141–2194. https://doi.org/10.5194/essd-10-2141-2018

Le Quéré, C., Moriarty, R., Andrew, R. M., Canadell, J. G., Sitch, S., Korsbakken, J. I., … Zeng, N. (2015). Global Carbon Budget 2015. *Earth System Science Data, 7*(2), 349–396.
https://doi.org/10.5194/essd-7-349-2015

Leon, E., Vargas, R., Bullock, S., Lopez, E., Panosso, A. R., & La Scala, N. (2014). Hot spots, hot moments, and spatio-temporal controls on soil CO_2 efflux in a water-limited ecosystem. *Soil Biology and Biochemistry, 77*, 12–21. https://doi.org/10.1016/j.soilbio.2014.05.029

Lewicki, J. L., Evans, W. C., Hilley, G. E., Sorey, M. L., Rogie, J. D., & Brantley, S. L. (2003). Shallow soil CO_2 flow along the San Andreas and Calaveras Faults, California. *Journal of Geophysical Research: Solid Earth, 108*(B4). https://doi.org/10.1029/2002JB002141

Li, L., and D. A. Barry (2000), Wave-induced beach groundwater flow, *Advances in Water Resources, 23*(4), 325-337, https://doi.org/10.1016/S0309-1708(99)00032-9.

Li, D., Wu, S., Liu, L., Zhang, Y., & Li, S. (2018). Vulnerability of the global terrestrial ecosystems to climate change. *Global Change Biology, 24*(9), 4095–4106. https://doi.org/10.1111/gcb.14327

Lickley, M., & Solomon, S. (2018). Drivers, timing and some impacts of global aridity change. *Environmental Research Letters, 13*(10), 104010. https://doi.org/10.1088/1748-9326/aae013

Lindzen, R. S. (1979). Atmospheric tides. In *Annual Review of Earth and Planetary Sciences* (Vol. 7). https://doi.org/https://doi.org/10.1007/978-94-010-3399-2

Liu, X., Wan, S., Su, B., Hui, D., & Luo, Y. (2002). Response of soil CO_2 efflux to water manipulation in a tallgrass prairie ecosystem. *Plant and Soil, 240*(2), 213–223. https://doi.org/10.1023/A:1015744126533

Longdoz, B., Yernaux, M., & Aubinet, M. (2008). Soil CO_2 efflux measurements in a mixed forest: Impact of chamber disturbances, spatial variability and seasonal evolution. *Global Change Biology, 6*, 907–917. https://doi.org/10.1046/j.1365-2486.2000.00369.x

Loisy, C., G. Cohen, C. Laveuf, O. Le Roux, P. Delaplace, C. Magnier, et al. (2013), The CO_2-vadose project: Dynamics of the natural CO_2 in a carbonate vadose zone, *International Journal of Greenhouse Gas* Control, 14, 97-112, doi: 10.1016/j.ijggc.2012.12.017.

López-Ballesteros, A., Oyonarte, C., Kowalski, A. S., Serrano-Ortiz, P., Sánchez-Cañete, E. P., Moya, M. R., & Domingo, F. (2018). Can land degradation drive differences in the C exchange of two similar semiarid ecosystems? *Biogeosciences, 15*(1), 263–278. https://doi.org/10.5194/bg-15-263-2018

López-Ballesteros, A., Serrano-Ortiz, P., Kowalski, A. S., Sánchez-Cañete, E. P., Scott, R., & Domingo, F. (2017). Subterranean ventilation of allochthonous CO_2 governs net CO_2 exchange in a semiarid Mediterranean grassland. *Agricultural and Forest Meteorology, 234–235*, 115–126. https://doi.org/10.1016/j.agrformet.2016.12.021

López-Ballesteros, A., Serrano-Ortiz, P., Sánchez-Cañete, E. P., Oyonarte, C., Kowalski, A. S., Pérez Priego, Ó., & Domingo, F. (2016). Enhancement of the net CO_2 release of a semiarid grassland in SE Spain by rain pulses. *Journal of Geophysical Research: Biogeosciences, 121*, 52–66. https://doi.org/doi: 10.1002/2015JG003091

Luo, H., Oechel, W. C., Hastings, S. J., Zuleta, R., Qian, Y., & Kwon, H. (2007). Mature semiarid chaparral ecosystems can be a significant sink for atmospheric carbon dioxide. *Global Change Biology, 13*(2), 386–396. https://doi.org/10.1111/j.1365-2486.2006.01299.x

MA. (2005). Ecosystems and Human Well-Being: Syntesis. In *Millenium Ecosystem Assesment.* https://doi.org/10.5822/978-1-61091-484-0_1

Ma, S., Baldocchi, D. D., Hatala, J. A., Detto, M., & Curiel Yuste, J. (2012). Are rain-induced ecosystem respiration pulses enhanced by legacies of antecedent photodegradation in semi-arid environments? *Agricultural and Forest Meteorology, 154–155*, 203–213. https://doi.org/10.1016/j.agrformet.2011.11.007

Ma, S., Baldocchi, D. D., Xu, L., & Hehn, T. (2007). Inter-annual variability in carbon dioxide exchange of an oak/grass savanna and open grassland in California. *Agricultural and Forest Meteorology, 147*(3), 157–171. https://doi.org/10.1016/j.agrformet.2007.07.008

Maestre, F. T., Eldridge, D. J., Soliveres, S., Kéfi, S., Delgado-Baquerizo, M., Bowker, M. A., … Berdugo, M. (2016). Structure and Functioning of Dryland Ecosystems in a Changing World. *Annual Review of Ecology, Evolution, and Systematics, 47*(1), 215–237. https://doi.org/10.1146/annurev-ecolsys-121415-032311

MAGNA (2010), Mapa Geológico de España Escala 1:50.000 (MAGNA 50). Instituto Geoloógico y Minero de España. Retrieved from: http://info.igme.es/cartografiadigital/geologica/Magna50.aspx (2019, January 16).

Magnani, F., Mencuccini, M., Borghetti, M., Berbigier, P., Berninger, F., Delzon, S., … Grace, J. (2007). The human footprint in the carbon cycle of temperate and boreal forests. *Nature, 447*(7146), 849–851. https://doi.org/10.1038/nature05847

Maier, M., & Schack-Kirchner, H. (2014). Using the gradient method to determine soil gas flux: A review. *Agricultural and Forest Meteorology, 192–193*, 78–95. https://doi.org/doi: 10.1016/j.agrformet.2014.03.006

Maier, M., Schack-Kirchner, H., Aubinet, M., Goffin, S., Longdoz, B., & Parent, F. (2012). Turbulence effect on gas transport in three contrasting forest soils. *Soil Science Society of America Journal, 76*(5), 1518–1528. https://doi.org/doi: 10.2136/sssaj2011.0376

Maier, M., Schack-Kirchner, H., Hildebrand, E. E., & Holst, J. (2010). Pore-space CO2 dynamics in a deep, well-aerated soil. *European Journal of Soil Science, 61*(6), 877–887. https://doi.org/doi: 10.1111/j.1365-2389.2010.01287.x

Maliva, R., & Missimer, T. (2012). Aridity and Drought. In R. and T. M. (eds.). ⌈Maliva (Ed.), *Arid Lands Water Evaluation and Management* (pp. 21–39). https://doi.org/10.1007/978-3-642-29104-3_2

Marañón-Jiménez, S., Castro, J., Kowalski, A. S., Serrano-Ortiz, P., Reverter, B. R., Sánchez-Cañete, E. P., & Zamora, R. (2011). Post-fire soil respiration in relation to burnt wood management in a Mediterranean mountain ecosystem. *Forest Ecology and Management, 261*(8), 1436–1447. https://doi.org/10.1016/j.foreco.2011.01.030

Martinez, M. J., and R. H. Nilson (1999), Estimates of barometric pumping of moisture through unsaturated fractured rock,

Transport in Porous Media, 36(1), 85-119, doi: 10.1023/a:1006593628835.

Massman, W. J., Sommerfeld, R. A., Mosier, A. R., Zeller, K. F., Hehn, T. J., & Rochelle, S. G. (1997). A model investigation of turbulence-driven pressure-pumping effects on the rate of diffusion of CO_2, N_2O, and CH_4 through layered snowpacks. *Journal of Geophysical Research: Atmospheres, 102*(D15), 18851–18863. https://doi.org/doi: 10.1029/97JD00844

Massman, W., Sommerfield, R., Zeller, K., Hehn, T., Hudnell, L., & Rochelle, S. (1995). *CO_2 flux through a Wyoming seasonal snowpack: diffusional and pressure pumping effects.*

Massmann, J., & Farrier, D. F. (1992). Effects of atmospheric pressures on gas transport in the vadose zone. *Water Resources Research, 28*(3), 777–791. https://doi.org/doi: 10.1029/91WR02766

Meyers, T. P. (2001). A comparison of summertime water and CO_2 fluxes over rangeland for well watered and drought conditions. *Agricultural and Forest Meteorology, 106*(3), 205–214. https://doi.org/10.1016/S0168-1923(00)00213-6

Mielnick, P., Dugas, W. A., Mitchell, K., & Havstad, K. (2005). Long-term measurements of CO_2 flux and evapotranspiration in a Chihuahuan desert grassland. *Journal of Arid Environments, 60*(3), 423–436. https://doi.org/https://doi.org/10.1016/j.jaridenv.2004.06.001

Migliavacca, M., Galvagno, M., Cremonese, E., Rossini, M., Meroni, M., Sonnentag, O., … Richardson, A. D. (2011). Using digital repeat photography and eddy covariance data to model grassland phenology and photosynthetic CO_2 uptake. *Agricultural and Forest Meteorology, 151*(10), 1325–1337. https://doi.org/10.1016/j.agrformet.2011.05.012

Mohr, M., Laemmel, T., Maier, M., & Schindler, D. (2016). Analysis of air pressure fluctuations and topsoil gas concentrations within a scots pine forest. *Atmosphere, 7*(10), 125. https://doi.org/doi: 10.3390/atmos7100125

Mörner, N.-A., & Etiope, G. (2002). Carbon degassing from the lithosphere. *Global and Planetary Change, 33*(1), 185–203. https://doi.org/10.1016/S0921-8181(02)00070-X

Mouat DA, Lancaster J (2006) Desertifi cation: impact. Encycl Soil Sci. doi: 10.1081/E-ESS- 120001732

Moya, M. R., Sánchez-Cañete, E. P., Vargas, R., López-Ballesteros, A., Oyonarte, C., Kowalski, A. S., … Domingo, F. (2019). CO 2 Dynamics

Are Strongly Influenced by Low Frequency Atmospheric Pressure Changes in Semiarid Grasslands. *Journal of Geophysical Research: Biogeosciences, 124*(4), 902–917. https://doi.org/10.1029/2018JG004961

Nachshon, U., Dragila, M., & Weisbrod, N. (2012). From atmospheric winds to fracture ventilation: Cause and effect. *Journal of Geophysical Research: Biogeosciences, 117*(2), G02016. https://doi.org/doi: 10.1029/2011JG001898

Nilson, R. H., Peterson, E. W., Lie, K. H., Burkhard, N. R., & Hearst, J. R. (1991). Atmospheric pumping: A mechanism causing vertical transport of contaminated gases through fractured permeable media. *Journal of Geophysical Research: Solid Earth, 96*(B13), 21933–21948. https://doi.org/doi: 10.1029/91JB01836

Nishina, K., Ito, A., Beerling, D. J., Cadule, P., Ciais, P., Clark, D. B., … Yokohata, T. (2014). Quantifying uncertainties in soil carbon responses to changes in global mean temperature and precipitation. *Earth Syst. Dynam., 5*(1), 197–209. https://doi.org/10.5194/esd-5-197-2014

Novick, K. A., Biederman, J. A., Desai, A. R., Litvak, M. E., Moore, D. J. P., Scott, R. L., & Torn, M. S. (2018). The AmeriFlux network: A coalition of the willing. *Agricultural and Forest Meteorology, 249*, 444–456. https://doi.org/10.1016/j.agrformet.2017.10.009

Noy-Meir, I. (1973). Desert Ecosystems: Environment and Producers. *Annual Review of Ecology and Systematics, 4*(1), 25–51. https://doi.org/10.1146/annurev.es.04.110173.000325

Ogle, K., Barber, J. J., Barron-Gafford, G. A., Bentley, L. P., Young, J. M., Huxman, T. E., … Tissue, D. T. (2015). Quantifying ecological memory in plant and ecosystem processes. *Ecology Letters, 18*(3), 221– https://doi.org/10.1111/ele.12399

Okuno, M., & Nakamura, T. (2003). Radiocarbon dating of tephra layers: recent progress in Japan. *Quaternary International, 105*(1), 49–56. https://doi.org/10.1016/S1040-6182(02)00150-7

Oyonarte, C., Rey, A., Raimundo, J., Miralles, I., & Escribano, P. (2012). The use of soil respiration as an ecological indicator in arid ecosystems of the SE of Spain: Spatial variability and controlling factors. *Ecological Indicators, 14*(1), 40–49. https://doi.org/10.1016/j.ecolind.2011.08.013

Papale, D., & Valentini, R. (2003). A new assessment of European forests carbon exchanges by eddy fluxes and artificial neural network

spatialization. *Global Change Biology*, 9(4), 525–535. https://doi.org/10.1046/j.1365-2486.2003.00609.x

Pastorello, G., Papale, D., Chu, H., Trotta, C., Agarwal, D., Canfora, E., … Torn, M. (2017). A New Data Set to Keep a Sharper Eye on Land-Air Exchanges. *Eos*, (April 2017), 1–10. https://doi.org/10.1029/2017eo071597

Pastorello, Gilberto, Trotta, C., Canfora, E., Chu, H., Christianson, D., Cheah, Y.-W., … Papale, D. (2020). The FLUXNET2015 dataset and the ONEFlux processing pipeline for eddy covariance data. *Scientific Data*, 7(1), 225. https://doi.org/10.1038/s41597-020-0534-3

Pereira, J. S., Mateus, J. A., Aires, L. M., Pita, G., Pio, C., David, J. S., … Rodrigues, A. (2007). Net ecosystem carbon exchange in three contrasting Mediterranean ecosystems – the effect of drought. *Biogeosciences*, 4(5), 791–802. https://doi.org/10.5194/bg-4-791-2007

Pérez-Priego, O., López-Ballesteros, A., Sánchez-Cañete, E. P., Serrano-Ortiz, P., Kutzbach, L., Domingo, F., … Kowalski, A. S. (2015). Analysing uncertainties in the calculation of fluxes using whole-plant chambers: random and systematic errors. *Plant and Soil*, 393(1), 229–244. https://doi.org/10.1007/s11104-015-2481-x

Pérez Priego, O., Serrano-Ortiz, P., Sánchez-Cañete, E., Domingo, F., & Kowalski, A. (2013). Isolating the effect of subterranean ventilation on CO2 emissions from drylands to the atmosphere. *Agricultural and Forest Meteorology*, 180, 194–202. http://dx.doi.org/10.1016/j.agrformet.2013.06.014

Pérez-Priego, O., Testi, L., Orgaz, F., & Villalobos, F. J. (2010). A large closed canopy chamber for measuring CO2 and water vapour exchange of whole trees. *Environmental and Experimental Botany*, 68(2), 131–138. https://doi.org/10.1016/j.envexpbot.2009.10.009

Pielke Sr., R. A., Pitman, A., Niyogi, D., Mahmood, R., McAlpine, C., Hossain, F., … de Noblet, N. (2011). Land use/land cover changes and climate: modeling analysis and observational evidence. *WIREs Climate Change*, 2(6), 828–850. https://doi.org/10.1002/wcc.144

Pimm, S. L. (1984). The complexity and stability of ecosystems. *Nature*, 307(5949), 321–326. https://doi.org/10.1038/307321a0

Polade, S. D., Gershunov, A., Cayan, D. R., Dettinger, M. D., & Pierce, D. W. (2017). Precipitation in a warming world: Assessing projected hydro-climate changes in California and other Mediterranean climate regions. *Scientific Reports*, 7(1), 10783. https://doi.org/10.1038/s41598-017-11285-y

Potts, D. L., Huxman, T. E., Cable, J. M., English, N. B., Ignace, D. D., Eilts, J. A., … Williams, D. G. (2006). Antecedent moisture and seasonal precipitation influence the response of canopy-scale carbon and water exchange to rainfall pulses in a semi-arid grassland. *New Phytologist, 170*(4), 849–860. https://doi.org/10.1111/j.1469-8137.2006.01732.x

Poulter, B., D. Frank, P. Ciais, R. B. Myneni, N. Andela, J. Bi, et al. (2014), Contribution of semi-arid ecosystems to interannual variability of the global carbon cycle, *Nature*, 509, 600, https://doi.org/doi: 10.1038/nature13376.

Pourbakhtiar, A., Poulsen, T. G., Wilkinson, S., & Bridge, J. W. (2017). Effect of wind turbulence on gas transport in porous media: experimental method and preliminary results. *European Journal of Soil Science, 68*(1), 48–56. https://doi.org/10.1111/ejss.12403

Prăvălie, R. (2016). Drylands extent and environmental issues. A global approach. *Earth-Science Reviews, 161*, 259–278. https://doi.org/https://doi.org/10.1016/j.earscirev.2016.08.003

Raich, J. W., & Schlesinger, W. H. (1992). The global carbon dioxide flux in soil respiration and its relationship to vegetation and climate. *Ecology, Evolution and Organismal Biology Publications Ecology, Evolution and Organismal Biology, 4*. https://doi.org/10.1034/j.1600-0889.1992.t01-1-00001.x

Rambal, S., Ourcival, J.-M., Joffre, R., Mouillot, F., Nouvellon, Y., Reichstein, M., & Rocheteau, A. (2003). Drought controls over conductance and assimilation of a Mediterranean evergreen ecosystem: scaling from leaf to canopy. *Global Change Biology, 9*(12), 1813–1824. https://doi.org/10.1111/j.1365-2486.2003.00687.x

Redeker, K. R., Baird, A. J., & Teh, Y. A. (2015). Quantifying wind and pressure effects on trace gas fluxes across the soil-atmosphere interface. *Biogeosciences, 12*(24), 7423–7434. https://doi.org/doi: 10.5194/bg-12-7423-2015

Reich, P. B. (2010). The carbon dioxide exchange. *Science, 329*(5993), 774–775. https://doi.org/10.1126/science.1194353

Reicherter, K. R., & Reiss, S. (2001). The Carboneras Fault Zone (southeastern Spain) revisited with Ground Penetrating Radar – Quaternary structural styles from high-resolution images. *Netherlands Journal of Geosciences, 80*(3–4), 129–138. https://doi.org/DOI: 10.1017/S0016774600023799

Reichstein, M., Falge, E., Baldocchi, D., Papale, D., Aubinet, M., Berbigier,

P., … Valentini, R. (2005). On the separation of net ecosystem exchange into assimilation and ecosystem respiration: review and improved algorithm. *Global Change Biology, 11*(9), 1424–1439. https://doi.org/10.1111/j.1365-2486.2005.001002.x

Reichstein, M., M. Bahn, P. Ciais, D. Frank, M. D. Mahecha, S. I. Seneviratne, et al. (2013), Climate extremes and the carbon cycle, *Nature*, 500, 287-295, https://doi.org/doi: 10.1038/nature12350.

Reichstein, M., Papale, D., Valentini, R., Aubinet, M., Bernhofer, C., Knohl, A., … Seufert, G. (2007). Determinants of terrestrial ecosystem carbon balance inferred from European eddy covariance flux sites. *Geophysical Research Letters, 34*(1). https://doi.org/10.1029/2006GL027880

Rey, A, Etiope, G., Belelli-Marchesini, L., Papale, D., & Valentini, R. (2012). Geologic carbon sources may confound ecosystem carbon balance estimates: Evidence from a semiarid steppe in the southeast of Spain. *Journal of Geophysical Research: Biogeosciences, 117*(G3). https://doi.org/doi:10.1029/2012JG001991

Rey, A, Pegoraro, E., Oyonarte, C., Were, A., Escribano, P., & Raimundo, J. (2011). Impact of land degradation on soil respiration in a steppe (Stipa tenacissima L.) semi-arid ecosystem in the SE of Spain. *Soil Biology and Biochemistry, 43*, 393–403. https://doi.org/doi: 10.1016/j.soilbio.2010.11.007

Rey, Ana, Oyonarte, C., Morán-López, T., Raimundo, J., & Pegoraro, E. (2017). Changes in soil moisture predict soil carbon losses upon rewetting in a perennial semiarid steppe in SE Spain. *Geoderma, 287*, 135–146. https://doi.org/https://doi.org/10.1016/j.geoderma.2016.06.025

Reynolds, J F, Stafford Smith, D. M., Lambin, E. F., Turner Ii, B. L., Mortimore, M., Batterbury, S. P. J., … Walker, B. (2007). Ecology: Global desertification: Building a science for dryland development. *Science, 316*(5826), 847–851. https://doi.org/doi: 10.1126/science.1131634

Reynolds, James F, Kemp, P. R., Ogle, K., & Fernández, R. J. (2004). Modifying the 'pulse–reserve' paradigm for deserts of North America: precipitation pulses, soil water, and plant responses. *Oecologia, 141*(2), 194–210. https://doi.org/10.1007/s00442-004-1524-4

Risk, D., Kellman, L., & Beltrami, H. (2002). Soil CO 2 production and surface flux at four climate observatories in eastern Canada . *Global Biogeochemical Cycles, 16*(4), 69-1-69–12. https://doi.org/10.1029/2001gb001831

Rodriguez-Caballero, E., Belnap, J., Büdel, B., Crutzen, P. J., Andreae, M. O., Pöschl, U., & Weber, B. (2018). Dryland photoautotrophic soil surface communities endangered byglobal change. *Nature Geoscience*, *11*(3), 185–189. https://doi.org/10.1038/s41561-018-0072-1

Roland, M., Serrano-Ortiz, P., Kowalski, A. S., Goddéris, Y., Sánchez-Cañete, E. P., Ciais, P., … Janssens, I. A. (2013). Atmospheric turbulence triggers pronounced diel pattern in karst carbonate geochemistry. *Biogeosciences*, *10*(7), 5009–5017. https://doi.org/10.5194/bg-10-5009-2013

Roland, M., Vicca, S., Bahn, M., Ladreiter-Knauss, T., Schmitt, M., & Janssens, I. A. (2015). Importance of nondiffusive transport for soil CO_2 efflux in a temperate mountain grassland. *Journal of Geophysical Research: Biogeosciences*, *120*(3), 502–512. https://doi.org/doi: 10.1002/2014JG002788

Rolston, D. E., and P. Moldrup (2012), Gas transport in Soils, in Handbook of Soil Science and Processes , Second edition, edited by Y. L. Pan Ming Huang, Malcolm E. , pp. 8-1 8-20, CRC Press, 2011.

Rubel, F., & Kottek, M. (2010). Observed and projected climate shifts 1901-2100 depicted by world maps of the Köppen-Geiger climate classification. *Meotorogische Zeitschrift*, *19,2*, 135–141. https://doi.org/doi: 10.1127/0941-2948/2010/0430

Rumpel, C., & Kögel-Knabner, I. (2011). Deep soil organic matter—a key but poorly understood component of terrestrial C cycle. *Plant and Soil*, *338*(1), 143–158. https://doi.org/10.1007/s11104-010-0391-5

Rutledge, S., Campbell, D. I., Baldocchi, D. D., & Schipper, L. A. (2010). Photodegradation leads to increased carbon dioxide losses from terrestrial organic matter. *Global Change Biology*, *16*(11), 3065–3074. https://doi.org/10.1111/j.1365-2486.2009.02149.x

Saleska, S. R., Miller, S. D., Matross, D. M., Goulden, M. L., Wofsy, S. C., da Rocha, H. R., … Silva, H. (2003). Carbon in Amazon Forests: Unexpected Seasonal Fluxes and Disturbance-Induced Losses. *Science*, *302*(5650), 1554 LP − 1557. https://doi.org/10.1126/science.1091165

Sanchez-Cañete, E. P., Serrano-Ortiz, P., Kowalski, A. S., Oyonarte, C., & Domingo, F. (2011). Subterranean CO_2 ventilation and its role in the net ecosystem carbon balance of a karstic shrubland. *Geophysical Research Letters*, *38*(9), L09802. https://doi.org/doi: 10.1029/2011GL047077

Sánchez-Cañete, E P, Oyonarte, C., Serrano-Ortiz, P., Curiel Yuste, J., Pérez-Priego, O., Domingo, F., & Kowalski, A. S. (2016). Winds

induce CO2 exchange with the atmosphere and vadose zone transport in a karstic ecosystem. *Journal of Geophysical Research: Biogeosciences, 121*(8), 2049–2063. https://doi.org/10.1002/2016JG003500

Sánchez-Cañete, Enrique P., Scott, R. L., van Haren, J., & Barron-Gafford, G. A. (2017). Improving the accuracy of the gradient method for determining soil carbon dioxide efflux. *Journal of Geophysical Research: Biogeosciences, 122*(1), 50–64. https://doi.org/10.1002/2016JG003530

Sánchez-Cañete, E.P. and Kowalski, A.S., (2014). Comment on "Using the gradient method to determine soil gas flux: A review" by M. Maier and H. Schack-Kirchner. Agricultural and Forest Meteorology, 197(0): 254- 255.

Sánchez-Cañete, E. P., Kowalski, A. S., Serrano-Ortiz, P., Pérez Priego, O., & Domingo, F. (2013a). Deep CO2 soil inhalation/exhalation induced by synoptic pressure changes and atmospheric tides in a carbonated semiarid steppe. *Biogeosciences, 10*, 6591–6600. https://doi.org/doi: 10.5194/bg-10-6591-2013

Sánchez-Cañete, E. P., Serrano-Ortiz, P., Domingo, F., & Kowalski, A. S. (2013b). Cave ventilation is influenced by variations in the CO2 dependent virtual temperature. *International Journal of Speleology, 42*(1), 1–8. https://doi.org/10.5038/1827-806X.42.1.1

Santer, B. D., Taylor, K. E., Wigley, T. M. L., Johns, T. C., Jones, P. D., Karoly, D. J., … Tett, S. (1996). A search for human influences on the thermal structure of the atmosphere. *Nature, 382*(6586), 39–46. https://doi.org/10.1038/382039a0

Scharlemann, J. P. W., Tanner, E. V. J., Hiederer, R., & Kapos, V. (2014). Global soil carbon: understanding and managing the largest terrestrial carbon pool. *Carbon Management, 5*(1), 81–91. https://doi.org/10.4155/cmt.13.77

Schlaepfer, D. R., Bradford, J. B., Lauenroth, W. K., Munson, S. M., Tietjen, B., Hall, S. A., … Jamiyansharav, K. (2017). Climate change reduces extent of temperate drylands and intensifies drought in deep soils. *Nature Communications, 8*(1), 14196. https://doi.org/10.1038/ncomms14196

Schlesinger, W. H. (1990). Evidence from chronosequence studies for a low carbon-storage potential of soils. *Nature, 348*(6298), 232–234. https://doi.org/10.1038/348232a0

Schimel, D., Pavlick, R., Fisher, J. B., Asner, G. P., Saatchi, S., Townsend, P., … Cox, P. (2015). Observing terrestrial ecosystems and the carbon cycle from space. *Global Change Biology, 21*(5), 1762–1776. https://doi.org/10.1111/gcb.12822

Schimel, D. S. (1995). Terrestrial ecosystems and the carbon cycle. *Global Change Biology, 1*(1), 77–91. https://doi.org/10.1111/j.1365-2486.1995.tb00008.x

Schimel, D., Pavlick, R., Fisher, J. B., Asner, G. P., Saatchi, S., Townsend, P., … Cox, P. (2015). Observing terrestrial ecosystems and the carbon cycle from space. *Global Change Biology, 21*(5), 1762–1776. https://doi.org/10.1111/gcb.12822

Schimel, D. S. (2010). Drylands in the Earth System. *Science, 327*(5964), 418–419. https://doi.org/doi: 10.1126/science.1184946

Schlesinger, W., Reynolds, J., Cunningham, G., Huenneke, L., Jarrell, W., Virginia, R., & Whitford, W. (1990). Biological Feedbacks in Global Desertification. *Science, 247*, 1043–1048. https://doi.org/10.1126/science.247.4946.1043

Schwinning, S., & Sala, O. E. (2004). Hierarchy of responses to resource pulses in arid and semi-arid ecosystems. *Oecologia, 141*(2), 211–220. https://doi.org/10.1007/s00442-004-1520-8

Seddon, A. W. R., Macias-Fauria, M., Long, P. R., Benz, D., & Willis, K. J. (2016). Sensitivity of global terrestrial ecosystems to climate variability. *Nature, 531*(7593), 229–232. https://doi.org/10.1038/nature16986

Seidl, R., Thom, D., Kautz, M., Martin-Benito, D., Peltoniemi, M., Vacchiano, G., … Reyer, C. P. O. (2017). Forest disturbances under climate change. *Nature Climate Change, 7*(6), 395–402. https://doi.org/10.1038/nclimate3303

Serrano-Ortiz, P, Roland, M., Sanchez Moral, S., Janssens, I. A., Domingo, F., Goddéris, Y., & Kowalski, A. S. (2010). Hidden, abiotic CO2 flows and gaseous reservoirs in the terrestrial carbon cycle: Review and perspectives. *Agricultural and Forest Meteorology, 150*, 321–329. https://doi.org/doi: 10.1016/j.agrformet.2010.01.002

Serrano-Ortiz, Penélope, Oyonarte, C., Pérez Priego, O., Reverter, B., Sánchez-Cañete, E., Were, A., … Domingo, F. (2014). Ecological functioning in grass–shrub Mediterranean ecosystems measured by eddy covariance. *Oecologia, 175*, 1005–1017. https://doi.org/10.1007/s00442-014-2948-0

Settele, J., R. Scholes, R. Betts, S. Bunn, P. Leadley, D. Nepstad, J.T. Overpeck, and M. A. T. (2014). Terrestrial and Inland water systems. In K. J. M. e [Field, C.B., V.R. Barros, D.J. Dokken, A. N. L. M.D. Mastrandrea, T.E. Bilir, M. Chatterjee, K.L. Ebi, Y.O. Estrada, R.C. Genova, B. Girma, E.S. Kissel, & and L. L. W. (eds.)]. S.

MacCracken, P.R. Mastrandrea (Eds.), *Climate Change 2014 Impacts, Adaptation and Vulnerability: Part A: Global and Sectoral Aspects* (pp. 271–359). https://doi.org/10.1017/CBO9781107415379.009

Shao, P., Zeng, X., Moore, D. J. P., & Zeng, X. (2013). Soil microbial respiration from observations and Earth System Models. *Environmental Research Letters, 8*(3), 34034. https://doi.org/10.1088/1748-9326/8/3/034034

Shen, W., Jenerette, G. D., Hui, D., Phillips, R. P., & Ren, H. (2008). Effects of changing precipitation regimes on dryland soil respiration and C pool dynamics at rainfall event, seasonal and interannual scales. *Journal of Geophysical Research: Biogeosciences, 113*(G3). https://doi.org/10.1029/2008JG000685

Sherwood, S., & Fu, Q. (2014). A Drier Future? *Science, 343*(6172), 737 LP – 739. https://doi.org/10.1126/science.1247620

Sitch, S., Smith, B., Prentice, I. C., Arneth, A., Bondeau, A., Cramer, W., … Venevsky, S. (2003). Evaluation of ecosystem dynamics, plant geography and terrestrial carbon cycling in the LPJ dynamic global vegetation model. *Global Change Biology, 9*(2), 161–185. https://doi.org/10.1046/j.1365-2486.2003.00569.x

Smith, K. A., Ball, T., Conen, F., Dobbie, K. E., Massheder, J., & Rey, A. (2018). Exchange of greenhouse gases between soil and atmosphere: interactions of soil physical factors and biological processes. *European Journal of Soil Science, 69*(1), 10–20. https://doi.org/10.1111/ejss.12539

Specht, R. L., & Moll, E. J. (1983). *Mediterranean-Type Heathlands and Sclerophyllous Shrublands of the World: An Overview BT - Mediterranean-Type Ecosystems* (F. J. Kruger, D. T. Mitchell, & J. U. M. Jarvis, Eds.). Berlin, Heidelberg: Springer Berlin Heidelberg.

Solomon Susan, Qin Dahe, M. M. (2007). *IPCC, 2007: Climate change 2007: The Physical Science Basis. Contribution of Working Group I to the Fourth Assessment Report of the Intergovernmental Panel on Climate Change* (C. U. Press, Ed.). Cambridge, United Kingdom and New York, NY, USA: Press, Cambridge University.

Sorensen, L. (2007). *A spatial analysis approach to the global delineation of dryland areas of relevance to the CBD Programme of Work on Dry and Subhumid Lands*. Cambridge.

Stull, R. B. (1988). *An introduction to boundary layer meteorology* (Vol. 13). https://doi.org/10.1007/978-94-009-3027-8

Subke, J.-A., Reichstein, M., & Tenhunen, J. D. (2003). Explaining

temporal variation in soil CO2 efflux in a mature spruce forest in Southern Germany. *Soil Biology and Biochemistry, 35*(11), 1467–1483. https://doi.org/10.1016/S0038-0717(03)00241-4

Sulkava, M., Luyssaert, S., Zaehle, S., & Papale, D. (2011). Assessing and improving the representativeness of monitoring networks: The European flux tower network example. *Journal of Geophysical Research: Biogeosciences, 116*(G3). https://doi.org/10.1029/2010JG001562

Sundareshwar, P. V, Murtugudde, R., Srinivasan, G., Singh, S., Ramesh, K. J., Ramesh, R., … Zimmerman, P. R. (2007). Environmental Monitoring Network for India. *Science, 316*(5822), 204 LP – 205. https://doi.org/10.1126/science.1137417

Takle, E. S., Massman, W. J., Brandle, J. R., Schmidt, R. A., Zhou, X., Litvina, I. V, … Rice, C. W. (2004). Influence of high-frequency ambient pressure pumping on carbon dioxide efflux from soil. *Agricultural and Forest Meteorology, 124*(3–4), 193–206. https://doi.org/doi: 10.1016/j.agrformet.2004.01.014

Tang, J., Baldocchi, D., Qi, Y., & Xu, L. (2003). Assessing soil CO2 efflux using continuous measurements of CO2 profiles in soils with small solid-state sensors. *Agricultural and Forest Meteorology, 118*, 207–220. https://doi.org/10.1016/S0168-1923(03)00112-6

Tian, H., Lu, C., Yang, J., Banger, K., Huntzinger, D. N., Schwalm, C. R., … Zeng, N. (2015). Global patterns and controls of soil organic carbon dynamics as simulated by multiple terrestrial biosphere models: Current status and future directions. *Global Biogeochemical Cycles, 29*(6), 775–792. https://doi.org/10.1002/2014GB005021

Tifafi, M., Guenet, B., & Hatté, C. (2018). Large Differences in Global and Regional Total Soil Carbon Stock Estimates Based on SoilGrids, HWSD, and NCSCD: Intercomparison and Evaluation Based on Field Data From USA, England, Wales, and France. *Global Biogeochemical Cycles, 32*(1), 42–56. https://doi.org/10.1002/2017GB005678

Torrence, C., & Compo, G. P. (1998). A practical guide to wavelet analysis. *Bulletin of the American Meteorological Society, 79*(1), 61–78. https://doi.org/doi: 10.1175/1520-0477(1998)079<0061:Apgtwa>2.0.Co;2

UNCCD. (1994). *Elaboration of an international convention to combat desertification in countries experiencing serious drought and/or desertification, particularly in Africa.* General Assembly, United Nations,.

UNEP. (1992). *World Atlas of Desertification* (N. and D. S. G. T.

[Middleton & (eds.)], eds.). London, UK,: Edward Arnold.

Valentini, R., Matteucci, G., Dolman, A. J., Schulze, E.-D., Rebmann, C., Moors, E. J., … Jarvis, P. G. (2000). Respiration as the main determinant of carbon balance in European forests. *Nature, 404*(6780), 861–865. https://doi.org/10.1038/35009084

Vargas, R. (2013). Progress and opportunities for monitoring greenhouse gases fluxes in Mexican ecosystems: The MexFlux network. *Atmósfera, 26*(3), 325–336. https://doi.org/10.1016/S0187-6236(13)71079-8

Vargas, R., D. Baldocchi, M. Allen, M. Bahn, T. A. Black, S. Collins, et al. (2010), Looking deeper into the soil: biophysical controls and seasonal lags of soil CO2 production and efflux, Ecological Applications, 20(6), 1569-1582.

Vargas, R., Carbone, M., Reichstein, M., & Baldocchi, D. (2011). Frontiers and challenges in soil respiration research: from measurements to model-data integration. *Biogeochemistry* (2011) 102:1–13 https://doi.org/doi:10.1007/s10533-010-9462-1

Vargas, R., Collins, S., Thomey, M., Johnson, J., Brown, R., Natvig, D., & Friggens, M. (2012). Precipitation variability and fire influence the temporal dynamics of soil CO2 efflux in an arid grassland. *Global Change Biology, 18(4)*, 1401–1414. https://doi.org/doi: 10.1111/j.1365-2486.2011.02628.x

Vargas, R., Sánchez-Cañete, E. P., Serrano-Ortiz, P., Curiel Yuste, J., Domingo, F., López-Ballesteros, A., & Oyonarte, C. (2018). Hot-Moments of Soil CO2 Efflux in a Water-Limited Grassland. *Soil Systems, 2*(3), 47. https://doi.org/doi: 10.3390/soilsystems2030047

Verhoef, A., Diaz-Espejo, A., Knight, J. R., Villagarcía, L., & Fernandez, J. (2006). Adsorption of Water Vapor by Bare Soil in an Olive Grove in Southern Spain. *Journal of Hydrometeorology, 7*, 1011–1027. https://doi.org/10.1175/JHM556.1

Villarreal, S., Guevara, M., Alcaraz-Segura, D., Brunsell, N. A., Hayes, D., Loescher, H. W., & Vargas, R. (2018). Ecosystem functional diversity and the representativeness of environmental networks across the conterminous United States. *Agricultural and Forest Meteorology, 262*, 423–433. https://doi.org/10.1016/j.agrformet.2018.07.016

Wagner, S. W., Reicosky, D. C., & Alessi, R. S. (1997). Regression Models for Calculating Gas Fluxes Measured with a Closed Chamber. *Agronomy Journal, 89*(2), 279–284. https://doi.org/10.2134/agronj1997.00021962008900020021x

Wårlind, D., Smith, B., Hickler, T., & Arneth, A. (2014). Nitrogen feedbacks increase future terrestrial ecosystem carbon uptake in an individual-based dynamic vegetation model. *Biogeosciences, 11*(21), 6131–6146. https://doi.org/10.5194/bg-11-6131-2014

Webb, S. W. (2006), Gas Transport Mechanisms, in Gas Transport in Porous Media, edited by C. K. Ho, Webb, Stephen W., p. 446, Springer, Netherlands, https://doi.org/doi: 10.1007/1-4020-3962-X.

Webb, S. W., and K. Pruess (2003), The use of Fick's law for modeling trace gas diffusion in porous media, Transport in Porous Media, 51(3), 327-341, https://doi.org/doi: 10.1023/A:1022379016613.

Weeks, E. P. (1994). Thermal and wind pumping as mechanisms for passive vapor extractions in hilly terrain. *Eos Trans. AGU, 75*(44), 263.

Were, A., Serrano-Ortiz, P., Moreno De Jong, C., Villagarcía, L., Domingo, F., & Kowalski, A. S. (2010). Ventilation of subterranean CO_2 and eddy covariance incongruities over carbonate ecosystems. *Biogeosciences, 7*(3), 859–867. https://doi.org/10.5194/bg-7-859-2010

Wilcox, L. J., Yiou, P., Hauser, M., Lott, F. C., van Oldenborgh, G. J., Colfescu, I., … Sutton, R. (2018). Multiple perspectives on the attribution of the extreme European summer of 2012 to climate change. *Climate Dynamics, 50*(9), 3537–3555. https://doi.org/10.1007/s00382-017-3822-7

Wofsy, S. C., Goulden, M. L., Munger, J. W., Fan, S.-M., Bakwin, P. S., Daube, B. C., … Bazzaz, F. A. (1993). Net Exchange of CO_2 in a Mid-Latitude Forest. *Science, 260*(5112), 1314 LP − 1317. https://doi.org/10.1126/science.260.5112.1314

WRB, I. W. G. (2015). *World Reference Base for Soil Resources 2014, update 2015 International soil classification system for naming soils and creating legends for soil maps. World Soil Resources Reports No. 106. FAO, Rome.*

Xiao, J., Zhuang, Q., Baldocchi, D. D., Law, B. E., Richardson, A. D., Chen, J., … Torn, M. S. (2008). Estimation of net ecosystem carbon exchange for the conterminous United States by combining MODIS and AmeriFlux data. *Agricultural and Forest Meteorology, 148*(11), 1827–1847. https://doi.org/https://doi.org/10.1016/j.agrformet.2008.06.015

Xu, L, Lin, X., Amen, J., Welding, K., & McDermitt, D. (2014). Impact of changes in barometric pressure on landfill methane emission. *Global Biogeochemical Cycles, 28*(7), 679–695. https://doi.org/doi: 10.1002/2013GB004571

Xu, Liukang, & Baldocchi, D. D. (2004). Seasonal variation in carbon dioxide exchange over a Mediterranean annual grassland in California. *Agricultural and Forest Meteorology, 123*(1), 79–96. https://doi.org/https://doi.org/10.1016/j.agrformet.2003.10.004

You, N., Meng, J., & Zhu, L. (2018). Sensitivity and resilience of ecosystems to climate variability in the semi-arid to hyper-arid areas of Northern China: a case study in the Heihe River Basin. *Ecological Research, 33*(1), 161–174. https://doi.org/10.1007/s11284-017-1543-3

Yu, G., Fu, Y., Sun, X., Wen, X., & Zhang, L. (2006). Recent progress and future directions of ChinaFLUX. *Science in China Series D: Earth Sciences, 49*(2), 1–23. https://doi.org/10.1007/s11430-006-8001-3

Zamanian, K., Pustovoytov, K., & Kuzyakov, Y. (2016). Pedogenic carbonates: Forms and formation processes. *Earth-Science Reviews, 157*, 1–17. https://doi.org/10.1016/j.earscirev.2016.03.003

Zeng, Z., Piao, S., Li, L. Z. X., Zhou, L., Ciais, P., Wang, T., … Wang, Y. (2017). Climate mitigation from vegetation biophysical feedbacks during the past three decades. *Nature Climate Change, 7*(6), 432–436. https://doi.org/10.1038/nclimate3299

Zhu, Z., Piao, S., Myneni, R. B., Huang, M., Zeng, Z., Canadell, J. G., … Zeng, N. (2016). Greening of the Earth and its drivers. *Nature Climate Change, 6*(8), 791–795. https://doi.org/10.1038/nclimate3004